Electronic Engineering

VOL. 39. No. 475.

The Publishers and staff of ELECTRONIC ENGINEERING join together this month in saying farewell to H. G. Foster, M.Sc., F.I.E.E., M.I.E.R.E., who has retired after being Managing Editor of the journal for eighteen years. He joined ELECTRONIC ENGINEERING in February 1949 when electronics was beginning to show itself outside the shadow of wartime restrictions. With his staff he built up ELECTRONIC ENGINEERING to become a world-wide journal of renown with particular emphasis on original contributions from experts in the whole range of electronics. Although there are now many other journals in the general field, as well as in particular fields of electronics, the firm foundation laid by H. G. Foster in the formative years has ensured that the journal retains its importance at the present time. It is, of course, the intention of all concerned to maintain this high standard now and in the future. H. G. Foster has made many friends and acquaintances in both publishing and the electronics industry. On our part we wish him a long and happy retirement, with time to sit in the sun and rest from the task which he performed so well here.

Large-signal characteristics and stability criteria of negative-impedance-convertor circuits

by A. C. Davies*, B.Sc.(Eng.)

Convertors differ in that the ideal circuit is symmetrical whereas the practical circuit invariably possesses dissimilar ports: one port is always found to be open-circuit unstable and the other short-circuit unstable. Details of this aspect of the behaviour of negative-impedance convertors are given, and the relationship between small-signal stability and the nature of the current/voltage characteristic at the ports discussed. The observed behaviour is related to quite elementary properties of amplifiers.

(Voir page 597 pour le résumé en français: Zusammenfassung in deutscher Sprache auf Seite 598)

THE negative-impedance convertor (n.i.c.), as normally defined, is a 2-port having an input impedance which is always equal to the negative of its load impedance (Fig. 1). If there is a common ground between terminals 1′ and 2′, two types of n.i.c. are possible: the voltage-inversion type, defined by

$$V_1 = -V_2$$
$$\text{and} \quad I_1 = -I_2$$

and the current-inversion type, defined by

$$V_1 = V_2$$
$$\text{and} \quad I_1 = I_2$$

In these, the conventional definitions, no distinction is made between port 11′ and port 22′: the device is apparently symmetrical. Nevertheless, practical n.i.c.s are

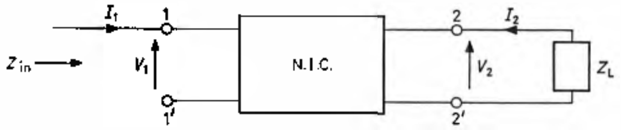

Fig. 1 Ideal negative-impedance converter ($Z_{in} = -Z_L$)

found to be definitely nonsymmetrical. One of the ports is always found to be open-circuit unstable, and the other short-circuit unstable. The negative-impedance property is necessarily produced by a cause-and-effect (feedback) relationship, and the simple definition ignores this, thus leading to an apparently symmetrical device.

Since the description of a transistorized n.i.c. by Linvill[1], the concept of the ideal symmetrical n.i.c. has proved a very useful basis for the development of techniques for synthesizing active-*RC* networks[2,3] (e.g. networks comprising only resistance, capacitance and active elements). Such networks are of interest because, firstly, all the properties of passive-*RLC* networks can be duplicated by active-*RC* networks, with the consequent possibility of avoiding the use of inductors in some filters and equalizers, and, secondly, active-*RC* networks can have properties unobtainable from passive-*RLC* networks.

Despite the usefulness of the ideal n.i.c. as a basis for active-network synthesis, the stability of the synthesized networks cannot be assured unless the inevitable asymmetry of practical n.i.c.s is taken into account. Even though the transfer functions or driving-point impedances to be synthesized are themselves stable, the practical circuits may not be, and it is often found that an interchange of the ports of the n.i.c. will render an unstable circuit stable, and *vice versa*.

Fig. 1 is an overidealized model; a circuit model which differentiates port 11′ from port 22′ is essential if the stability or instability of networks containing n.i.c.s is to be taken into account.

* *The City University, London*

Voltage-inversion negative-impedance convertor

Controlled-source model of the n.i.c.

Initially, only the voltage-inversion type of n.i.c. will be considered. This may be represented[2] by a single voltage-controlled voltage source (with $\mu = 2$, nominally), as in Fig. 2. Many practical n.i.c. circuits[4,5,6] are direct implementations of this model. Fig. 3 is a redrawn version of Fig. 2, intended to show its relationship to an amplifier with feedback. It is now apparent that there is a clear distinction between the ports. It would be expected that short-circuiting port 11′ would lead to a stable condition, since the controlled source would be reduced to zero voltage, while short-circuiting port 22′ (with $Z_s > 0$) would lead to instability (or, exceptionally, conditional stability), because of the presence of positive feedback with a loop gain greater than unity. (The nature of the instability is not apparent from the simple model in Fig. 3, just as it is not apparent from the voltage-gain expression $\dfrac{A}{1 - A\beta}$ for an amplifier with positive feedback and $A\beta > 1$). The model in Fig. 2 is thus a more useful basis for considering the behaviour of practical n.i.c. circuits than the over-idealized Fig. 1, though the conceptual usefulness of the latter cannot be denied.

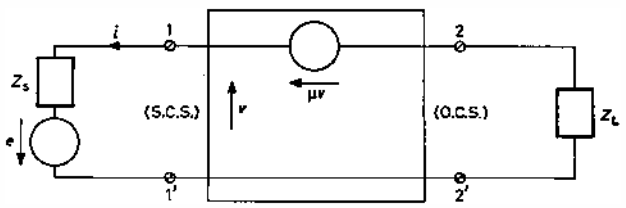

Fig. 2 Controlled-source model of voltage-inversion n.i.c. ($\mu = 2$)

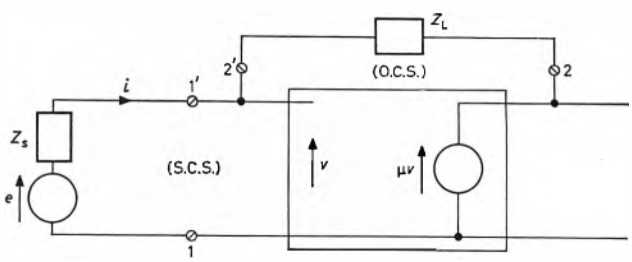

Fig. 3 Circuit of Fig. 2 redrawn as a feedback amplifier

Stability condition for resistive loads

A simplified approach to the stability conditions is possible as follows. Suppose that Z_s and Z_L are resistive, denoted R_s and R_L, respectively:

$$e - iR_s = v \quad \ldots\ldots\ldots\ldots\ldots\ldots \quad (1)$$

$$i = (v - \mu v)/R_L \quad \ldots\ldots\ldots\ldots\ldots \quad (2)$$

Therefore

$$v/e = \frac{R_L}{R_L + (1 - \mu)R_s} \quad \ldots\ldots\ldots\ldots\ldots \quad (3)$$

If $\mu = 0$, the circuit is certainly stable, and the limiting case of stability occurs when the denominator is zero. (The same result may be obtained by noting that the voltage-feedback fraction is $\frac{R_s}{R_L + R_s}$; and so, for stability, $\frac{\mu R_s}{R_L + R_s}$ must be less than unity). Thus, for stability,

$$R_L + (1 - \mu)R_s > 0$$

or

$$R_L/R_s > (\mu - 1)$$

If μ has a nominal value $+2$, the stability criterion becomes

$$R_L > R_s \quad \ldots\ldots\ldots\ldots\ldots\ldots \quad (4)$$

This is a well known property of the n.i.c.; the circuit is unstable when the resistance connected to the open-circuit-unstable port is greater than the resistance connected to the short-circuit-unstable port.

In order to investigate the stability conditions further, it is necessary to consider the practical restrictions on the frequency behaviour of the gain μ; this is done later in this article.

Large-signal characteristics

It is well known that, in practice, devices or circuits which possess negative resistance do so only for a limited range of voltages and currents. The resistance invariably becomes positive for sufficiently large voltage and current excursions. It will be seen that, in the present context, this follows from the fact that a real amplifier cannot remain linear for sufficiently large input signals. The n.i.c., in conjunction with a positive resistor R, can be used to produce a negative resistance $-R$ in two different ways: if R is connected across port 22′, $-R$ will be produced between 1 and 1′, and *vice versa.*

To simplify the discussion, suppose that the amplifier has a gain of $+2$ for small signals, and a sudden overload point, as shown in Fig. 4. If a voltage $v_{11'}$ is applied at port 11′, the current i_1 which flows in at terminal 1 is given by

$$i_1 = \frac{v_{11'} - v_{12}}{R} \quad \ldots\ldots\ldots\ldots\ldots\ldots\ldots \quad (5)$$

when R is connected across 22′. For small signals,

$$i_1 = \frac{v_{11'} - 2v_{11'}}{R} = -\, v_{11'}/R$$

Therefore $v_{11'}/i_1 = -R$

For large signals, the $v_{11'}/i_1$ characteristic may be obtained by first deriving from Fig. 4 a graph of $(v_{11'} - v_{12})/v_{11'}$; this is shown in Fig. 5. From equation (5), i_1 is proportional to $(v_{11'} - v_{12})$, and so Fig. 5 is identical in shape

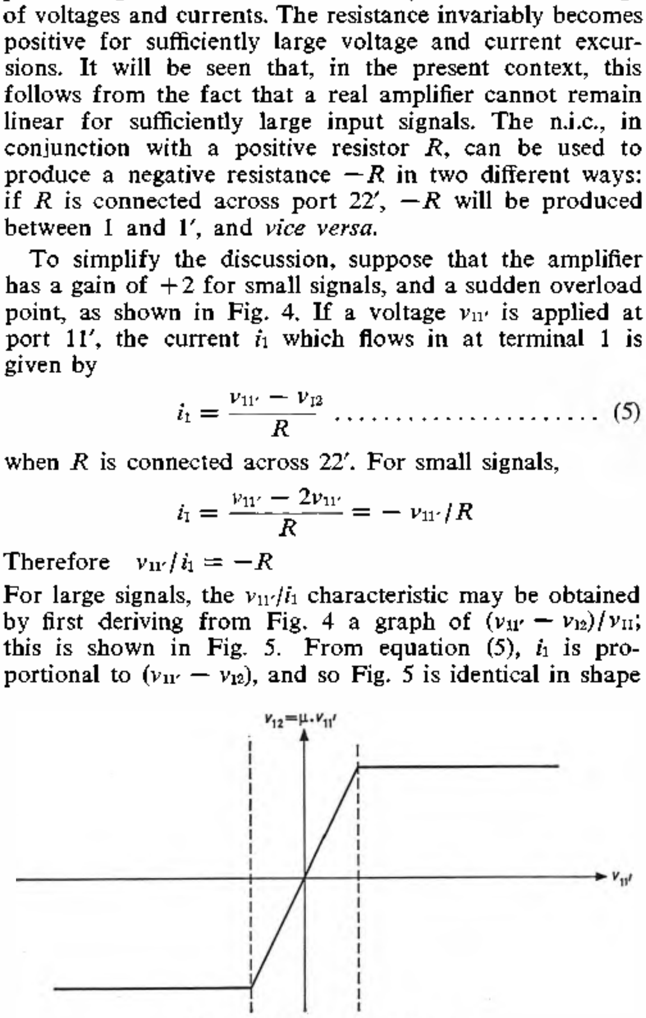

Fig. 4 **Overload characteristic**

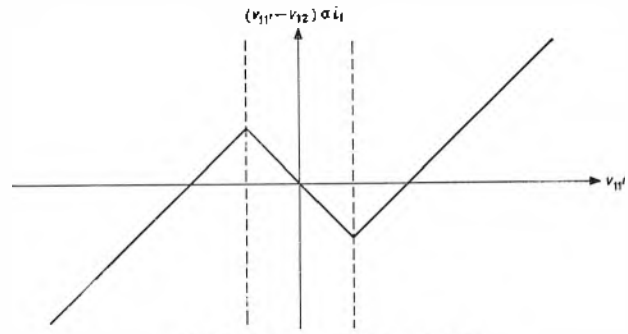

Fig. 5 **Resultant** I/V **characteristic**

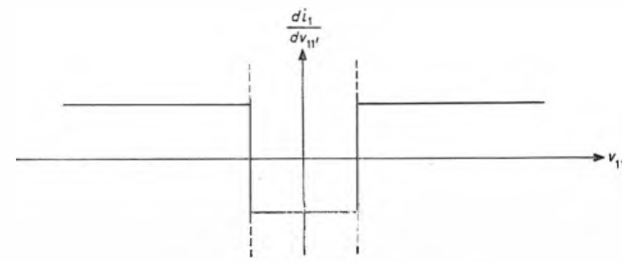

Fig. 6 **Slope resistance**

to the current/voltage (I/V) characteristic of the 'negative resistor' produced at port 11′. For sufficiently large $v_{11'}$, $di_1/dv_{11'}$ therefore becomes positive (Fig. 6).

Any practical amplifier must have an 'overload' point, above which the output does not continue to increase with increasing input, and therefore any practical method of producing a negative resistance in this manner must necessarily give rise to an N-shaped I/V characteristic; if the overload is not sudden as it was in the example, this merely alters the details but not the nature of the N-shaped characteristic. Thus it is seen that the open-circuit-unstable (and short-circuit-stable) port 11′ is associated with the N-type I/V characteristic (e.g. a voltage-controlled negative resistance).

The second method of producing a negative resistance with this amplifier is by connecting the positive resistor across 11′ and 'looking in' at port 22′. If a voltage $v_{22'}$ is applied at port 22′, the current i_2 which flows in at terminal 2 is given by

$$i_2 = +v_{11'}/R$$

and

$$v_{22'} = v_{11'} - v_{12}$$

Consequently, assuming the $v_{12}/v_{11'}$ characteristic of Fig. 4 again, a graph of $v_{22'}/i_2$ will have the same shape as $(v_{11'} - v_{12})/v_{11'}$.

Thus Fig. 5 is identical in shape to the V/I characteristic of the negative resistor produced at port 22′. Once again, for sufficiently large $v_{22'}$, $dv_{22'}/di_2$ becomes positive, and this method of producing a negative resistance must necessarily give rise to an S-shaped I/V characteristic; and so the short-circuit-unstable (and open-circuit-stable) port 22′ is associated with the S-type I/V characteristic (e.g. a current-controlled negative resistance).

Open-circuit and short-circuit stability or instability appear to be solely small-signal properties, and the connection between the N-type I/V graph and open-circuit instability is not at once apparent (nor, similarly, is the connection between the S-type I/V graph and short-circuit instability). Even if load lines are drawn on the characteristics, it is necessary to invoke the requirement that a single intersection corresponds to a stable condition and that the centre intersection of a triple intersection is unstable. Yet the difference in behaviour between circuits biased at P and Q (Fig. 7) is not easy to explain if the characteristics are assumed linear up to the overload point.

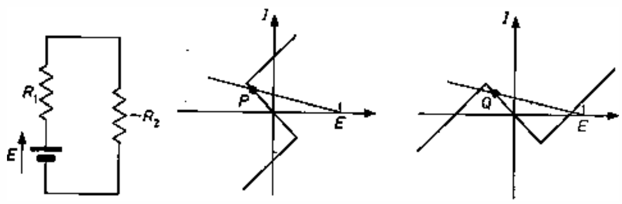

Fig. 7 Stable and unstable bias points

P represents a stable point and Q represents an unstable point, but it seems reasonable to ask how P and Q differ from a small-signal point of view, since voltages, currents and their rates of change are identical in both cases. In practice, of course, the central section of the characteristic would not be completely linear; but it seems undesirable to have to take this into account when trying to assess the small-signal stability.

Small-signal characteristics

In order to resolve this point, it is necessary to return to a consideration of the mechanism by which the negative resistance is produced in the two cases.

(i) SHORT-CIRCUIT-STABLE PORT

For the amplifier loaded at port 22′ with an impedance $Z_L(s)$, the impedance looking in at port 11′ is obtained as follows:

$$I_{in} = \frac{V_{in}(1-\mu)}{Z_L(s)}$$

therefore

$$V_{in}/I_{in} = Z_{in}(s) = \frac{Z_L(s)}{(1-\mu)} \quad \dots\dots\dots\dots (6)$$

The gain μ will be a function of s, and can be written as a ratio of polynomials:

$$\mu(s) = kN(s)/D(s)$$

where $N(s)$ and $D(s)$ are monic polynomials.

Let $N(s) = s^n + a_{n-1}s^{n-1} + \dots + a_1 s + a_0$

and $D(s) = s^m + b_{m-1}s^{m-1} + \dots + b_1 s + b_0$

$Z_L(s)$, assumed passive, will be positive real, and may also be written as a ratio of polynomials:

$$Z_L(s) = P(s)/Q(s)$$

[$Z_L(s)$ could be a positive-real irrational function of s and still be a realizable passive impedance, but this would not significantly affect the argument].

Thus the input impedance may be written as

$$Z_{in}(s) = \frac{P(s)\,D(s)}{Q(s)\,[D(s) - kN(s)]} \quad \dots\dots\dots (7)$$

The following assumptions are made about $\mu(s)$:

(a) In any practical amplifier, $\mu(s)$ must have at least one zero at $s = \infty$; therefore

$$\text{degree of } D(s) > \text{degree of } N(s)$$

thus $\qquad m - n > 0$

This restriction on $\mu(s)$ may be attributed to either the presence of some time delay in the amplifier or the effect of stray reactance, both being inevitable in any practical amplifier.

(b) If the amplifier is to be stable without $Z_L(s)$ present, $D(s)$ must have only left-halfplane (l.h.p.) zeros. The signs of all coefficients in $D(s)$ must therefore be the same, and, with no loss of generality, it can be assumed that they are positive.

(c) Case I: If the amplifier is 'low-pass' (e.g. with gain extending to $s = 0$),

$$\mu(0) = +2$$

therefore

$$ka_0/b_0 = +2 \quad \dots\dots\dots\dots\dots\dots (8)$$

Case II: If the amplifier is not 'low-pass', there must be some frequency ω_0 so that

$$\mu(j\omega_0) = +2$$

Now, in equation (7), $P(s)$ and $D(s)$ cannot have any right-halfplane (r.h.p.) zeros, and so $Z_{in}(s)$ cannot have r.h.p. zeros either. The port 11′ must therefore be short-circuit stable.

For case I, where the negative-impedance property extends to zero frequency, the coefficient of s^0 in $D(s) - kN(s)$ is $b_0 - ka_0$, which must be negative, by equation (8). But the coefficient of s^m in $D(s) - kN(s)$ must be positive [condition (b)]. Consequently, the signs of the coefficients of $D(s) - kN(s)$ are not all the same, and this is a sufficient condition for the existence of r.h.p. zeros. $Z_{in}(s)$ therefore has r.h.p. poles, and the circuit is not stable on open circuit. Thus, for the case of a low-pass amplifier, open-circuit instability and short-circuit stability at port 11′ are necessary conditions.

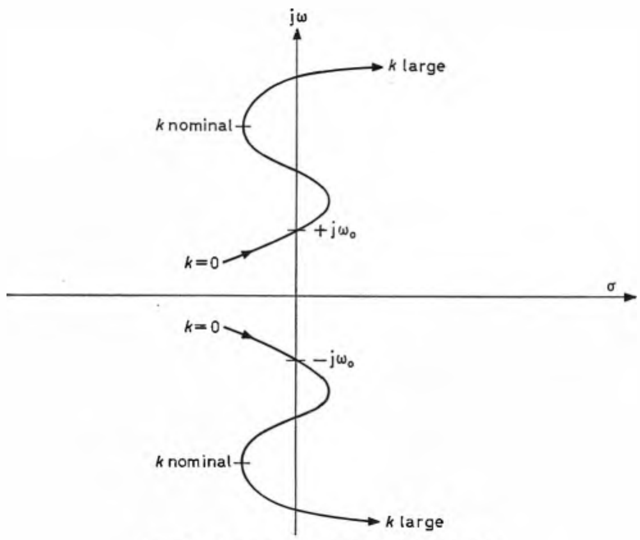

Fig. 8 Root locus of $D(s) - kN(s) = 0$

For case II, where the negative-impedance effect does not extend to zero frequency, it is not so easy to determine whether $D(s) - kN(s)$ must have r.h.p. zeros. Suppose that the amplifier is a conventional RC-coupled type, with a fall in gain at low frequencies due to coupling capacitors, and a fall in gain at high frequencies due to stray capacitance; this will be referred as to case II(a). The gain function $\mu(s)$ has the form

$$\frac{kN(s)}{D(s)} = \frac{2}{\underbrace{[1+(s/\omega_1)][1+(s/\omega_2)]\dots}_{q\text{ factors}}\;\underbrace{[1+(\omega_A/s)][1+(\omega_B/s)]\dots}_{r\text{ factors}}} \quad \dots\dots\dots\dots (9)$$

where there are q factors of the form $[1+(s/\omega_i)]$ due to stray-capacitance time constants, and r factors of the form $[1 + (\omega_i/s)]$ due to RC coupling-network time constants.

For a normally designed amplifier, there must be a 'midfrequency' range over which these factors have negligible effect; so that

$$(\omega_A, \omega_B, \ldots \ldots) \ll \omega \ll (\omega_1, \omega_2, \ldots \ldots)$$

and $\quad kN(s)/D(s) \simeq +2$ (for midfrequency)

Rearranging equation (9) gives

$$\frac{kN(s)}{D(s)} = \frac{2\,(\omega_1\omega_2 \ldots)s^r}{(s+\omega_1)(s+\omega_2)\ \ldots\ (s+\omega_A)(s+\omega_B)\ \ldots}$$

Using the approximation $(\omega_1,\omega_2 \ldots) \gg (\omega_A,\omega_B \ldots)$ to eliminate certain terms, this becomes

$$\frac{2\,(\omega_1\omega_2 \ldots)s^r}{s^{q+r} + \ldots + (\omega_1\omega_2 \ldots)s^r + \ldots (\omega_A\omega_B\omega_1\omega_2 \ldots)}$$

and therefore

$$D(s)-kN(s)=s^{q+r}+ \ldots +(\omega_1\omega_2 \ldots)s^r-2(\omega_1\omega_2 \ldots)s^r+ + \ldots +(\omega_A\omega_B\omega_1\omega_2 \ldots)$$

Clearly, in this case, the coefficient of s^r is negative while other coefficients are positive. Therefore $D(s)$-$kN(s)$ has r.h.p. zeros, and for a conventional RC-coupled amplifier, port 11′ is open-circuit unstable, as for case I.

It may be noted in passing that, although nominal amplifier gain has been taken as +2, similar conclusions may be reached about the stability for any positive gain greater than unity.

Although it has been shown that, for a low-pass amplifier [case I] and a conventional RC-coupled amplifier [case II(a)], $D(s)$-$kN(s)$ must have r.h.p. zeros, this is not necessarily true for all amplifiers. The general case will be referred to as case II(b).

For this general case, it is known that, at some frequency ω_0,

$$\left.\frac{kN(s)}{D(s)}\right|_{s=j\omega_0} = +2$$

Therefore

$$kN(j\omega_0) = 2D(j\omega_0)$$

so that

$$D(j\omega_0) - kN(j\omega_0) = -D(j\omega_0) \quad \ldots\ldots\ldots (10)$$

But, if k is reduced to zero,

$$\left. D(j\omega_0) - kN(j\omega_0)\right|_{k=0} = +D(j\omega_0) \quad \ldots\ldots (11)$$

It follows from equations (10) and (11) that

$$D(j\omega_0) - (k/2)N(j\omega_0) = 0$$

Thus $D(s) - kN(s)$ has zeros on the $j\omega$ axis (at $\pm j\omega_0$) when k has half its nominal value.

The problem of investigating the zeros of $D(s) - kN(s)$ may now be regarded as a 'root-locus' problem.

The root locus as k is increased from zero must start in the l.h.p., since $D(s)$ has all its zeros there, by condition (b), and when k has half its nominal value, there are zeros on the $j\omega$ axis.

As k is increased towards its nominal value, two possibilities exist: either the locus crosses into the r.h.p., and there are r.h.p. zeros as in cases I and II(a), or the locus moves back into the l.h.p. Even for the latter case, for sufficiently large k (greater than nominal), $D(s) - kN(s)$ must have r.h.p. zeros, because

$$D(s) - kN(s) = (s^m + b_{m-1}s^{m-1} + \ldots) - k(s^n + a_{n-1}s^{n-1} + \ldots)$$

and $m > n$, so the coefficient of s^m is independent of k and positive, while the coefficient of s^n is $(b_n - k)$, which will certainly become negative if k is made large enough. Therefore the signs of the coefficients are not all the same, and there are r.h.p. zeros for sufficiently large k.

A possible root locus is shown in Fig. 8. It is thus apparent that, in the unlikely event of an amplifier having a root-locus $D(s) - kN(s)$ of this form being used to construct an n.i.c., the port 11′ could be both open-circuit stable and short-circuit stable (the arrangement being essentially a conditionally stable feedback system). A numerical example is given in the Appendix, to show that a gain function with this root locus is possible.

Nevertheless, it seems highly improbable that such a root locus would ever arise unintentionally, and it may be concluded that, for almost every amplifier, $D(s) - kN(s)$ would have r.h.p. zeros and port 11′ would be unstable on open circuit.

(ii) OPEN-CIRCUIT-STABLE PORT

For the amplifier loaded at port 11′ with an impedance $Z_L(s)$, the impedance looking in at port 22′ is found by similar means to be given by

$$Z_{in}(s) = Z_L(s)(1 - \mu) \quad \ldots\ldots\ldots\ldots (12)$$

Therefore

$$Z_{in}(s) = \frac{P(s)\,[D(s) - kN(s)]}{Q(s)D(s)} \quad \ldots\ldots\ldots (13)$$

By comparison with equation (7), it can be seen that the same arguments can be used to show that $Z_{in}(s)$ cannot have r.h.p. poles, and is therefore open-circuit stable, while r.h.p. zeros and consequent short-circuit instability occur for all except the 'improbable' case discussed under case II(b).

The product of the input impedances at the two ports [equations (7) and (13)] is $[Z_L(s)]^2$, so that the two impedances are 'generalised duals'[8] with respect to $[Z_L(s)]^2$.

Current-inversion negative-impedance convertor

Small-signal characteristics and stability conditions

The current-inversion n.i.c. can also be represented[2] by a single-controlled-source model, as in Fig. 9, which is redrawn as Fig. 10 to show the relation to a feedback amplifier. Again, many practical n.i.c. circuits[4,6] are direct

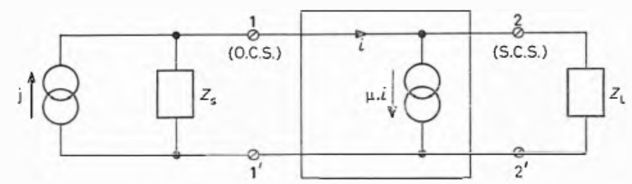

Fig. 9 Controlled-source model of current-inversion n.i.c. (μ = 2)

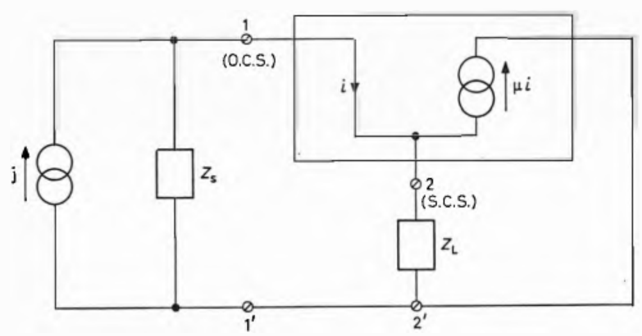

Fig. 10 Circuit of Fig. 9 redrawn as a feedback amplifier

implementations of this model. Open-circuiting port 11′ is expected to lead to a stable condition, since the controlled source is then reduced to zero, while open-circuiting port 22′ clearly leads to positive feedback (with $\mu > 1$) and expected instability.

This may be verified in the same manner as for the voltage-inversion n.i.c. Thus, if Z_L and Z_s are resistive, denoted R_L and R_s, respectively,

$$j/i = \frac{R_s}{R_s + (1 - \mu)R_L}$$

If $\mu = 0$, the circuit is certainly stable, and the limiting case occurs when the denominator is zero.

Thus, for stability,

$$R_L/R_s < (\mu - 1)$$

and if μ has a nominal value $+2$, the stability criterion becomes

$$R_L < R_s \quad \ldots\ldots\ldots\ldots\ldots\ldots \quad (14)$$

Taking into account the inevitable frequency dependence of μ, and using the same symbols as before, the input impedance at port 11′ is

$$Z_{in}(s) = \frac{P(s)[D(s) - kN(s)]}{Q(s)D(s)} \quad \ldots\ldots\ldots\ldots \quad (15)$$

so that the port is open-circuit stable and normally short-circuit unstable.

The input impedance at port 22′ is

$$Z_{in}(s) = \frac{P(s)D(s)}{Q(s)[D(s) - kN(s)]} \quad \ldots\ldots\ldots\ldots \quad (16)$$

so that the port is short-circuit stable and normally open-circuit unstable.

Therefore, the conclusions about small-signal stability and pole-zero locations apply in an exactly similar manner to both the voltage-inversion and the current-inversion types of n.i.c.

Large-signal characteristics

These may be derived in a manner similar to that for those of the voltage-inversion n.i.c. (see p. 537). The current amplifier may be assumed to have an overload characteristic of the same shape as the voltage-amplifier characteristic of Fig. 4. The short-circuit-unstable (and open-circuit-stable) port 11′ is found to have an S-type I/V characteristic, while the open-circuit-unstable (and short-circuit-stable) port 22′ is found to have an N-type I/V characteristic.

Example

One of the simplest but realistic examples to which equations (7), (13), (15) and (16) can be applied is as follows.

Suppose that the load impedance is a pure resistance and that the amplifier has a single dominant time constant, causing a high-frequency fall in gain of 6dB/octave; thus,

$$Z_L(s) = R \text{ and } \mu(s) = \frac{2}{1 + (s/\omega_0)}$$

For the short-circuit-stable port [equation (7) or (16)],

$$Z_{in}(s) = \frac{R}{1 - \mu(s)} = -R\frac{[1 + (s/\omega_0)]}{[1 - (s/\omega_0)]}$$

Therefore

$$Y_{in}(s) = -(1/R) + \frac{2s/\omega_0 R}{[1 + (s/\omega_0)]} \quad \ldots\ldots\ldots \quad (17)$$

Fig. 11 shows a network corresponding to equation (17) from which it can be seen that the effect of the amplifier time constant is to produce an apparent parasitic capacitance at the port. Obviously the time constant of Fig. 11 is negative and the network is unstable unless a resistor of lower resistance than R is connected across the terminals.

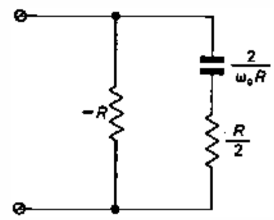

Fig. 11 Network model of driving-point impedance of s.c.s. port

For the open-circuit-stable port [equations (13) or (15)],

$$Z_{in}(s) = R[1 - \mu(s)] = -R\frac{[1 - (s/\omega_0)]}{[1 + (s/\omega_0)]}$$

Therefore

$$Z_{in}(s) = -R + \frac{2sR/\omega_0}{[1 + (s/\omega_0)]} \quad \ldots\ldots\ldots\ldots \quad (18)$$

Fig. 12 shows a network corresponding to equation (18), and in this an apparent parasitic inductance is produced. (The appearance of inductive effects should not cause surprise, since one of the motives for using active-*RC* networks is to avoid the use of actual inductors). The time constant is negative and the network unstable unless a resistor of higher resistance than R is connected across the terminals.

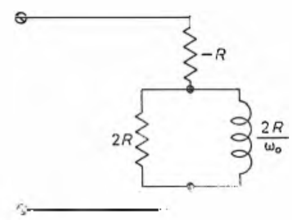

Fig. 12 Network model of driving-point impedance of o.c.s. port

These two networks are thus valid and useful models of the short-circuit-stable and open-circuit-stable ports. Although the capacitor and inductor have definite values, depending on R and ω_0, the stability criteria for the models are independent of these values; infinitesimally small capacitance and inductance would give the same criteria. It is of interest to refer to the conclusions of Herold[7] regarding negative-resistance devices and circuits. He suggested that the open-circuit-stable type of negative resistance is one in which stray inductance has a dominant effect, and the short-circuit-stable type is one in which stray capacitance has a dominant effect. Although these assumptions explain the observed behaviour, the theory has no predictive value: it is necessary to know in advance whether the negative resistance in question is open-circuit stable or short-circuit stable before choosing whether to take account of stray inductance or stray capacitance. The networks of Figs. 11 and 12 possess the type of stray reactance expected from Herold's theory, but they are only *models* of the driving-point impedances. There is no suggestion that the capacitance in Fig. 11 or the inductance in Fig. 12 have any physical existence (e.g. they are not to be identified with stray lead inductance or with capacitance between terminals). Thus, although infinitesimal capacitive and inductive parasitics can be used to explain the observed behaviour, there is no reason to assume their physical reality[3].

Relationship between small-signal stability and the large-signal characteristic

If the exceptional case where $D(s) - kN(s)$ does not have r.h.p. zeros is excluded from consideration, it is seen that, for both types of n.i.c., short-circuit stability, open-circuit instability and an N-type I/V characteristic are always associated at one port, while open-circuit stability, short-circuit instability and an S-type I/V characteristic are always associated at the other port.

This association has been observed with all negative-resistance devices[7,8] and it is often assumed that there must therefore be a causal connection between the small-signal stability and the type of I/V characteristic. And yet it is clear that, in the case of the n.i.c. circuits discussed in the previous sections, the small-signal stability is determined by the gain/frequency response of the amplifier, and the N or S shape of the I/V characteristic is determined by the overload characteristic of the amplifier. The facts that all amplifiers cease to be linear if the input signals are increased sufficiently, and that the gain/frequency response $\mu(s)$ falls to zero for sufficiently high values of complex frequency, are two necessary, but apparently quite unrelated, properties of amplifiers (it has been suggested that a relationship does exist[8]).

It seems that the association between the type of small-signal instability and the type of I/V characteristic is necessary but coincidental; the two effects stem from unrelated amplifier limitations.

Conclusions

The single-controlled-source model of the n.i.c. has been shown to be capable of predicting the observed large-signal and small-signal behaviour, and it is known that many practical n.i.c. circuits are based directly on such a model.

It has been shown that (apart from an exceptional case in which n.i.c. plus load impedance may be regarded as a conditionally stable feedback system) the open-circuit-unstable port invariably has an N-type I/V characteristic, while the short-circuit-unstable port invariably has an S-type I/V characteristic, but that these two characteristics arise from apparently unrelated limitations of the amplifier used to construct the n.i.c. If the n.i.c. is directly coupled, having a response extending to zero frequency, even the conditionally stable case cannot occur. Unless it is possible to find a causal relationship between the necessity for an amplifier to overload for very large signals and the necessity for an amplifier to have zero gain at infinite complex frequency, it is not possible, for the n.i.c. circuits discussed, to find a causal relation between the small-signal instability and the shape of the I/V characteristic.

In view of the fact that similar properties are found with all negative-resistance devices and circuits, it may be conjectured that they all rely for their behaviour on a process which can be represented by one of the controlled-source models. If this is so, conclusions reached about the n.i.c. may be applicable to other cases as well.

The stability properties of practical n.i.c. circuits are often regarded as rather mysterious and inexplicable. It is hoped that the ideas put forward in this article may help to provide a better understanding of the behaviour of these circuits.

Appendix

Conditions for simultaneous open-circuit and short-circuit stability

For simultaneous open-circuit and short-circuit stability at the ports, it is necessary that $D(s) - kN(s)$ should have no r.h.p. zeros. This condition is satisfied if the root locus of $D(s) - kN(s) = 0$ (for various k) is as in Fig. 8.

If $D(j\omega') - kN(j\omega') = 0$, there is a real-frequency zero at ω' and the ratio $kN(j\omega')/D(j\omega')$, which is $\mu(j\omega')$, must be real. Therefore, to give the Fig. 8 locus, the imaginary part of $\mu(j\omega)$ must be zero at three distinct positive values of ω. This imaginary part is a polynomial in ω^2, and so must be of at least 6th degree in ω, and factorizable to the form

$$(\omega^2 - \alpha)(\omega^2 - \beta)(\omega^2 - \gamma)$$

with α, β, γ, positive.

The above condition is not sufficient to guarantee the desired root locus, but it does indicate the degree of complexity required of $\mu(s)$ in order that such a root locus should be possible. (This problem should be distinguished from the much easier one of producing an open-circuit- and short-circuit-stable active driving-point impedance having a negative real part at some frequency: the object here is to achieve this result with the specific configuration of Fig. 2 or Fig. 9).

A gain function which does satisfy all required conditions is

$$\mu(s) = \frac{kN(s)}{D(s)} = \frac{k(s+0{\cdot}0833)(s+0{\cdot}1)}{s(s+0{\cdot}0167)(s+0{\cdot}02)(s+0{\cdot}5)(s+1)} \quad .. \quad (19)$$

The imaginary part of $\mu(j\omega)$ is

$$\omega^6 - (0{\cdot}282037)\omega^4 + (0{\cdot}00133796)\omega^2 - (0{\cdot}0000013911)$$

which factorizes to

$$(\omega^2 - 0{\cdot}00153138)(\omega^2 - 0{\cdot}00327651)(\omega^2 - 0{\cdot}277229)$$

If k is $-0{\cdot}0179156$, then, at a frequency $s = j0{\cdot}0572408$ [corresponding to the centre bracket of Im $\mu(j\omega)$],

$$\mu(s) = +2{\cdot}000$$

and

$$D(s) - kN(s) = s^5 + 1{\cdot}5367s^4 + 0{\cdot}555384s^3 + 0{\cdot}0367670s^2 + 0{\cdot}00345100s + 0{\cdot}000149240$$

The roots of this polynomial are

$$s_1 = -1{\cdot}02836$$
$$s_2 = -0{\cdot}450132$$
$$s_3 = -0{\cdot}0525935$$
$$s_4 = -0{\cdot}00280759 + j0{\cdot}0812710$$
$$s_5 = -0{\cdot}00280759 - j0{\cdot}0812710$$

Thus all zeros of $D(s) - kN(s)$ are in l.h.p., but $\mu(s) = +2$ at $s = j0{\cdot}0572408$.

Consequently, if an amplifier having a voltage gain $\mu(s)$ given by equation 19 were used to construct an n.i.c., there would be a frequency $\omega = 0{\cdot}0572408$ at which n.i.c. action would occur, but each of the ports 11′ and 22′ would be both open-circuit stable and short-circuit stable.

References

1 Linvill, J. G.: Transistor Negative Impedance Converter. *Proc. Inst. Radio Engrs. 41*, 725 (June 1953).
2 Sipress, J. M.: Synthesis of Active-RC Networks. *IRE Trans. CT-8*, 260 (Sept. 1961).
3 Storey, D. J., Cullyer, W. J.: Network Synthesis Using Negative Impedance Convertors. *Proc. IEE, 111*, 891 (May 1964).
4 Hakim, S. S.: Some New Negative Impedance Convertors. *Electronics Letters, 1*, 9 (March 1965).
5 Antoniou, A.: Negative Impedance Convertors Using Operational Amplifiers. *ibid., 1*, 88 (June 1965).
6 Larky, A. I.: Negative Impedance Converters. *IRE Trans. CT-4*, 124 (1957).
7 Herold, E. W.: General Theory of Negative Resistance Devices. *Proc. Inst. Radio Engrs. 23*, 1201 (1935).
8 Brownlie, J. D.: Small-Signal Responses Realizable from D.C. Biased Devices. *Proc. IEE, 110*, 823 (May 1963).
9 Mitra, S. K., Herbst, N., Declaris, N.: Generalized Dual and Inverse: An Extended Definition. IEEE Convention Record, Part II (Automatic Control and Circuit Theory), 76 (1963).

Short-range shock-measuring telemetry system

by J. Morrison*

This article describes a short-range f.m. transmitter/receiver system which was designed to measure impact accelerations up to 1000g. These measurements were required to optimize a shock-absorber design, which was tested by dropping a 600lb steel cylinder on to the absorber from heights up to 60ft.

(Voir page 597 pour le résumé en français: Zusammenfassung in deutscher Sprache auf Seite 598)

A SYSTEM was required which would measure the impact shock experienced by a falling weight hitting a shock absorber. Decelerations up to 1000*g*, lasting 20ms, were expected, with frequency components in the range 100Hz-10kHz; a measurement accuracy of 5-10% was required. The transmitter should, of course, be shock-mounted to avoid detuning on impact.

Fig. 1 Transmitter circuit

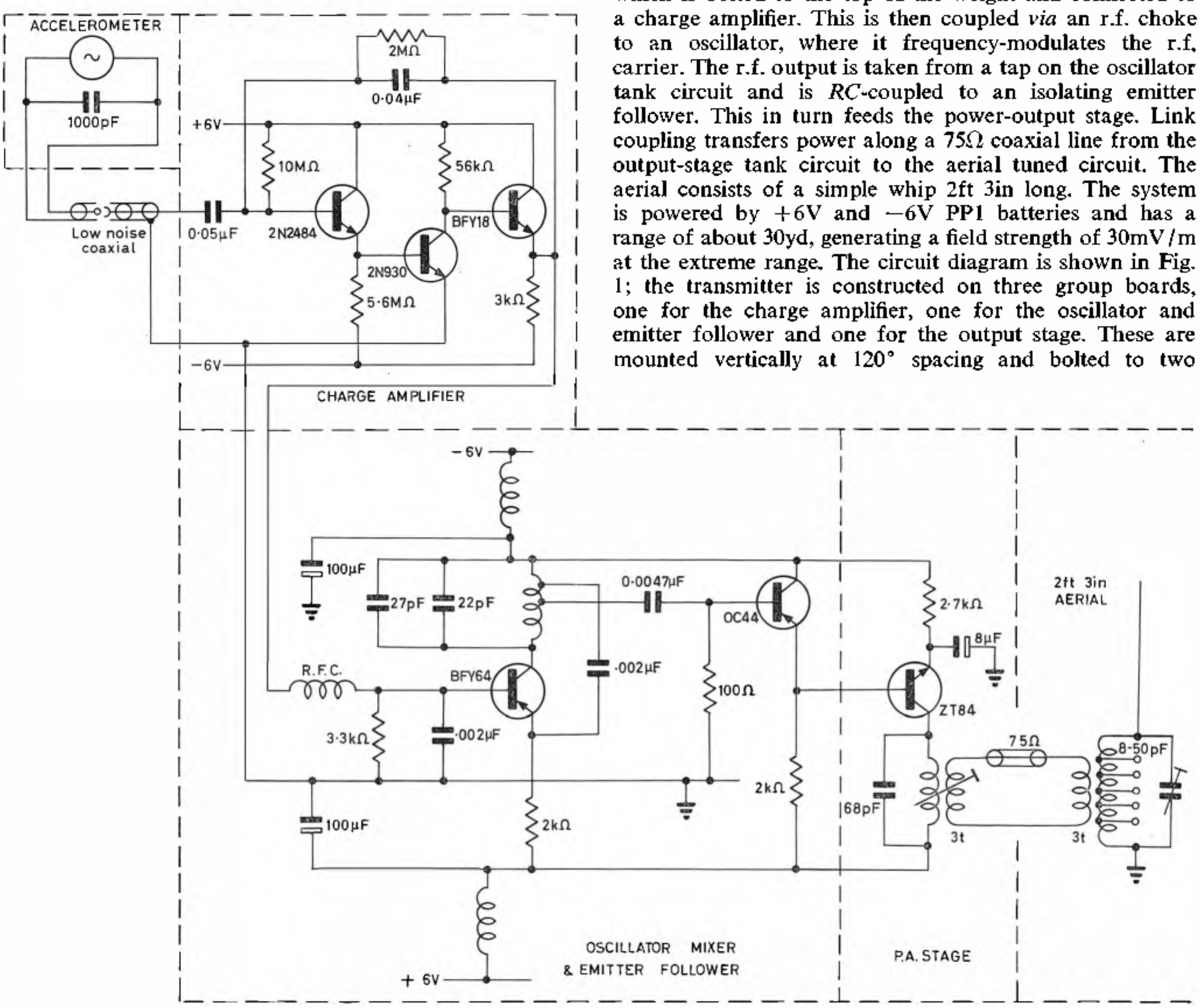

Construction

The system consists of two parts: a transmitter and a receiver. The transmitter system consists of a piezolectric accelerometer (B & K type-4311 or Endevco type-2213) which is bolted to the top of the weight and connected to a charge amplifier. This is then coupled *via* an r.f. choke to an oscillator, where it frequency-modulates the r.f. carrier. The r.f. output is taken from a tap on the oscillator tank circuit and is *RC*-coupled to an isolating emitter follower. This in turn feeds the power-output stage. Link coupling transfers power along a 75Ω coaxial line from the output-stage tank circuit to the aerial tuned circuit. The aerial consists of a simple whip 2ft 3in long. The system is powered by +6V and −6V PP1 batteries and has a range of about 30yd, generating a field strength of 30mV/m at the extreme range. The circuit diagram is shown in Fig. 1; the transmitter is constructed on three group boards, one for the charge amplifier, one for the oscillator and emitter follower and one for the output stage. These are mounted vertically at 120° spacing and bolted to two

* British Aircraft Corporation (Operating) Ltd

circular Tufnol discs (Fig. 3). The aerial is made from ¼in-diameter steel tubing and is mounted vertically through the centre of the disks. The whole assembly is potted in aerated silicone rubber and forms a piston when mounted inside its supporting tube. It also contains the batteries, shock-mounted on pads of plastic foam. The tube, which is 3in-internal-diameter steel 2ft long, is attached to the top of the weight by bolting through two welded lugs. The transmitter assembly is positioned at the top of its mounting tube before each drop; so that it acts as a piston on impact and thus isolates the transmitter from large shocks which could cause detuning or damage.

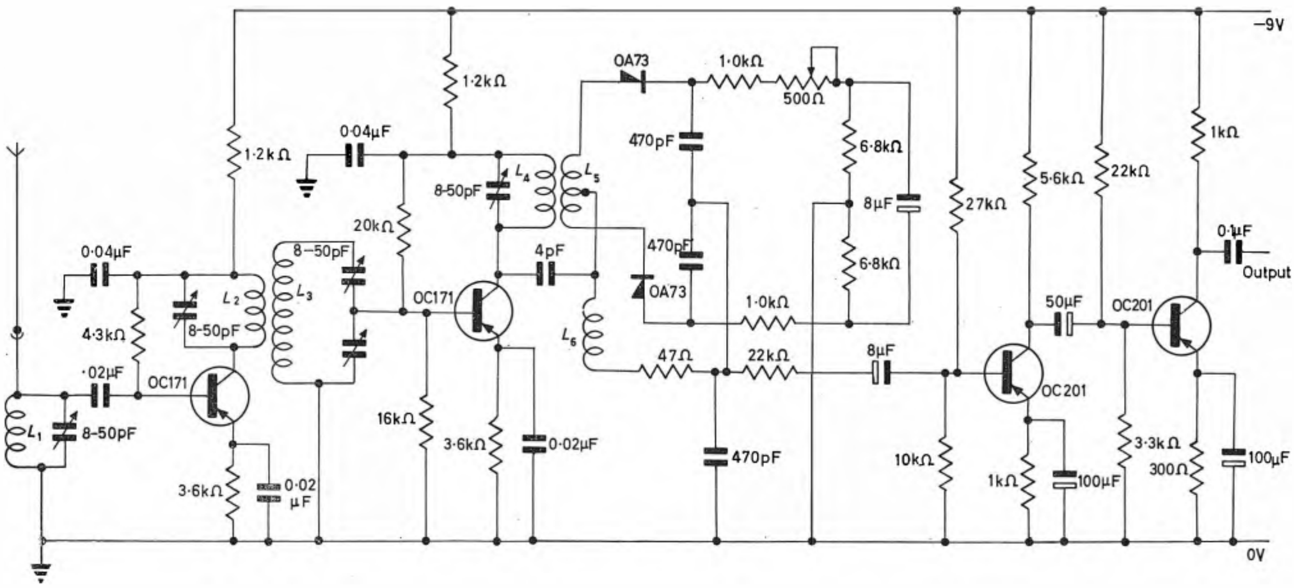

Fig. 2 Receiver circuit

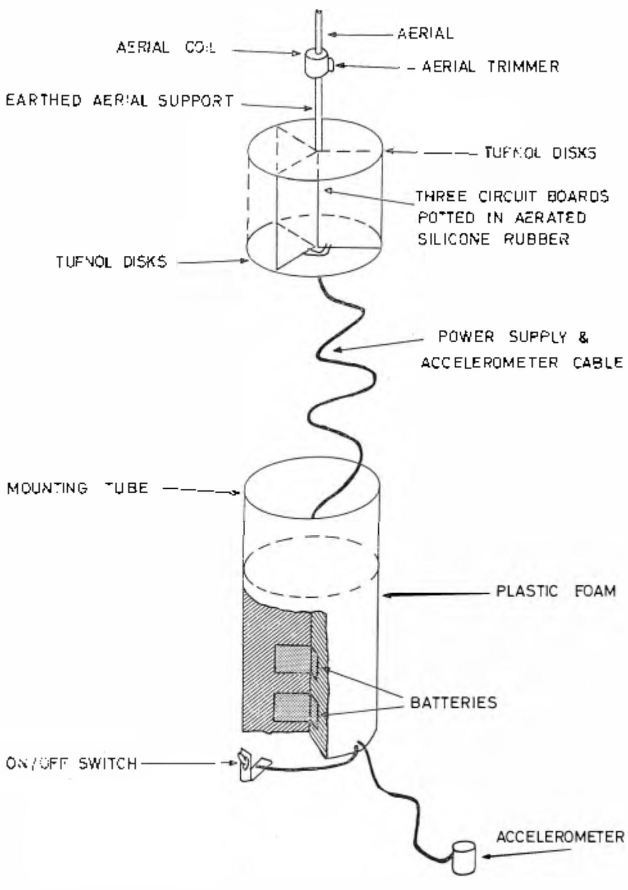

Fig. 3 Transmitter assembly

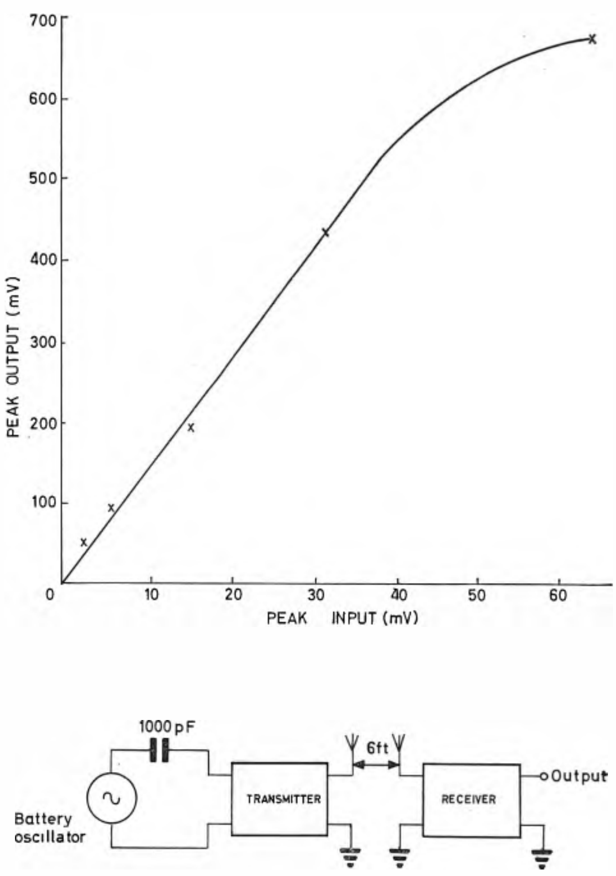

Fig. 4 System linearity measured at 1kHz

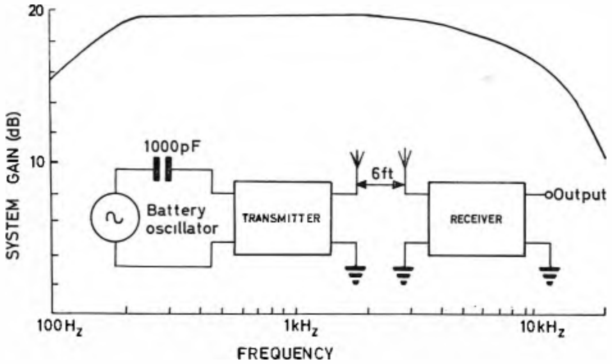

Fig. 5 System frequency response at 400mV peak output with a 1000pF capacitor in the charge amplifier

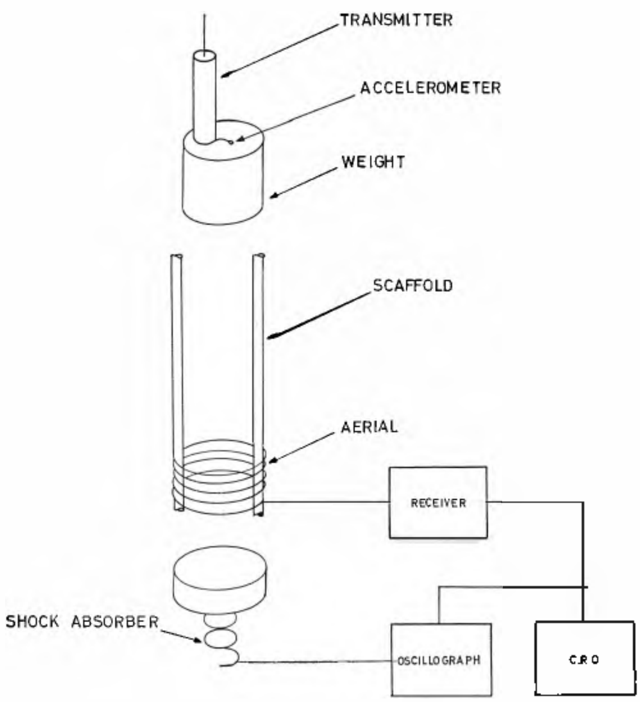

Fig. 6 Drop-test configuration

The receiver is a conventional t.r.f. set containing two stages of r.f. amplification, followed by a ratio detector and two stages of a.f. amplification; it is constructed on Veroboard which is mounted inside an aluminium chassis (Fig. 2). The aerial used for test purposes was a 6ft vertical wire, but this was unsatisfactory when mounted on the rig, because of severe screening by the earthed scaffolding. However, a frame aerial consisting of several turns of wire wound round the innermost scaffold proved satisfactory.

Performance

Bench tests were carried out at a 6ft range, where linearity and frequency response were measured using a battery-driven oscillator coupled through a 1000pF capacitor to the transmitter, which represents the accelerometer impedance. These tests showed that the system was linear to within 10% over a dynamic range of 40:1, representing a deviation of ± 27kHz. Frequency response was 3dB down at 130Hz and 11kHz, the low-frequency limitation being imposed by the a.c.-coupled a.f. amplifier in the receiver. The gain of the charge amplifier was finally adjusted by changing the feedback capacitor to $0{\cdot}05\mu$F before the rig tests were carried out, to cater for the expected maximum g. The results are shown in Figs. 4 and 5.

Drop-test procedure

The system was connected as shown in Fig. 6, which includes a force cell placed underneath the shock absorber to define the time of impact. The receiver and force-cell outputs were recorded on an oscillograph (Southern Instruments). Before raising the weight, the transmitter-aerial circuit was tuned by adjusting its trimmer while injecting a 1kHz signal into the system from the battery oscillator and monitoring the receiver output on an oscilloscope. This technique also gave the system gain and hence a calibration factor in mV/g when combined with the known accelerometer sensitivity. The oscillator was then disconnected and the accelerometer reconnected. The weight was raised to a predetermined height, the oscillograph chart motor was switched on and the weight-release mechanism was operated. A $\frac{1}{2}$V peak-to-peak squarewave from the oscilloscope CAL terminal was then connected to the recorder as a calibration signal. Finally the film was processed and analysed.

Results

Several drops were carried out; the first, from 30ft, showed weaknesses in mechanical mounting, namely sheared bolts, broken ON/OFF switch and cracked welds, which led to the revised design in Fig. 7. Subsequent drops from 8-9ft with the B&K accelerometer showed that the system functioned correctly, although some spurious signals were produced after impact by the lateral oscillations of the weight causing the aerial and mounting tube to collide with the scaffolding.

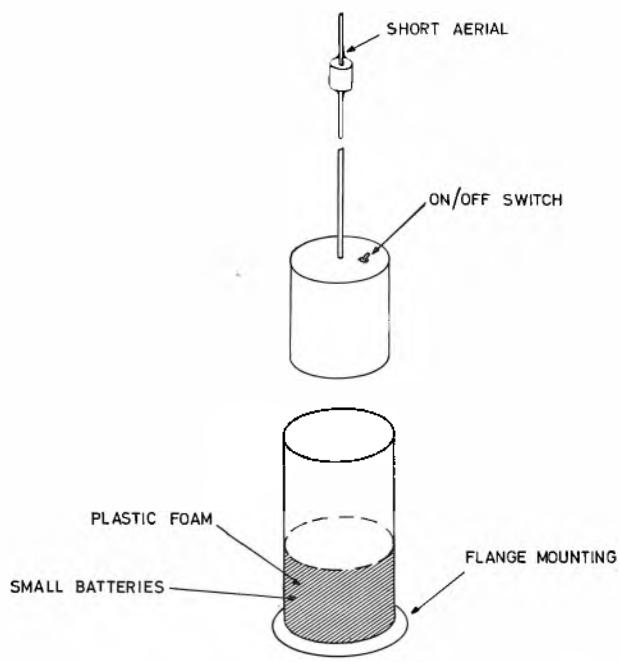

Fig. 7 Revised transmitter assembly

For future work, the aerial will be shortened and the weight should be restrained to prevent this effect.

Typical results are shown in Fig. 8, which indicates

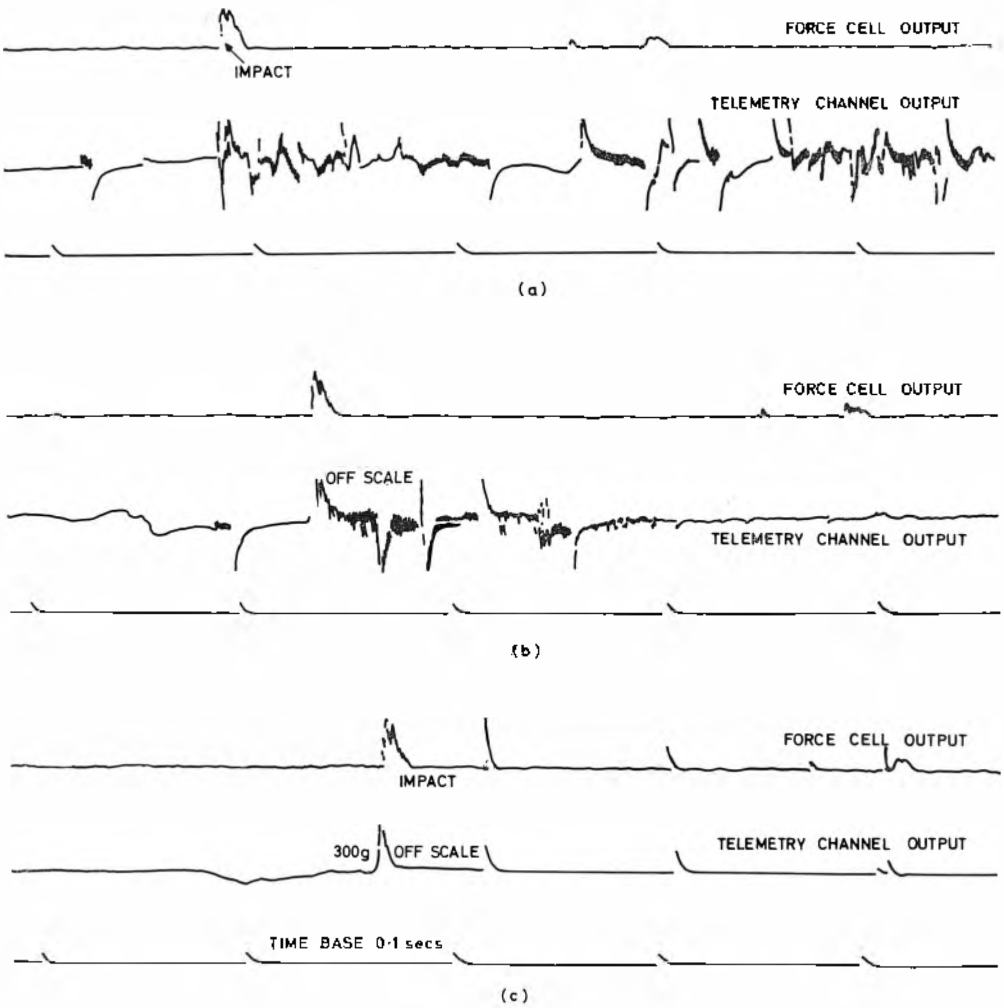

Fig. 8 Typical results

a 500g peak shock on impact which decays to zero in 90ms.

Conclusions

A shock-measuring telemetry system has been developed and demonstrated satisfactorily. Improvements in signal/noise ratio can be obtained if an accelerometer with low lateral sensitivity is used and if the weight is restrained laterally after impact. Multichannel operation is feasible by modifying the receiver to a superheterodyne configuration, and it should be possible to adapt the system for use with other types of transducer.

Electronic sketch-pad

How often has a designer wished that he could discuss a problem with a computer in terms of the problem itself and not in terms of computer 'language'? A new range of high-definition displays introduced by Marconi goes a long way towards realizing this ideal. The new 'electronic sketch-pad' is capable of presenting diagrammatic or graphical outputs from a computer, or tabulator information in written form. A 'light-pen' used directly on the face of a cathode-ray tube, in the same way as a pencil on paper, allows the 'sketch-pad' to be used as an input device for a computer, able to accept either original design sketches or modifications to displays already produced. In addition, tabular information can be fed into a computer from a standard typewriter keyboard and written out simultaneously on the display, the computer's replies being presented on the same display, as required.

The light-pen contains a tiny optical system with a very narrow angle of field, which can 'see' a point of light on the display. It transmits this through a flexible-fibre optical system to a photomultiplier tube, where it is converted into an electrical signal. This is fed into the computer, in which it can be related to the position of the original point of light on the display. If the pen is now moved across the tube face, its subsequent positions are traced by a spot of light moving through a 'search' pattern until impulses from the pen tell the computer that the spot has reached each new position of the pen. Each position is marked by a permanent trace on the tube face. All points on the trace will then be stored in co-ordinate form in the computer.

Two other input devices can be used: a rolling ball, where rolling of a ball across the screen is translated by pick-off devices into perpendicular co-ordinates, and touch wires, where touching any one of a matrix of tiny contacts mounted in a transparent mask on the screen produces a signal which is fed into a computer.

Extraction of signals from noise using digital techniques

by A. B. E. Ellis, A.M.I.E.R.E.*

An instrument is described which improves a noisy signal; the presence and approximate waveshape of a 10mV signal can be extracted from 100mV noise. The description has been treated from both circuit and operational aspects. Some applications are mentioned, notably in the fields of ionospheric research, ultrasonics, biomedical research and radioastronomy. Particular results in the field of ionospheric research are given. The approach adopted results in a compact unit capable of good performance.

(Voir page 597 pour le résumé en français: Zusammenfassung in deutscher Sprache auf Seite 598)

IN a number of applications, a requirement exists for extracting signals immersed in noise. The particular characteristics of the signal, e.g. frequency spectrum, repetition period or specific coding of information, may be used to provide the basis for an enhancement process. Several methods have been used to approach the problem, including visual integration[1], integration using delay-line techniques[2] and integration using digital techniques[3]. (Integration is used here to indicate a process of continual addition of information to that already held.) In this article an approach is made using the known repetition rate as the basis for improvement; this has wide applications in many radar-type systems.

Digital techniques are used, since these promise to give the most versatile system. The digital approach can cover a range of pulse-repetition frequencies (p.r.f.s) and resolutions by alteration of relative timing circuits, whereas those employing delay lines, for example, are tied to the electrical properties of time delay.

Basic approach

The basic system for postdetection digital integration is shown in Fig. 1. The noisy signal is converted to digital form and is then gated in time at the p.r.f. of the signal source. A count is made over a fixed time and recorded; the gate delay is progressively increased and the process repeated. The final record comprises a histogram of the counts at each delay. Whereas noise adds in a random manner, the presence of a signal introduces a statistical increase in the probability of a count.

This approach, however, is slow and cumbersome; in the device described, a count is taken in a number of consecutive range gates during one sweep. Further sweeps increase the accumulated totals. Two input methods may be used—one in which a direct analogue-to-digital conversion is made and one which simply provides a go/no-go decision based on whether the noise at the time of the decision is above or below a threshold. In the former method, a more precise reproduction of the signal may be made, particularly with respect to the linearity of the system. However, this requires more information than a simple go/no-go method and requires greater complexity for an equivalent improvement. Either method may be selected in the system to be described, in order to maintain optimum conditions. The encoded input would be used to improve a signal which is already comparatively clear of noise (e.g. an 8dB signal/noise ratio); the go/no-go or threshold method would be used for extracting signals well below noise.

The amount of information which can be integrated depends on the capabilities of the storage medium. In this

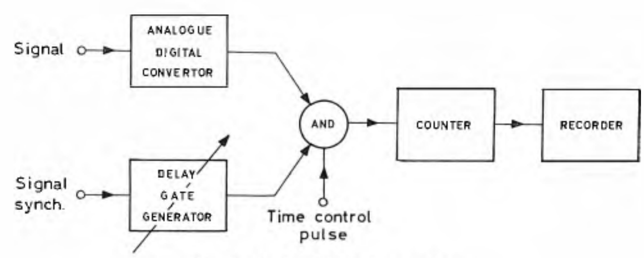

Fig. 1 Basic integrating system

case, to maintain flexibility, a magnetic-core store has been used. A finite top limit is therefore fixed by the store capacity. In order to prevent overfilling the store, two alternative approaches are made:

(a) the single-integration mode, in which the device switches itself off when the store is filled at any address

(b) the continuous-integration mode, in which the whole of the store content is divided by 2 when any address is filled, and the system then continues as before, enabling a running average to be made.

A facility is also provided to enable the store contents to be recycled without further integration; this enables the resulting waveform to be examined, photographed or read out for further processing. Micrologic circuits are used wherever they can be applied easily, although no attempt is made to take advantage of a smaller construction in this model.

Circuit operation

The operation of the circuit is as follows (referring to Fig. 2 and assuming that the system is reset to zero initially):

On pressing the START key, synchronising pulses (e.g. transmitter pulses) from the external-signal system are

* *The Marconi Co. Ltd, Chelmsford.*

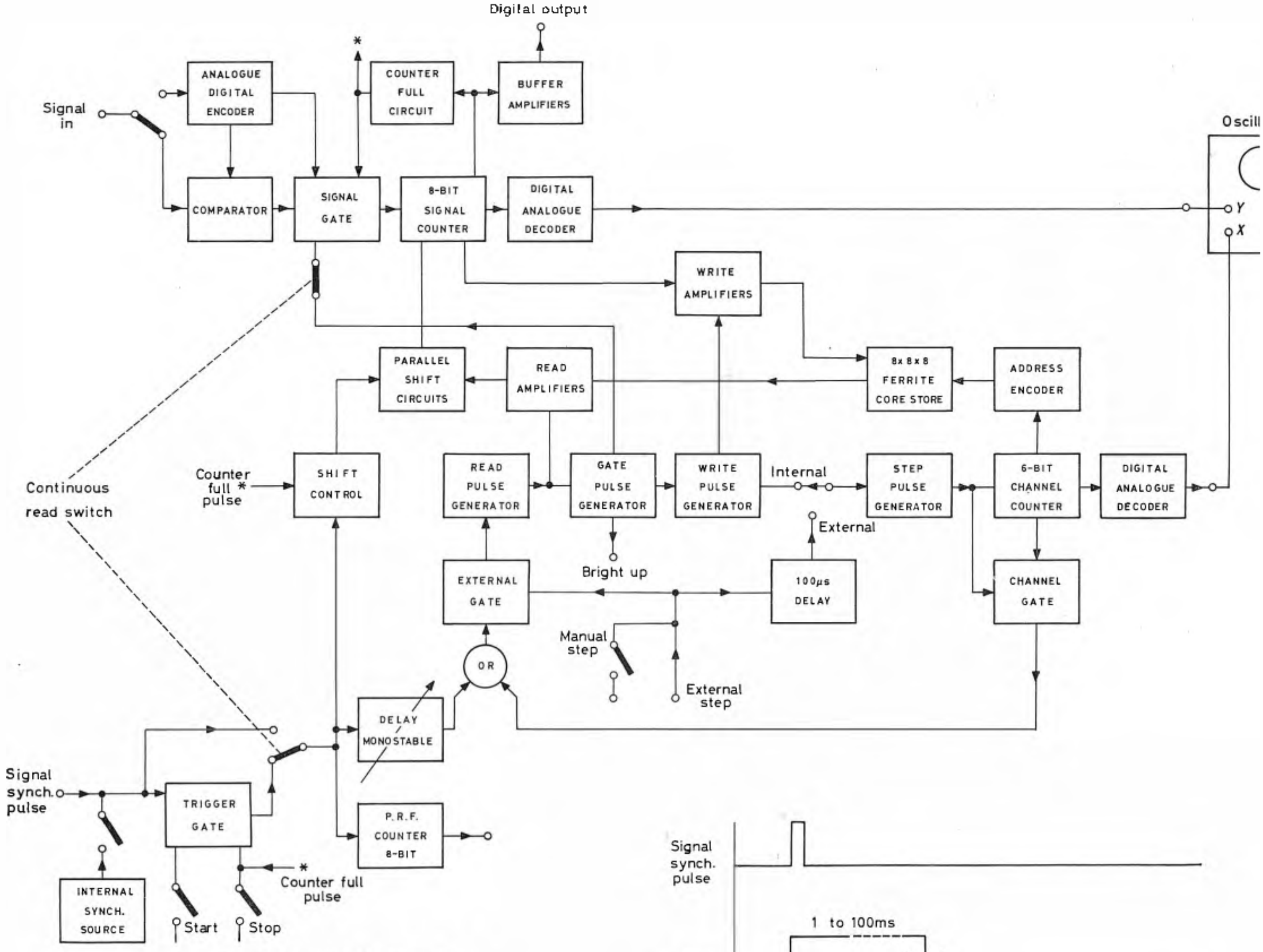

Fig. 2 Integrator block diagram

used to operate a coarse delay. In the present model, two ranges of coarse delay are provided—1-10 and 10-100ms. This delay enables a section of the system p.r.f. period to be selected by the operator. The trailing edge of the coarse-delay pulse is fed *via* the external gate to the read-pulse generator (r.p.g.). This edge now initiates a sequence of four pulses to control the READ, COUNT, WRITE and STEP functions of the equipment (Fig. 3).

The function of these pulse generators is as follows: the READ pulse (3μs) causes stored information from the first address to be read into the signal counter (during the first p.r.f. period this will be zero, as the store would have been cleared). The gate pulse (91μs) opens the signal gate. In the threshold condition, signals are compared with a manually set threshold voltage in a comparator. Signals (comprising noise pulses) exceeding the set threshold are sharpened and limited to trigger the signal counter *via* the signal gate. The signal counter records the number of counts in the gate-pulse period. If a number has already been set into the counter from the store, counts during the signal gate are added to this number.

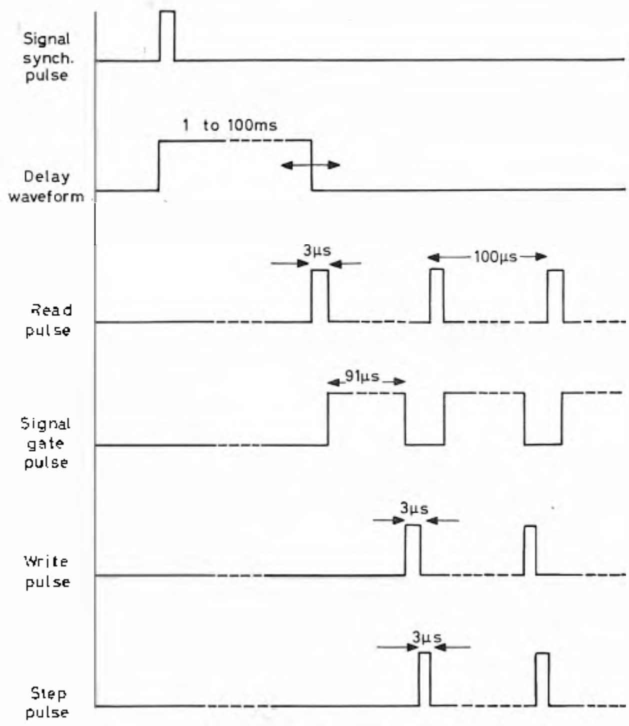

Fig. 3 Timing waveforms

The WRITE pulse (3μs) now causes the new number in the counter to be written into the same store address. The STEP pulse (3μs) triggers the channel counter, advancing it by one count; this changes the store address to the next in sequence. The channel gate is opened after the first address, allowing the STEP pulse to retrigger the r.p.g. *via* the external gate. Thus an active time of 91μs with a store process time of 9μs provides a 91% coverage of the signal. The input-signal bandwidth is of the order 5kHz, ensuring that no information is lost during the process time. The sequence described now repeats on the second address, continuing until the channel counter has selected each of the 64 addresses in turn, and returns to the first address. This condition closes the channel gate and prevents further recycling until another coarse-delay pulse is generated in the next p.r.f. period.

The channel counter provides two 3 bit outputs, which are decoded to provide the required 8 × 8-line address matrix for the store. The channel counter is also decoded to provide x-shift for an oscilloscope display. In the mode described, the output comprises a staircase waveform of 64 × 100μs steps (6·4ms). The signal counter is similarly decoded to provide a y-deflection for the oscilloscope; the oscilloscope is brightened by the gate pulse. The signal counter also provides an 8bit binary output *via* buffers, for use in recording data on to paper or magnetic tape for subsequent processing or storage.

The alternative input to the threshold mode is the encoder mode, in which the input amplitude is converted to an equivalent binary number. The method used is by comparison of the signal with a sawtooth waveform, by counting clock pulses from a fixed start until the sawtooth exceeds the signal. The amplitude is now converted to time and the time is in turn converted to a number of clock pulses, which are counted to provide a binary number equivalent to the analogue amplitude. This approach was chosen since three of the main circuits were already in existence, i.e. comparator, gate and counter. Only the clock-pulse generator and sawtooth generator are required to provide the encode facility.

In order to make maximum use of the store capacity, the integrating process is controlled by the signal counter. A COUNTER FULL circuit senses when the counter registers a full count. In the single-integration mode, this COUNTER FULL signal inhibits the synchronising pulses, preventing further triggering of the coarse delay, stopping the process after completion of the store cycle. In the continuous-integration mode, a COUNTER FULL signal is remembered by a shift-control circuit which causes a parallel shift operation to shift each digit read out of the store to the next least significant place, thus effectively dividing the readout by 2. This is maintained over one p.r.f. period, dividing the whole of the store contents by 2. The COUNTER FULL signal now disappears and the shift control reverts to normal READ, until the signal counter again registers full, when the operation is repeated.

The result is a picture which continually builds to a peak, halves and rebuilds to a peak, until the process is terminated. This process does not in itself improve the output signal continually, owing to the reduced weight of the divided signal when further normally weighted counts are added; however, it does prolong the integration and allow the process to be studied visually.

In order to freeze the integration process for display and examination of the result, a CONTINUOUS READ switch is incorporated. This closes the signal gate, preventing further additions of signal counts, and at the same time recycles the store continuously, using the trigger pulse bypassing the trigger gate. This facility can be used for any mode of operation.

Integration of a signal with respect to range or time is not always required, and provision is made to operate the channel counter by an external or manual stepping signal. In this mode, the feedback system of the step pulse to retrigger the r.p.g. is broken, enabling only one READ-GATE-WRITE sequence for each input trigger pulse, this sequence occurring at the coarse-delay trailing edge.

The step-pulse generator is now triggered from a manual or external signal *via* a 100μs delay. At the same instant, a 150μs external gate is produced, preventing a coarse-delay trigger reaching the r.p.g. This prevents spurious operation of the system.

A simple p.r.f. generator may be switched in in place of the external-trigger source, to provide an internal-trigger source for test or operational purposes. The threshold control may be set to such a position that, with no signal input, the comparator is set to a d.c. condition, rendering a continuous output which is equivalent to a large signal input. This results in a continuous increase in all store addresses, and the display exhibits a uniformly rising horizontal line. Faulty operation of individual addresses is readily seen.

A STOP switch resets all bistables to zero. A second position on this switch enables the signal counter to be set and held at zero, to enable a complete cycle of 64 addresses to clear the store contents to zero. The store can be operated in such a way that, when power is removed from the equipment, stored information is not destroyed.

Circuit description

The system is divided into the following subsystems (Fig. 2):

(i) Signal-counting chain

(ii) Timing circuits

(iii) Core store and ancillary circuits

(iv) Control requirements and p.r.f. counter

Signal-counting chain

The input circuits are shown in block form in Fig. 4. The input signal is fed *via* a gain control to one input of a comparator. Two modes are possible:

(a) Threshold mode

(b) Encoder mode

In the threshold mode, a direct current is fed *via* a multiturn threshold potentiometer and switch to the other input of the comparator. When the input signal exceeds this threshold, a negative pulse appears at the comparator output. This pulse is fed to an AND gate to provide an output when a signal gate pulse is present. This output is used to operate an 8bit counter. Thus noise pulses exceeding the threshold within the signal gate pulse are counted to provide a signal. These counts are subsequently stored and reused in the following p.r.f. period.

In the encoder mode, an 80μs sawtooth is fed to the comparator in place of the threshold voltage. This sawtooth occurs within the signal gate and runs from a positive voltage down to earth. The sawtooth operates once for each address. When the sawtooth falls below the level of the incoming signal, the comparator produces a pulse whose duration is proportional to the signal amplitude. This pulse is used to operate the AND gate, which now has clock pulses at 800kHz fed to its second input in place of the signal gate pulse. The number of clock pulses passed to the counter will depend on the duration of the comparator output, and hence on the input-signal amplitude. The values are chosen to provide a nominal 6bit encode accuracy (i.e. 1·5%).

The eight outputs from the signal counter are used to operate an 8-input AND gate, to provide an output when all inputs are present (i.e. when the counter is at 11 111 111). This is the COUNTER FULL signal which is fed as a

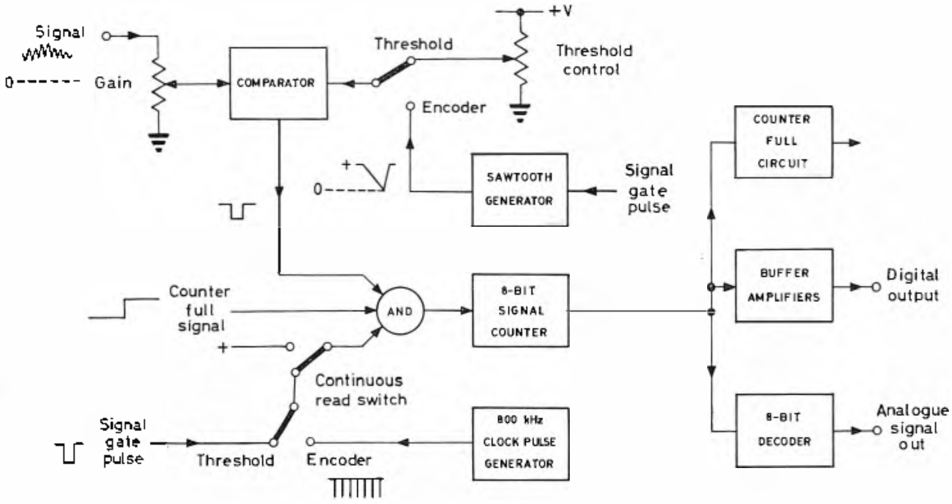

Fig. 4. Input circuits

third input to the comparator AND gate. This prevents further pulses reaching the counter when the COUNTER FULL pulse is present, thus preventing recycling of the signal counter. The COUNTER FULL signal is also used in the control circuits described later.

The signal-counter output is fed *via* buffers for external use and is also decoded to provide an analogue output for the display oscilloscope. The decoder is an 8bit current-switched operational amplifier.

When it is required to staticize the information in the store, the signal gate is rendered inoperative by the CONTINUOUS READ switch, preventing further counting by the signal counter. At the same time, the incoming synchronising pulse is fed directly to the coarse-delay monostable, initiating a normal READ-WRITE-STEP sequence for each address, and thus recycling and displaying the stored information.

Timing circuits

The pulse-timing circuits are shown in Fig. 5. In the initial state, the channel counter is reset to 000 000 and the 7-input AND gate associated with it is in such a condition to inhibit the step pulse fed to it.

The gated trigger initiates a delay monostable which may provide a delay from 1 to 100ms, using a continuous control and two switched ranges. The trailing edge of the delay pulse is used to trigger a 3μs READ-pulse generator, *via* the external AND gate. The trailing edge of this pulse is used to trigger a SIGNAL-gate-pulse generator (91μs) from which the trailing edge triggers a WRITE-pulse generator (3μs) and finally the trailing edge of the WRITE-pulse triggers a step-pulse generator (3μs). Thus from the delay-monostable edge, a consecutive series of pulses is generated to control the system in a READ-COUNT-WRITE-STEP sequence, the timing of which is shown in Fig. 3.

The leading edge of the step pulse triggers the channel counter, causing the store-address code to be advanced one position. As the counter is now no longer in the 000 000 condition, its AND gate no longer inhibits the step pulse and the trailing edge is fed back to retrigger the r.p.g. This causes a continuation of the READ-COUNT-WRITE-STEP sequence for each address of the store.

After the final store address has been cycled, the step pulse reverts the channel counter to 000 000 and inhibits the step-pulse trailing edge, breaking the feedback path. The system now remains at rest until the next p.r.f. period, in which a new delay pulse is generated to start a new address sequence.

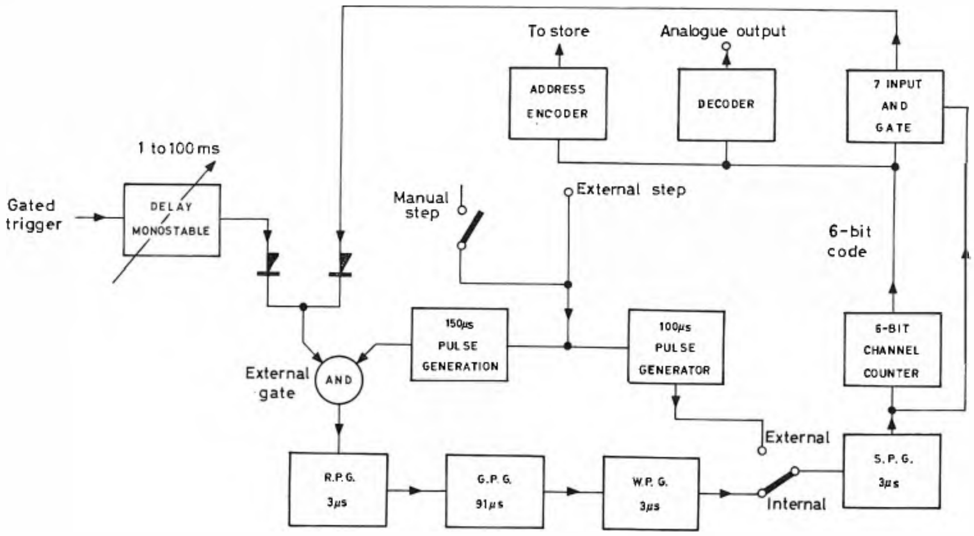

Fig. 5 Timing circuits

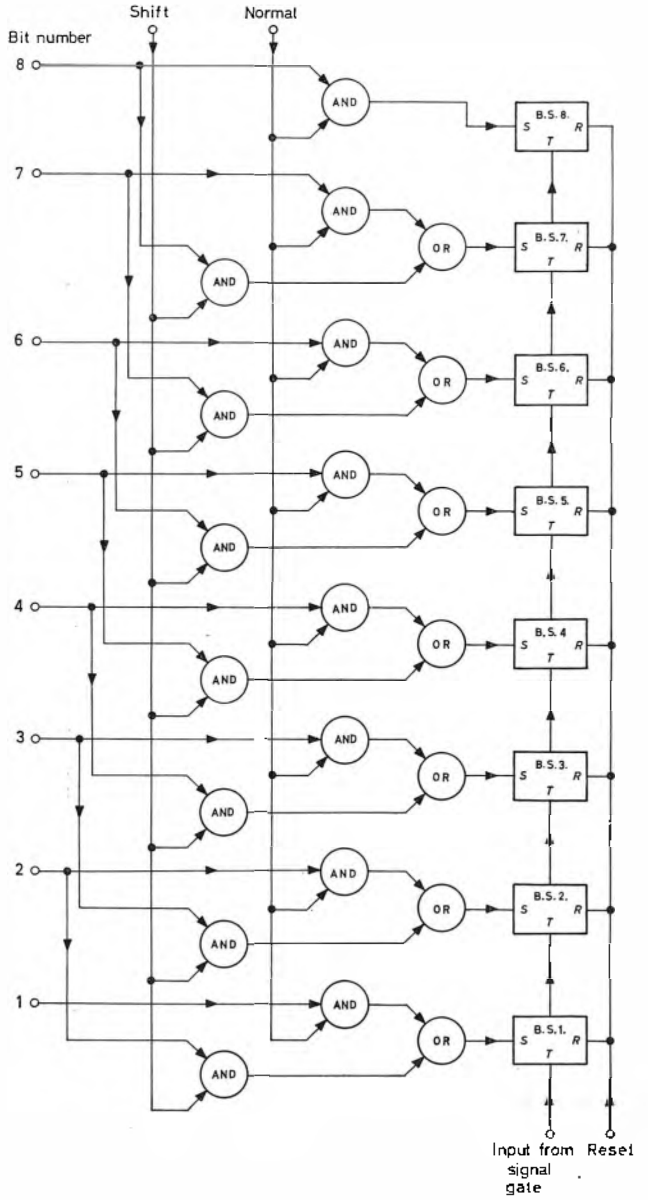

Fig. 6 Parallel shift circuit

In the event of an external or manual stepping mode, the s.p.g. is triggered from the external or manual sources, and there is no feedback. Thus a single READ-COUNT-WRITE cycle is initiated once only in each p.r.f. period.

As the manual or external step source is no longer synchronised to the p.r.f., precautions must be taken to prevent a step occurring during a READ-COUNT-WRITE cycle. This is done by two monostables triggered by the step source. A 150μs monostable inhibits any delay monostable edge for this period while a 100μs monostable triggers the s.p.g. from its trailing edge. Thus triggering of the READ-COUNT-WRITE sequence is prevented while a step is being carried out and the step is not actually carried out until after a delay of 100μs, to enable the READ-COUNT-WRITE circuits (97μs) to clear any sequence which may have been started just before the step initiation.

The output of the channel counter is fed to a digital-to-analogue converter to provide a horizontal output to the display oscilloscope. It is also used to provide the 64 x-y address codes.

Core store and ancillary circuits

The core-drive circuits and READ amplifiers are conventional and will not be elaborated. The address system uses an 8 × 8 matrix supplied by two sets of 3bit information from the 6bit channel counter. Provision is made to read the contents of any selected store address into the 8bit signal counter in parallel form during the READ pulse. Counter information is written into the store during the write pulse.

In the continuous-integration mode, it is required to halve the contents of each store address for one p.r.f. period only. A control signal for this purpose is generated in the control circuits described later. The control signal is used to route each of the 8bit READ amplifiers to set the next least significant bistable, the least significant bit being lost. A simplified logic diagram for this purpose is shown in Fig. 6. The store may be cleared before use by initiating a complete store cycle while maintaining the signal counter in a reset condition.

Control circuits

The main control circuits are shown in simplified form in Fig. 7. Incoming p.r.f. synchronizing pulses are fed to an AND gate which is controlled by an ON/OFF bistable. This bistable BS_1 can be set or reset by START and STOP switches or pulses. In addition, on single integration, the COUNTER FULL signal is used to trigger the bistable off. This prevents further cycles after completion of the current period. The AND gate supplies pulses to the delay monostable to initiate the timing sequence. Provision is made to override the AND gate when in the continuous-read mode.

In the continuous-integration mode, it is required to generate the shift-control signal previously referred to. The COUNTER FULL signal is fed to a memory bistable BS_2 which is set. The output of the bistable opens an AND gate, allowing the next p.r.f. sychronizing pulse to pass, triggering the period bistable BS_3 to the set condition. The second p.r.f. pulse toggles BS_3 to the reset condition, which in turn also toggles BS_2 to the reset condition, closing the AND gate and preventing further operation until another COUNTER FULL signal is received.

Thus BS_3 provides an output pulse for one p.r.f. period only immediately following the period in which a full-store position was noted. This output is used to divide all information read from the store during that period by 2 (Fig. 6). Provision is made to manually reset the bistables.

A further 8bit counter has been included as an additional facility. This counter counts the p.r.f. pulses and

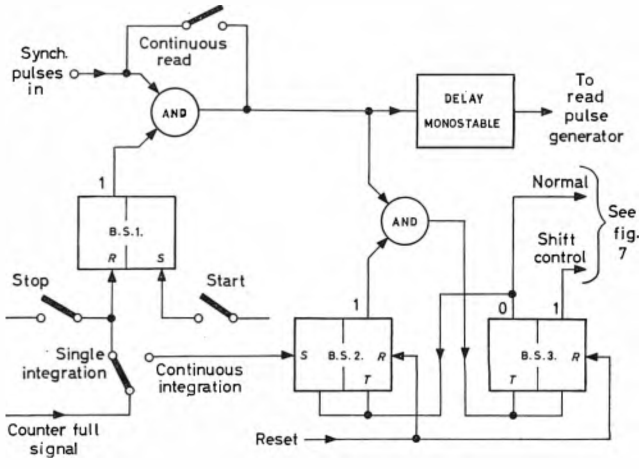

Fig. 7 Control circuits

enables the integrator to be controlled, i.e. switched off or stepped after a preset number of p.r.f. periods. This mode was used when operating on angle information described later.

Evaluation

A test circuit was constructed in order to evaluate the performance of the equipment. The test waveform comprised a single cycle at 330Hz after full-wave rectification; the p.r.f. was approximately 30Hz. Photographs of the test waveform, together with typical reproductions after integration, are shown in Fig. 8.

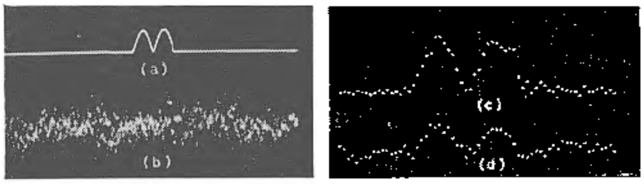

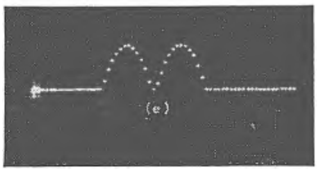

Fig. 8 Test result
(a) Test signal (enlarged)
(b) Test signal plus noise
(c) Integration result; 100mV p-p noise, 10mV p signal
(d) Integration result; 100mV p-p noise, 5mV p signal
(e) Encoded output of test signal only

In order to provide some measure of the improvement obtained, the following simple experiment was conducted. A 10mV peak test signal was immersed in 100mV peak-to-peak noise (10mV r.m.s.). Ten single integrations were carried out and these were superimposed on a storage oscilloscope. This resulted in a band of random counts from which a signal was clearly seen. On the second beam, the input signal to the integrator was displayed, and the gain adjusted until the band of noise at the input, when averaged over a short period (a few seconds), was equal to the stored noise band. The cusp signal amplitude was now increased until the peak amplitude equalled that of the stored picture. The resulting input was stored to provide two equivalent pictures. The new cusp amplitude was noted and the increase gave the effective improvement due to integration.

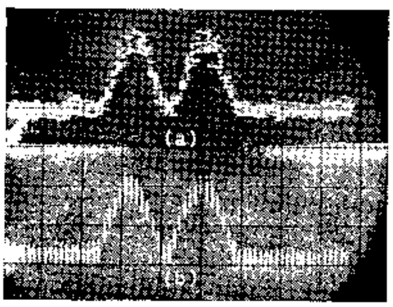

Fig. 9 Calibration result
(a) Stored picture of ten single integrations of input signal
(b) Stored picture of input signal plus noise, with signal amplitude increased 20 times

In this method, the d.c. (mean noise level) resulting from the integration was ignored, but as no d.c. was present at the input this was considered justifiable. A photograph of the result is shown in Fig. 9, in which the test signal was increased by 20 times in Fig. 9(b). This is equivalent to stating that, in order to obtain a similar apparent signal/noise ratio, the signal amplitude must be increased 20 times.

Operation

One application requires measurement of time and vertical angle to be carried out on returns from an h.f. backscatter sounder, for ionospheric research. The sounder transmits a pulse of energy in the h.f. band which follows a path *via* the ionosphere to a distant ground point. Most of the energy is reflected on forming a second hop. However, a little is returned as backscatter and may retrace the outward path of the pulse to provide a signal at the receiver. In order to carry out measurements, an aerial system having low sensitivity has to be used. Fig. 10 shows typical backscatter signals received

(a) on a high-gain aerial array (horizontal scale 2ms/division)

(b) on a low-gain measuring array.

The result of integrating (b) between the range limits shown by the dotted line is shown in (c).

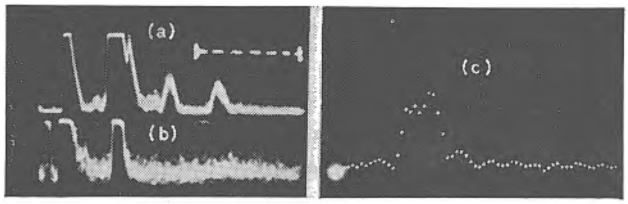

Fig. 10 Backscatter integration
(a) High-gain-aerial reception showing limits of integration
(b) Low-gain-aerial reception
(c) Integration of (b) between the limits shown in (a)

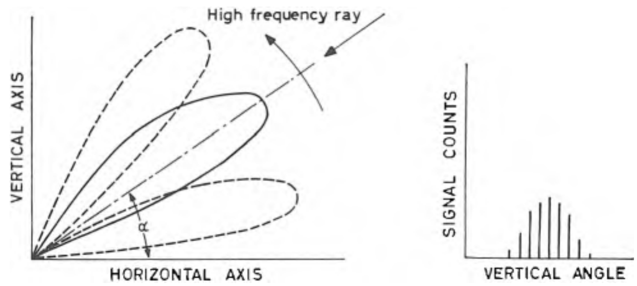

Fig. 11 Angle-measurement method

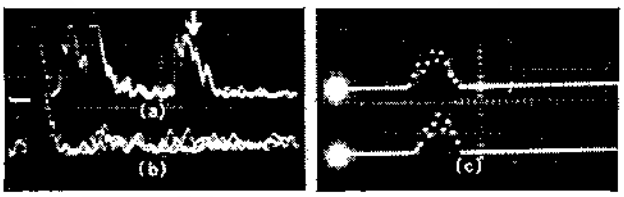

Fig. 12 Angle integration
(a) High-gain-aerial reception showing limits of integration
(b) Low-gain-aerial reception
(c) Two integrations of (b) in vertical angle at range as in (a)

A further application has been made in which a lobe pattern is switched through a series of vertical angles. Integration is carried out on each angle and an indication is given of the angle receiving maximum energy. A schematic drawing of this is shown in Fig. 11 and a typical photograph of the results obtained on a signal is shown in Fig. 12, in which (a) shows the reception on a high-gain array, (b) shows reception on the measuring array and (c) the result of several integration runs on (b) at the range indicated by the arrow.

The procedure for obtaining angle integration makes use of a fixed-range gate and the address change of the inte-

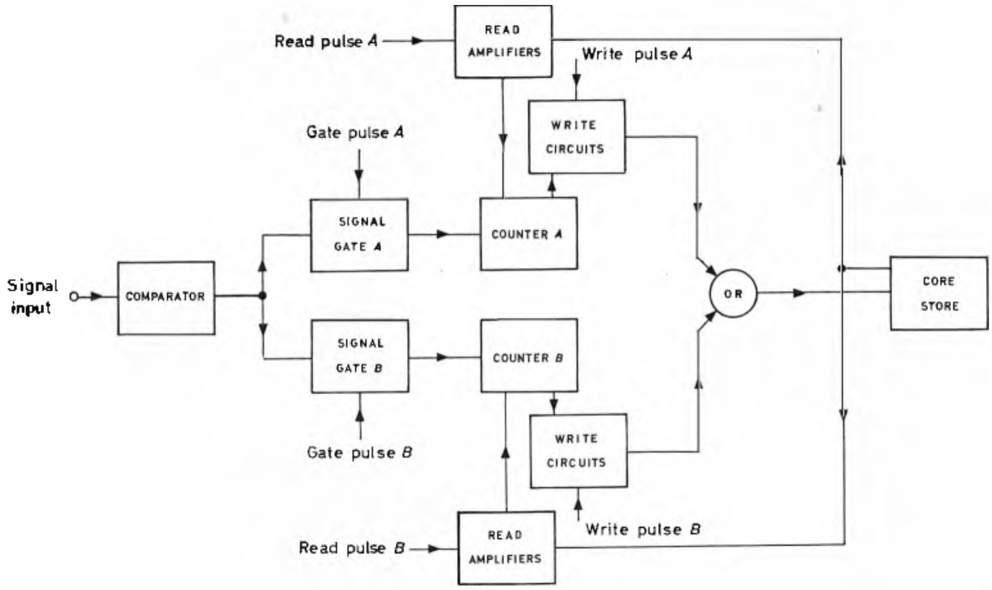

Fig. 13 Time-sharing system

grator is accomplished by the external-step mode of operation. Thus the horizontal scale in Fig. 12(c) is in terms of vertical angle.

Alternative uses

It is felt that such a device should have wider application than those already mentioned. The technique has already been used in more complex radar systems, but some other fields which this particular device might benefit are those of underwater echo-sounding systems, including fish-locating equipment, ultrasonics and seismology, in which controlled explosions are used to generate shock waves. The field of radio astronomy may well offer some application and the use of the equipment in medical research in which a stimulus is applied and a response is to be measured.

The above fields involve a wide range of p.r.f.s and resolution requirements. However the integrating device described is readily adaptable to a wide range in these parameters. Circuits which are affected are the delay circuit and the delay circuit and gate-pulse generator. The delay circuit is required to cover the range of interest within the p.r.f. period, the gate-pulse generator determines the resolution of the system and the width of the 64 channels. These two factors are interdependent, and it is possible to trade one for the other. Further addresses could be added to cover a wider range or provide greater resolution than the 1 in 64 of the present system.

In view of the method of storage, there is no reason why the p.r.f. period should not extend over days or weeks if required. Typical extremes of specification could be

from: p.r.f. 0·1 per s, 10s period;

delay up to one period;

gate-pulse width 100ms, giving a total range of 6·4s for 64 channels.

to: p.r.f. 500 per s, 2ms period;

delay up to 1ms;

gate-pulse width 10μs (plus approximately 10μs for READ-WRITE-STEP sequence), giving a total range of 1·28ms (64 × 20μs) for 64 channels.

Usefulness at lower p.r.f.s is governed by the stability of the delay device.

The usefulness at high p.r.f.s is ultimately governed by the store cycle which could be made much faster than the present 10μs. An alternative to this, however, is shown schematically in Fig. 13, and is basically a time-sharing facility in which the incoming signal is switched between two counters, these may feed a common-store system, allowing one counter to count while the other counter store carries out the READ-WRITE-STEP cycle. This enables almost 100% of the incoming signal to be processed.

Conclusion

A system has been described which makes use of up-dated radar-type techniques in which an improvement of signal/noise ratio may be achieved with repetitive waveforms. Some unusual innovations contribute to a useful tool for a wide range of research activities, as well as providing a useful ancillary to commercial fields, including ionospheric prediction and echo sounding. Some results for ionospheric data measurement are given. Suggestions for further improvement are made. The basic device is versatile and may be used over a wide range of p.r.f. and timing conditions.

Acknowledgment

The author wishes to thank the Director of Engineering, The Marconi Co. Ltd, and the Ministry of Aviation (for whom the work on the equipment was carried out) for permission to publish this article.

REFERENCES

1 Tucker, D. G.: Detection of Pulse Signals in Noise. *J. Brit. Inst. Radio Engrs. 17*, 6, 319 (June 1957).
2 Cooper, D. C., Griffiths, J. W. R.: Video Integration in Radar and Sonar Systems. *ibid., 21*, 5, 421 (May 1961).
3 Dimson, G. P., Reed, I. S.: An Analysis of Signal Detection and Location by Digital Methods. *IRE Trans. IT-2*, 29 (March 1956).
4 Griffiths, J. W. R.: Visibility of Pulse Signals in Noise. *J. Brit. Inst. Radio Engrs. 17*, 6, 330 (June 1957).
5 Hideo Seki: Some Studies on Delayed Feedback Circuits. *Proc. Inst. Radio Engrs. 46*, 4, 758 (April 1958).
6 Tucker, D. G., Griffiths, J. W. R.: Detection of Pulse Signals in Noise. *Wireless Eng. 32*, 11, 290 (Nov. 1955).
7 Kaplan, E.: Signal Detection Studies with Applications. *Bell Syst. Tech. J., 34*, 2, 403 (March 1955).
8 Tucker, D. G.: Signal-to-Noise Performance of Multiplier and Addition Types of Detector. *Proc. IEE, 102B*, 558 (1955).
9 Marcum, J. I., Swerling, P.: Studies of Target Detection by Pulsed Radar. *IRE Trans. IT-6*, 2 (April 1960).
10 Harrington, J .V.: An Analysis of the Detection of Repeated Signals in Noise by Binary Integration. *ibid. IT-1*, 1 1 (March 1955).
11 Harrington, J. V.: Signal-to-Noise Improvement Through Integration in a Storage Tube. *Proc. Inst. Radio Engrs. 38*, 10, 1197 (Oct. 1950).
12 Raether, M., Bitzer, D.: Polarity Coincidence Detector for the Measurement of Very Small Signal-to-Noise Ratios. *Rev. Sci. Instrum. 35*. 837 (July 1964).
13 Kjell Mellberg: Digitrac Video Correlator for Binary Detection of Radar Targets. *Elect. Commun. I.T.T. 39*, 4, 481 (1964).

New shutdown amplifier (s.d.a.) for nuclear reactors

(Part 2)

by I. G. Morris*, Dip.El., C.Eng., M.I.E.R.E., A.M.I.C.E., A.M.I.Mech.E., M.I.E.E.

This second part discusses briefly some of the aspects considered during the design of the various circuit elements, in order to provide equipment with optimum fail-safe properties without impairing its operation or building in too many redundant components

ALL the individual circuits are oriented towards 'fail-to-safety' where each circuit is based on a chopper d.c. amplifier using internally stabilised a.c. amplifiers to define the overall d.c. gain. This technique eliminates the conventional overall d.c. feedback, which, although providing a more stable gain characteristic, introduces a larger risk of failing to danger. In general, however, the components define transistor d.c. operating conditions and, in the event of a component failure, the amplifier is biased off. This usually reduces the overall gain to zero and operates one or other of the trip circuits, i.e. 'fails safe'.

There are, however, two major problems with this general case, which are as follows:

(a) A short circuit between the base of the output chopper and earth converts the device to a diode, which is then capable of rectifying the output pulses to provide a signal differing very little in magnitude from the original, but not phase sensitive. This problem is 'designed out' on the trip boards by rectifying the signal at the base of the chopper to provide a collector supply for one of the amplifier transistors. Failure of this signal, due for example to a short circuit to earth, cuts off the supply to the amplifier transistor and substantially reduces the gain of the amplifier, i.e. it fails safe.

(b) Amplifiers requiring gain adjustment can fail in the dangerous direction by increasing gain. In amplifier *A*, this is owing to the necessity of a.c. coupling of the gain-defining networks. This coupling prevents faults in the feedback line from affecting the d.c. bias conditions. Adjustable feedback in the d.c. path places such restrictions on adjustment that the circuit becomes impracticable. Amplifier *B* has fixed gain, but adjustment of the output voltage is made by attenuating the input signal. In both cases where gain controls are employed, failures can be 'caught' by one of two trips, and are less likely to cause dangerous failures. In the third case—the zero-margin trip—the use of gain controls is avoided by using 'adjust on test' resistors to set the gain within a predetermined range. Failure of this fixed resistor is considerably less likely than failure of a variable resistor of the same function.

Overall circuit

The impracticability of making each board fail safe becomes apparent. However, with the circuits employed, the safety requirements of each amplifier and trip unit are followed to their practical limits. These individual circuits, when interconnected in the overall circuit, operate so that failures, dangerous on one trip, are safely 'caught' by one of the others.

Each circuit is assessed separately for open-circuit and short-circuit faults in each component, and these faults are graded according to their safeness as follows:

A Faults which give an immediate indication on either of the two main trips (z.m.t. and e.m.t.).

B Faults which give an immediate indication on one of the three subsidiary trips (a.z.m.t., a.e.m.t. or e.h.t./screen/reference-voltage trip).

C Faults which, though not immediately indicated, render the z.m.t. more sensitive (i.e. in a safe direction).

D Faults which give no indication of their presence but do not affect the accuracy to any appreciable extent.

E Faults which give no indication of their presence but reduce the sensitivity of trips other than the z.m.t.

F Faults which give no indication of their presence but degrade the operation of the main trip circuit (z.m.t.).

In order to place the various faults into categories, some assumptions must be made with regard to

(a) ion-chamber output for maximum reactor power

(b) the settings of the various trip levels in relation to the reactor power.

To estimate these values, typical parameters have been assumed in the following paragraphs. The ion-chamber output-current range that the circuit is at present catering for is 40 to 400μA for 2400MW power, which will, of course, be much reduced when the equipment is finally installed and the parameters of a particular system are known more accurately. The s.d.a. has a full-scale deflexion of 600MW, corresponding to input currents in the range 10 to 100μA. At 100μA, the gain of the circuit is very much reduced by feedback; failures such as open-circuit feedback therefore give large changes in gain and are safe; using a 10μA f.s.d. input, the safety factor is ten times lower. On the other hand, the gain of the circuit using a 10μA f.s.d. input is safer for short-circuit-feedback resistors, which reduce the gain to unity. To simplify the assessment, the worst cases have been considered and it has been assumed that, if satisfactory, the circuit will also be satisfactory when set up at the other extreme.

It is general practice to vary all the trip levels of the s.d.a. simultaneously, by employing a motorized ganged potentiometer, and typical levels considered are

(a) At levels below 200MW, the levels in relation to the s.d.a. scale are constant, preset within the following ranges:

z.m.t.	6MW ±2MW	a.e.m.t.	32 to 50MW
a.z.m.t.	6 to 23MW	e.m.t.	50 to 61MW
margin indicator	23 to 32MW		

(b) Above 200MW, the levels are preset ratios of the power level. Figures at 2000MW reactor power would give levels in relation to the s.d.a. scale in the following ranges:

* *Formerly with the Electronics Division of the Rank Organisation*

z.m.t. 6MW ±2MW a.e.m.t. 271 to 446MW
a.z.m.t. 6 to 181MW e.m.t. 446 to 556MW
margin indication 181 to 271MW

Examination of these lists shows that the levels at 2000MW impose the more stringent requirements. Assume, for example, that the reactor is running at the maximum level equal to 271MW margin on the s.d.a. To be detected, any loss of gain must take the reading below the lowest setting of the a.z.m.t. (i.e. 6MW). This requires a loss in gain by a factor exceeding 50 to be safe. Conversely, assuming that the reactor is running at 181MW margin, an increase in gain must take the level beyond 556MW to be safe, say, by a factor of 3.

It is possible for some faults to cause a fixed change in the level, e.g. zero drift. To ensure that these are detected in all cases by the a.z.m.t. or the a.e.m.t., these shifts must exceed ±265MW. Thus the categories previously quoted can be more accurately defined as follows:

A Z.M.T. gain falls by a factor of 50
or e.m.t. gain rises by a factor of 11
or reading shifts by more than −265MW or +375MW.
B A.Z.M.T. gain falls by a factor of 50
or a.e.m.t. gain rises by a factor of 3
or reading shifts by more than ±265MW.
C Z.M.T. gain falls by a factor of less than 50 and the change is not detected by the other trips; in general, this is safe, since the trip operates sooner than it ought.
D Covers all other cases where the sensitivities of the trips are not affected to any appreciable extent (e.g. z.m.t. still within 6MW ±2MW).
E Covers all other cases when the sensitivities of the trips, except the z.m.t., are degraded.
F Covers all other cases when the sensitivity of the z.m.t. is degraded.

These are the figures for gain change employed in the assessment and allocation of fault grades on the amplifiers and trip circuits. It should, however, be noted that trip settings as extreme as those quoted would be regarded as being very unusual; in most cases the trips will be set near to the centre of their range. With such ideal settings, category *C*, for example, would include all faults causing gain changes in excess of 3 instead of 50.

The figures applied to changes in the resistor network from which the reference current is derived (R_1, RV_1 and RV_2 of Fig. 1) are lower than those quoted. The reason for this can be seen from the following example: Assume that the reactor is running at 2000MW and giving an indication of 271MW margin. If the reference current equivalent to this level dropped by the equivalent of 265MW, the z.m.t. would operate. This is a change of only 13.3% compared with a factor of 50 in amplifier gain estimated under similar conditions. This percentage applies to a margin above 200MW, where the various levels vary in proportion to one another. However, below 200MW, the levels are fixed, and we find the worst conditions at shut down.

With the reactor shut down the input current is virtually zero and the reference current equivalent to powers between 23 and 32MW. At this level, any fault must cause the current to change by a factor of 6 to be safe.

On this basis, the faults in R_1, RV_1 and RV_2 are allocated grades comparable to those given above, and are

A Current falls by a factor of 6 or current rises by a factor of 3
B Current rises by a factor of 2 or reference voltage by 20%
C Current falls by a factor of less than 6
D Current remains unchanged
E Current rises by a factor of less than 2 or the reference voltage by less than 20%.

The wide range of input currents (40-400μA) is too great for the potentiometer RV_2 alone. The value of RV_2 is the maximum available in the range of wire-wound resistors, carbon resistors of higher values not being stable enough for this circuit. A resistor in series with either RV_1 or RV_2 tends to increase the number of fail-to-danger faults. To overcome this and still cover the required range, the circuit shown in Fig. 1 has been used. The diodes MR_1 and MR_2 incorporated are low-temperature-coefficient types. With the circuit as shown and RV_1 at maximum voltage, RV_2 can be set to give currents in the range 40 to 130μA. Should the current from the ionisation chamber lie in the range 75 to 400μA, the alternative circuit would be used. Here, MR_2 is omitted and R_1 is decreased to give the correct current through RV_1 and MR_1.

To cover the ranges specified, for all ranges of Zener-diode tolerances, RV_2 is used over the range of resistance 20 to 90kΩ. Employing the circuit described, assessment has shown that the full range of reference currents can be safely covered. The actual component values could probably be optimised to provide even greater safety if the range of input currents were known more accurately.

The result of a short circuit across MR_1 is to alter the trip-point stability by less than 1MW on the z.m.t. This is still within the 6 ±2MW required, and is acceptable.

Failure rates

These have been assessed by employing the figures for component failure listed in Table 1, which are applicable to transistorized equipment operating in similar conditions. These figures are, however, considered as somewhat pessimistic in some quarters; in which case, the picture here, while more than acceptable, could be painted even brighter.

TABLE 1

COMPONENTS		FAILURE RATE, % PER kh	
		o/c	s/c
Resistors,	metal oxide	0·008	0·002
	metal film	0·018	0·002
Variable resistors, per failure mode,			
	'flat pot'	0·01	0·01
	wire wound	0·02	0·02
	carbon track	0·04	0·04
	precision wire wound	0·05	0·05
Capacitors,	polystyrene film	0·005	0·005
	other synthetic films	0·025	0·025
	tantalum foil	0·05	0·05
	tantalum—sintered anode	0·005	0·005
Diodes,	germanium alloy	0·02	0·02
	silicon alloy	0·01	0·01
	silicon planar	0·001	0·001
Relays,	per winding	0·015	0·015
K3000,	per contact pair		
	per contact	0·005	0·01
Miniature,	per contact pair		
	per contact	0·1	0·2
Plugs and sockets, per open-circuit pin		0·02	

AMPLIFIER A

This amplifier feeds both the z.m.t. and the e.m.t. and is thus monitored for both rise and fall in sensitivity. The analysis given shows that none of the faults is fail-to-danger but that 11 faults are in categories *C* and *D*. These faults can, under certain running conditions, remain concealed indefinitely, or until some change in the operating conditions or a maintenance check reveals their existence.

The total failure rate of the amplifier is assessed as 0·51% per kh. Most of these faults will cause at least one of the four trips to operate, but a probability of 0·114% per kh will remain concealed (category *C* 0·08% per kh plus category *D* 0·034% per kh).

AMPLIFIER B

Amplifier *B* accepts the a.c. signal from amplifier *A*, amplifying it to the level required to feed the output meters (10V d.c. for f.s.d.); the same output also provides the input signal for the e.m.t., a.e.m.t. and a.z.m.t. As in amplifier *A*, amplifier *B* is monitored for an excessive fall in output signal by the e.m. and a.e.m. trips on the one hand and the a.z.m. trip on the other. Considerably more faults fall into category *E;* however, this is not fail-to-danger, since these faults have no direct effect on the prime trip circuit (the z.m.t.). On this basis, category *D* and *E* faults are combined under the heading of unrevealed faults (category *C* faults cannot occur).

The total failure rate is assessed at 0·75% per kh. However, a large proportion of these faults are in the unrevealed category: 0·337% per kh (0·08% *D* and 0·257% *E*). Most of these unrevealed faults occur in the output stage of the amplifier. The reason for this is that so much power and feedback have been built into this amplifier to achieve the required d.c. output with reasonable linearity that many faults merely introduce excessive nonlinearity (limiting). These faults, though causing incorrect output signals, do not generate sufficient change to guarantee detection by the trips.

AMPLIFIER *C* (Z.M.T.)

Since there is only one output, the circuit is monitored only for failure signals in one direction, i.e. reducing gain. This makes the circuit the most critical of the whole unit with respect to fail-safe design. The inclusion of normal gain controls to accommodate the anticipated range of component tolerances would introduce many possible fail-to-danger faults. To overcome this, the circuit has been designed using gain defined by fixed resistors. The size of input resistor that determines the gain is selected during test to eliminate most of the spread due to component tolerances. Final adjustment of gain for the complete z.m.t. signal is carried out by RV_1 of amplifier *A*.

If resistor R_{10} is short-circuited, the gain of the system is increased by approximately 15%. This is obviously in the dangerous direction but of a magnitude which is still well within the specified ±2MW stability figures quoted for the z.m.t.

If one assumes a perfect chopper d.c. amplifier, R_{10} can be considered redundant; but, unfortunately, some resistance is required in the circuit to limit current surges when the amplifier output and chopper drive signal are not exactly in phase. The value chosen for R_{10} is a compromise between the two conflicting requirements.

The trip circuit has only one output, which causes the output relay to de-energise on a falling signal. Faults which increase amplifier gain or prevent the relay de-energising are therefore dangerous. Two faults fall in the dangerous category:

(a) Short circuit of the input resistor: as with all the other resistors used in this circuit, this is a metal oxide type having an extremely low failure rate. The UKAEA at Risley has used 0·002% per kh, i.e. a probability of one failure every 5000 years.

(b) Short circuit of the relay contacts which are normally open circuit in the de-energised condition: the figure quoted for this type of fault is 0·2% per kh, i.e. a probability of one failure every 50 years.

The total failure probability is 1·1% per kh; of these faults, 0·202% per kh are fail-to-danger (category *F*) and 0·103 per kh are unrevealed faults which are in themselves not dangerous. The latter figure is made up of 0·096% per kh category-*C* faults and 0·007% per kh category-*D* faults.

AMPLIFIER D (STANDARD TRIP UNIT)

To overcome certain fail-to-danger faults in this circuit, which occur with modes of use, two types have been designed. To illustrate the faults that could occur, consider the trip board shown in Fig. 6—amplifier D_1. When operated correctly, the energised condition occurs with a negative d.c. signal across the input chopper. VT_1 is turned on by a negative-going signal which chops the d.c. signal to earth, i.e. a positive-going signal. From this, it is obvious that any condition which allows the chopper drive signal to reach the amplifier directly will cause a phase inversion

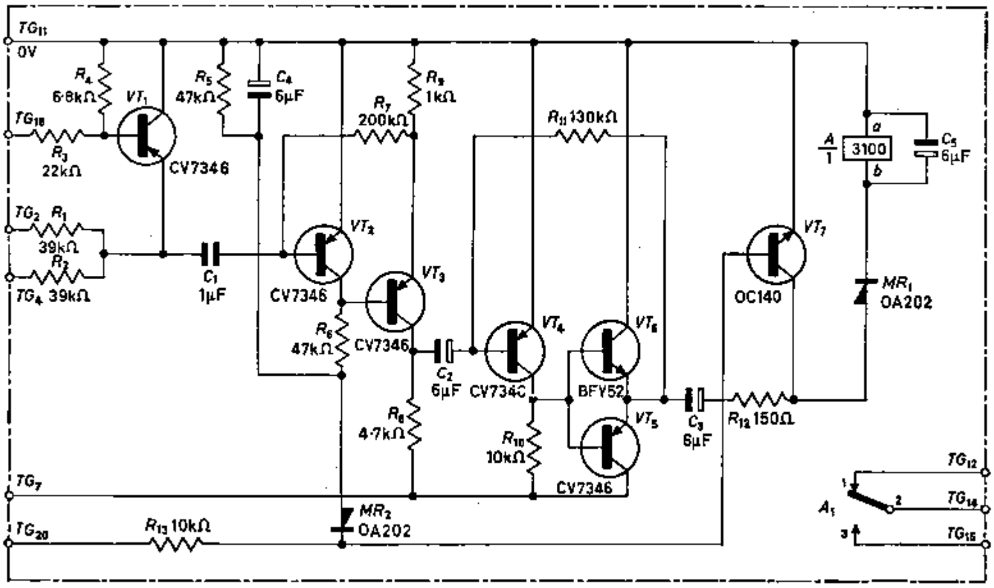

Fig. 6 Amplifier D_1 (trip board)

of the output signal. Under these conditions, the output chopper phase is incorrect and no rectified d.c. output is produced.

Contrasting this with the other case where the input is a positive d.c. signal, by changing the output phasing the circuit can be made to operate as efficiently as before as a d.c. chopper amplifier. However, the base-drive waveform and the amplifier input waveform are now in phase, and, should a base-emitter fault occur in VT_1, the signal to VT_2 will still be in the correct phase relation to the output chopper. As a result, the output relay will be continuously energised—a fail-to-danger condition. This fault has been corrected by the introduction of a second version of the trip board—amplifier D_2. The input chopper of this board is an *n-p-n* instead of a *p-n-p* transistor. The consequence of this is that the phase of the required input chopper drive is reversed and this circuit can therefore be used in all cases where the input to energise the relay must be positive. Between them, these boards cover all the required conditions of trip operation used.

The overall categories into which the faults are placed depend to some extent on the functions of the trip. This assessment is based on the most critical of its uses in the e.m.t. The individual trips only monitor failures which cause a loss in sensitivity. Other faults are all classified as unrevealed, since none of them can directly interfere with operation of the main unit trip (the z.m.t.). The following are the assessed failure rates:

Total failure rate	1·03% per kh
Unrevealed faults	0·35% per kh
	(*D* 0·14% and *E* 0·21%)

This is based on the second version of the board, which having a germanium input chopper, has slightly worse properties than that of Fig. 6.

Overall safety assessment

The fail-to-danger probability of the s.d.a. is the sum of three figures:

(a) Direct fail-to-danger faults on the z.m.t. are given as 0·202% per kh (category *F* faults).

(b) Failures of slave relays, in this case assumed to be all K3000 types with high-voltage contacts for increased contact spacing and nylon lifting pins to reduce the risk of short circuit: the fault on these relays is a short circuit between the contacts, and the assessed rate is 0·01% per kh.

(c) Combinations of one unrevealed fault with any other fault in the system: to assess a figure for the probability of such a combination, it is assumed pessimistically that 10% of the total unrevealed faults can, when combined with 10% of the z.m.t. faults, form fail-to-danger combinations. The z.m.t. faults in this case encompass any fault in the signal path, i.e. amplifier *A* plus amplifier *C*. The unrevealed-faults total includes figures for the three trips of amplifier-*D* type (i.e. e.m., a.e.m., and a.z.m. trips); using a maintenance period of 10 000h (approximately 1 year), the probability of such faults occurring are 1·85% for z.m.t. and 1·74% for unrevealed faults. The product of these is 0·015%, giving a probability of 0·0015% per kh.

The sum of all these fail-to-danger faults is therefore 0·211% per kh, or 2·115% over a one-year maintenance period. However, it would be reasonable to expect routine checks at much shorter intervals, say, once every 1000 h. A check which involved the dropping out of each of the guard lines in turn, carried out at 1000 h intervals, would reduce the probability of an undetected fail-to-danger fault to 0·23%.

Faults in the remaining circuit modules from which the s.d.a. is constructed are detected by their affect on the various trips:

(a) Failure of the chopper-drive oscillator prevents any of the choppers from functioning and all the trips de-energise.

(b) If the h.v. supply drops by 20%, the reference voltage rises by 20% or the signal/h.v. cable-screen continuity fails, the trip monitoring these three parameters will energise.

(c) Loss of the reference supply will cause the output of the amplifier to fail to zero; both the z.m.t. and the a.z.m.t. will operate.

(d) Loss of the +20V supply will prevent the chopper-drive oscillator from functioning and all the trips will de-energise.

(e) Loss of the −20V supply will prevent all trip circuits from operating and all the trip relays will de-energise.

Appendix A

Low-current test facility

General

Designed for the situation where an installation includes a requirement for indication of the ionization-chamber current with the reactor shutdown, an indication of currents in the order of 10^{-8}A is catered for in order to check for any degradation of the chamber. The circuit of this additional unit is shown in Fig. 7.

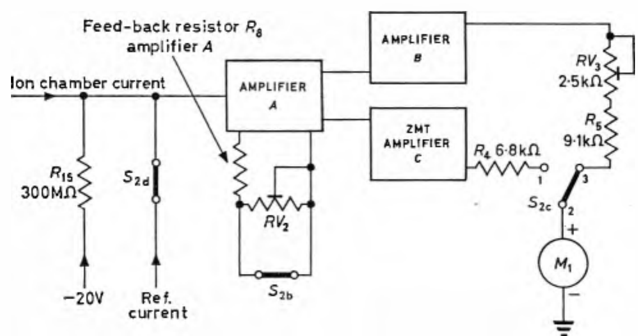

Fig. 7 Low-current test facility

Problems

There are two major problems associated with this requirement:

(a) With the possibility of a servosystem being used to control the trips, the reference current remains at the equivalent of 20MW when the reactor is shut down. This could be a current of between, say, 3×10^{-7} and 3×10^{-6}A, depending on the ionization-chamber sensitivity. Currents of this order will swamp the effect of the 10^{-8}A, which the circuit is required to measure.

(b) The gain of the circuit must be greatly increased to amplify 10^{-8}A, in order to give a meaningful reading on the meter.

Test-circuit reference current

The problem of reference test current has been solved by switching out the normal reference current and leaving a test reference current of approximately 7×10^{-8}A. Ion-chamber currents up to this level can be read on the meter scale, the subtraction of input from reference currents being carried out as in normal circuit operation.

The voltage from the reference potentiometer, with the reactor shut down, is extremely low and ill-defined. To overcome this, the normal -20V supply line and a high-value resistor R_{15} have been employed to generate the desired current. R_{15} is left in circuit during normal operation, since loss of the test current gives a small shift in the safe direction, whereas a gain in current due to short-circuited switch contacts would be in the dangerous direction.

Amplifier gain

The gain of the amplifier must be increased by between 600 and 6000 times for the period of the test. This has been carried out in three stages:

(a) The largest part of the gain (up to 200 times) is achieved by switching the meter from its normal output to the z.m.t. output.

(b) The adjustable part of the gain is obtained by increasing the feedback resistor in amplifier *A*.

(c) For reasons associated with circuit safety, the resistor used in series with the meter is selected so that in no case is the increase in gain of amplifier *A* less than three times.

Using all three methods, the desired test sensitivity can be safely obtained.

Table 2 lists all the components added to the s.d.a. for required test facility. Examination of the table reveals no significant increase in the fail-to-danger probabilities compared with the unmodified unit.

TABLE 2

R_{15}	o/c	*C*	Z.M.T. operates at 10 MW in the worst case
	s/c	*A*	Very large reference current, e.m.t. operates
R_4	o/c		No effect on the circuit safety since this component is used only during test
	s/c		
RV_2	o/c		RV_2 is short-circuited during normal operation and cannot affect circuit safety
	s/c		
S_{2d}	o/c	*A*	No reference current, z.m.t. operates
	s/c		Test circuit cannot function, but it has no effect on circuit safety
S_{2b}	o/c	*B*	Provided that the increase in gain, with RV_2 in circuit, exceeds 3, the a.e.m.t. will operate
	s/c		Test circuit cannot function but it has no effect in circuit safety
S_{2c} 1	o/c		No reading in test position
S_{2c} 2	o/c	*D*	No reading in either position
S_{2c} 3	o/c	*D*	No reading in normal position. Note that in the last two cases the shedding of the meter load will cause the trip output levels, other than z.m.t., to rise by approximately 10%
S_{2c} 1–2	s/c	*C*	The additional load on the z.m.t. will cause it to operate with a greater margin than the normal 6MW
S_{2c} 2–3	s/c		Test reading will be low, no safety implications

APPENDIX B

Response time of the s.d.a.

The important response time in this unit is the time taken for the z.m.t. to operate after the appropriate step signal has been applied to the input of the s.d.a. The input circuit is current sensitive and there are no large input time constants to consider. The two delays constituting the main part of the overall response are due to (a) the charging up of the output capacitor C_5 of the z.m.t., and (b) the slugging of the slave relays.

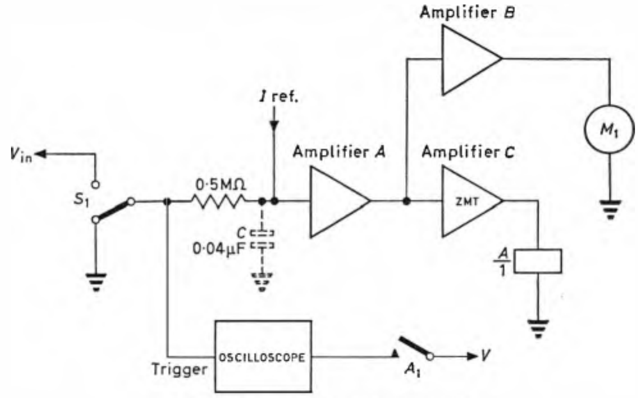

Fig. 8 Response-time test circuit

Tests have been carried out (using the circuit in Fig. 8) on a prototype circuit to assess the overall response time.

(i) With S_1 in position 1, the reference current was adjusted to give the required margin indicated on M_1.

(ii) With S_1 in position 2, the input voltage was adjusted to cancel out the reference current, giving zero margin indication.

(iii) S_1 was switched back to position 1 and the circuit allowed to settle down.

(iv) S_1 was then switched back to position 2 and the time between S_1 operating and RLA_1 opening was measured using an oscilloscope.

TABLE 3 Results of the tests

INITIAL MARGIN	CIRCUIT ADJUSTED FOR MAXIMUM GAIN (10µA IN FOR F.S.D.)	CIRCUIT ADJUSTED FOR MAXIMUM GAIN (100µA IN FOR F.S.D.)	CABLE CAPACITANCE C
	ms	ms	µF
20MW	35	40	0
300MW	85	80	
20MW	35	40	
300MW	85	80	0.014

Capacitor *C* was added to simulate cable capacitance, but, as can be seen from the table, it has negligible effect. Changes in circuit gain have a small effect, but the main variation is, as one might expect, due to the magnitude of the original margin setting. It is possible that the variation in this figure from unit to unit in a production batch is likely to be fairly high, since some of the main determining factors C_4 and C_5 and the drop-out voltage of RL_1 are not very closely defined parameters. With this in mind, a suitable assumption for this equipment is that the z.m.t. main relay contact will break in less than 150ms in response to a step input which reduces a 300MW margin to zero. If the equipment is employed in a safety system which employs several slave relays to give sufficient output contacts, these relays would be slugged by the diode damping circuit, which provides an additional delay of 150ms.

Equipment design rights

The design rights on the equipment detailed in this article and in Part 1 (August issue) are held by English Electric's Reactor Equipment division, who are manufacturing it for the CEGB Wylfa nuclear power station.

Acknowledgments

The author wishes to thank the Rank Organization for permission to publish, and J. Galvin and D. Halton for valuable assistance.

Random and pseudorandom number generators

by M. Davio*

A comparison is made between two types of number generator: random number generators, in which the output binary numbers are obtained by polarity sampling of classical noise sources, and pseudorandom number generators, where the output binary numbers are obtained from selected cells of a maximal-length programmed shift register. Comparison of the spectral properties of the two decoded output signals favours the former, which has a bandwidth about four times as good as that of a comparable pseudorandom signal.

IN many engineering applications, it is highly desirable to obtain a random signal whose statistical properties (whatever they are) are known and stable. Digital implementation gives a suitable solution to this problem and, in recent years, many generators of this kind have been described in the literature. All these generators consist of two main parts: a digital register, in which a random or pseudorandom sequence of binary numbers appears, and a digital-to-analogue converter. Two types of solution are available for the synthesis of the binary-number sequence:

(a) *Random sequence*: each $n$bit binary number is obtained by polarity sampling of the output voltage of n conventional noise sources (thyratrons, diodes etc.)

(b) *Pseudorandom sequence*[2-5]: the register in which the binary numbers appear is an $n$bit shift register coupled to a linear feedback network (i.e. comprising only modulo-2 adders); it is well known that, for a suitable choice of feedback network, the shift register generates a maximal-length sequence[6] (i.e. a sequence of length $2^n - 1$).

In both cases, the output signal of any flip-flop [Fig. 1(a)] is a sequence of 1s and 0s which appear with an equal probability of 1/2. According to the conclusions of Zierler[7], the autocorrelation function $\phi_{ff}(\tau)$ of that signal is a triangular function in the vicinity of the τ origin. The base of the triangle has a width 2θ, where θ is a sampling period (random sequence) or a clock period (pseudorandom sequence). Furthermore, in the pseudorandom case, f and $\phi_{ff}(\tau)$ are periodic, with a period $T = (2^n - 1)\,\theta$. For the sake of simplicity, the autocorrelation function is normalized, as shown in Fig. 1(b), in such a way that $\phi_{ff}(0) = 1$ and $\phi_{ff}(\tau) = 0$, for $\tau > \theta$.

This normalization is achieved by choosing suitable weights in the analogue interpretation of the logical levels

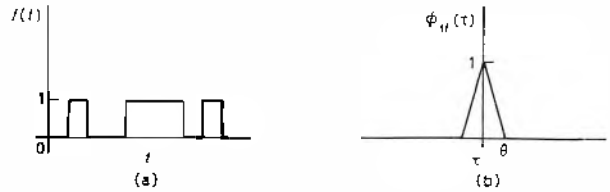

Fig. 2 (a) Typical decoded output signal
(b) Its autocorrelation function
***A* random case**
***B* pseudorandom case (consecutive outputs)**

0 and 1. It is then easy to find the power spectrum $\Phi_{ff}(\omega)$ of the signal by computing the Fourier transform of $\phi_{ff}(\tau)$. $\Phi_{ff}(j\omega)$ follows the law

$$\left[\frac{\sin(\omega\theta/2)}{\omega\theta/2}\right]^2$$

It becomes zero for $\omega = 2n\pi/\theta$ (n an integer), is flat to zero frequency, and is 6dB down for $\omega \simeq 2{\cdot}8/\theta$ (Fig. 3, curve A). In the second part of the generator (i.e. the digital-to-analogue decoder), a signal $g(t)$ is produced. This is the weighted sum of, say, m signals, $f_k(t)$ all having the same statistical properties and, in particular, the same correlation function $\phi_{ff}(\tau)$:

$$g(t) = \sum_{k=0}^{m-1} (1/2^k)\, f_k(t) \quad \ldots\ldots\ldots\ldots \quad (1)$$

The probability density of $g(t)$ is easily shown to be uniform inside the existence domain of that function[5].

Study of the autocorrelation function $\phi_{gg}(\tau)$ of $g(t)$ requires more care. One has to distinguish here between the random and pseudorandom cases (as defined above). In the random case, the summand functions $f_k(t)$ are statistically independent (i.e. the crosscorrelation functions $\phi_{f_if_j}(\tau)$ ($i \neq j$) are all zero). The correlation function $\phi_{gg}(\tau)$ is then the weighted sum of m identical functions $\phi_{ff}(\tau)$, and the result has the same triangular shape:

$$\phi_{gg}(\tau) = \phi_{ff}(\tau)\,(1 + 1/2 + 1/4 + \ldots) \simeq 2\,\phi_{ff}(\tau) \quad \ldots. \quad (2)$$

[Fig. 2(b), curve A]. In the pseudorandom case, however, the summand functions are obviously correlated, as they just differ by a timeshift. If, for instance,

$$f_k(t) = f_0\,(t - k\theta) \quad \ldots\ldots\ldots\ldots\ldots\ldots \quad (3)$$

nonzero crossterms appear when computing zero the autocorrelation function $\phi_{gg}(\tau)$ from equation (1). One shows[5] that these crossterms have the same triangular shape but are shifted along the τ axis. The resulting function is then given by

$$\phi_{gg}(\tau) = \sum_{k=0}^{m-1} \sum_{k=0}^{m-1} (1/2^{k+p})\, \phi_{ff}\,[\tau + (k - p)\theta] \quad \ldots. \quad (4)$$

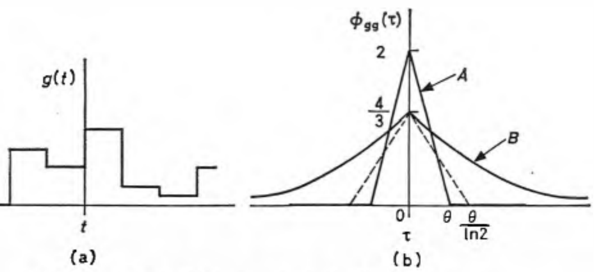

Fig. 1 (a) Typical binary output signal
(b) Its autocorrelation function

* *Louvain University, Heverlee, Belgium*

Now, from equation (4),

$$\phi_{gg}(r\theta) = \sum_{k=0}^{m-1} \sum_{k=0}^{m-1} (1/2^{k+p})\, \phi_{ff}\,[(k + r - p)\theta] \quad \ldots\ldots \quad (5)$$

where ϕ_{ff} is nonzero when $k + r - p = 0$, i.e. when $p = r + k$.

Thus, k being positive,

$$\phi_{gg}(r\theta) = \sum_{k=0}^{m-r-1} 1/2^{2k+r} = 1/2^r \sum_{k=0}^{m-r-1} 1/2^{2k} \quad \ldots\ldots \quad (6)$$

When m increases

$$\lim_{m\to\infty} \phi_{gg}(r\theta) = 4/(3{\cdot}2r) \quad \ldots\ldots\ldots\ldots \quad (7)$$

$\phi_{gg}(\tau)$ appears thus to be divided by 2 every θ-interval. This is the characteristic property of an exponential with the time constant $\theta/\ln 2$. While $\phi_{gg}(\tau)$ is a linear function of τ between the breakpoints $r\theta$, a numerical computation shows that the approximation

$$\phi_{gg}(\tau) \simeq 4/3\ \exp\left(-\frac{|\tau|\ \ln 2}{\theta}\right) \quad \ldots\ldots\ldots\ldots \quad (8)$$

is fairly good for all $m \geqslant 6$ [Fig. 2(b), curve B]. A simple inspection of the Fig. 2(b) shows that the frequency band of the output signal is wider in the random case than in the pseudorandom one. Quantitatively, the power spectrum computed from equation (8) is given by an expression of the form

$$\Phi_{gg}(j\omega) = k\ \frac{\omega\theta}{1 + (\omega\theta/\ln 2)^2} \quad \ldots\ldots\ldots\ldots \quad (9)$$

and is 6dB down for $\omega = \ln 2/\theta \simeq 0{\cdot}7/\theta$. The cutoff frequency is about four times smaller than in the random case. The origin of this bandwidth loss obviously lies in the interdependancy of $f_k(t)$. One might then raise the question: is it possible to improve in a simple way the spectrum performances for the pseudorandom case?

Without changing the decoding network, one may just think of one modification to the circuit, i.e. modifying the connections between the shift register and the decoder. Those connections are represented by equation (3) and the associated equation (4). These formulas are easily generalized by the hypothesis

$$f_k(t) = f_0\,(t \pm rk\theta)\ \ (r \text{ an integer}) \quad \ldots\ldots\ldots \quad (10)$$

The autocorrelation function then becomes

$$\phi_{gg}(\tau) = \sum_{k=0}^{m-1} \sum_{p=0}^{m-1} (1/2^{k+p})\, \phi_{ff}\,[\tau \mp r(k - p)\theta] \quad \ldots\ldots \quad (11)$$

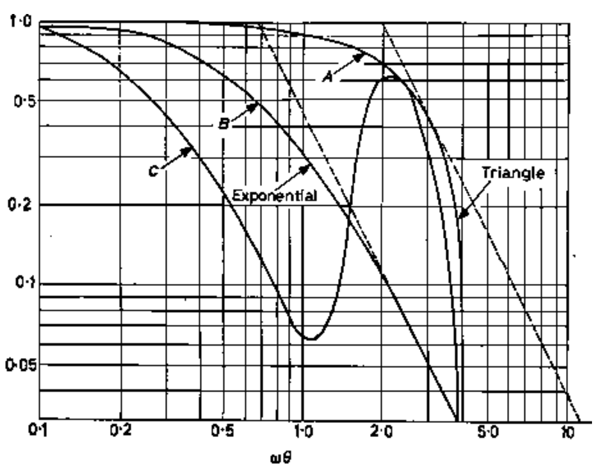

Fig. 3 Power spectrum of the decoded signal
A random case
B pseudorandom case (consecutive outputs)
C pseudorandom case (equidistant outputs $r = 3$)

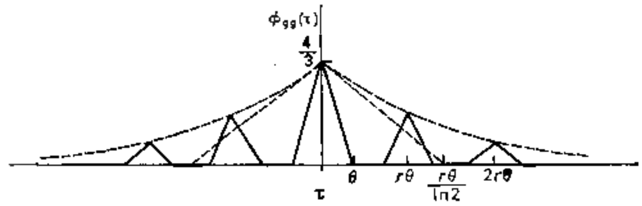

Fig. 4 Autocorrelation function of the decoded signal (pseudorandom case, equidistant outputs $r = 3$)

and it has the shape shown in Fig. 4. The corresponding power spectrum is easily computed if one notes that the Fourier transform of two triangular waves centred on $\pm r\theta$ is simply given by

$$2\left(\frac{\sin \omega\theta/2}{\omega\theta/2}\right)^2 \cos \omega r\theta$$

Hence

$$\Phi_{gg}(j\omega) = \left(\frac{\sin \omega\theta/2}{\omega\theta/2}\right)^2 \left(1 + \cos \omega r\theta + \frac{\cos 2\omega r\theta}{2} + \ldots + \frac{\cos m\omega r\theta}{2^{m-1}}\right) \ldots \quad (12)$$

Now, when m is great enough, the second factor of this product may be considered as an approximation of a Fourier expansion of an even function, periodic in ω and with a period $2\pi/r\theta$. One sees furthermore that the envelope of the discrete spectrum of that function has an exponential shape. From the symmetry of the Fourier-transform relations, one may then deduce, with fairly good approximation, that this is the Fourier expansion in an interval $\pm\,(\pi/r\theta)$ of the function

$$\frac{1}{1 + (\omega r\theta/\ln 2)^2} \quad \ldots\ldots\ldots\ldots\ldots \quad (13)$$

Finally, the power spectrum of the new signal will have a rather complicated shape, entirely contained under a $(\sin x/x)^2$ curve. The foregoing computation shows, however, that, for any r, the spectrum will have a first point 6dB down for $\omega = \ln 2/r\theta$. The answer to the previous question is thus negative.

The spectral properties of the decoded signal are thus well known, and one is lead to the conclusion that the simplicity gained in the pseudorandom synthesis is paid for by a double loss in spectral qualities:

(a) The spectrum is discrete, and this could be a source of trouble when testing highly selective networks.

(b) The random generator provides, in any case, an output signal having a wider spectrum than the signal provided by a comparable pseudorandom generator; as shown, for the latter, a change in the connections between the register and the converter does not improve the performance of the delivered signal.

REFERENCES

1 Dag, T., and Skinner, M.: A random signal generator, *Electronic Engng.*, *38*, 2-7 (Jan. 1966).
2 Kramer: A low frequency pseudorandom noise generator, *ibid.*, *37*, 465-467 (July 1965).
3 Stern, Cazemajou, Machefrez, Valat and Vignon: Génération d'un créneau pseudoaléatoire par un registre à décalage à contreréaction binaire, Rapport CEA R.2230 (Aug. 1964).
4 Stern, Blaquiere and Valat: Reactivity measurement using pseudo-random source excitation, *Reactor Sci. Tech.*, *16*, 499-508 (1962).
5 Davio, M.: Synthèse et propriétés d'un générateur de nombres aléatoires, *Revue MBLE*, *7*, 249-265 (Dec. 1964).
6 Peterson, W. W.: *Error-correcting codes*, MIT Press and Wiley, 1961.
7 Zierler, N.: Linear recurring sequences, *Soc. Industr. Appl. Math.*, *7*, 31-48 (March 1959).
8 Huffman, D. A.: The generation of impulse equivalent pulse trains, *IRE Trans. IT-8*, 10-14 (Sept. 1962).
9 Simpson, H. R.: Statistical properties of a class of pseudorandom sequences, *Proc. IEE*, *113*, 2075-2080 (Dec. 1966).

Some novel *RC* oscillators for radio frequencies

(Part 2)

by R. S. Sidorowicz*, Dipl.Ing., D.I.C., M.I.E.E.

Oscillator with two tuning elements

Equation (21) shows that the circuit of Fig. 11 can produce phase shifts of up to $2\phi \leqslant 180°$. This fact suggests that it is possible to arrange an oscillator by connecting the circuit in cascade with a simple series *RC* network that can provide a phase shift $\phi_1 \leqslant 90°$. This combined circuit should be able to produce an overall shift of 180° at a 'sensible' (noninfinite) frequency. The block schematic of an oscillator based on this concept is shown in Fig. 14. It is seen that the oscillator contains an inverting amplifier, as well as the combined phase shifter. This amplifier must develop enough gain to compensate for the attenuation of the phase shifter at the frequency of oscillation. It should be emphasized that the oscillator circuit must be designed so that operation of the combined phase-shift network is linear; this requirement implies that the amplitude limiting during oscillation should be done entirely by the amplifier.

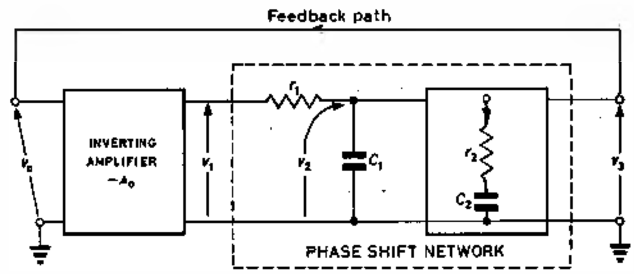

Fig. 14 *RC* **oscillator with one active all-pass stage**

The conditions of oscillation for the circuit of Fig. 14 can readily be formulated mathematically, if it is assumed that

(i) the passive r_1C_1 network does not load the amplifier

(ii) the input resistance of the all-pass stage is very high

(iii) the input impedance of the amplifier does not significantly load the output of the all-pass stage.

The voltage transfer function of the circuit with the feedback path interrupted is

$$v_3/v_0 = \mathrm{k}(\omega) = -A_0\mathrm{g}(\omega)\,\mathrm{f}(\omega) \quad \ldots\ldots (27)$$

where $\mathrm{g}(\omega) = 1/(1 + \mathrm{j}\omega C_1r_1)$ is the transfer function of the passive network and $\mathrm{f}(\omega)$ is the transfer ratio of the all-pass stage. Explicitly

$$\mathrm{k}(\omega) = -\frac{A_0A_1(B - \mathrm{j}\omega C_2r_2)}{(1 + \mathrm{j}\omega C_1r_1)(B + \mathrm{j}\omega C_2r_2)} \quad \ldots\ldots (28)$$

The circuit will oscillate if $\mathrm{k}(\omega) = 1$. From equation (28) it follows, therefore, that

$$(1+\mathrm{j}\omega_0C_1r_1)(B+\mathrm{j}\omega_0C_2r_2) = -A_0A_1(B-\mathrm{j}\omega_0C_2r_2) \quad \ldots\ldots (29)$$

By separating the real and imaginary parts of equation (29), the following expressions are obtained:

$$\left.\begin{aligned} B - \omega_0^2C_1C_2r_1r_2 &= -A_0A_1B \\ BC_1r_1 + C_2r_2 &= A_0A_1C_2r_2 \end{aligned}\right\} \quad \ldots\ldots (30)$$

from which $\quad A_0 = (1 + BC_1r_1/C_2r_2)/A_1 \quad \ldots\ldots (31)$

$$f_0 = (1/2\pi)\sqrt{\frac{B(2 + BC_1r_1/C_2r_2)}{C_1C_2r_1r_2}} \quad \ldots\ldots (32)$$

Equation (31) determines the gain necessary for oscillation, while equation (32) gives the frequency of oscillation. It is seen that A_0 is dependent on the ratio C_1r_1/C_2r_2. When the oscillator is tuned, A_0 must be kept constant. This means that C_1r_1/C_2r_2 must be a constant, which can be achieved only if C_1 and C_2 are varied simultaneously. For the case when $r_1 = r_2 = r$ and $C_1 = C_2 = C$, the formulas for the gain and frequency become

$$A_0 = (1 + B)/A_1 \quad \ldots\ldots (33)$$

$$f_0 = \frac{\sqrt{[B(2 + B)]}}{2\pi Cr} \quad \ldots\ldots (34)$$

Since B must always be greater than unity, it follows that the numerator of equation (34) is appreciably larger than unity. If it is assumed that $B = 3$, the frequency is given by $f_0 = \sqrt{15}/2\pi Cr$. For $r = 4{\cdot}7\mathrm{k}\Omega$ and $C = 100\mathrm{pF}$, this gives $f_0 = 1{\cdot}3\mathrm{MHz}$.

A transistorized oscillator, based on the concept of Fig. 14, was built in order to verify the above theoretical conclusions. A detailed circuit diagram of the oscillator is shown in Fig. 15. The oscillator circuit employs three silicon-junction *n-p-n* transistors, type 2N706, with a typical f_T of 400MHz. One transistor is used as the inverting amplifier, while the other two form the phase-shift stage. In addition, the circuit of Fig. 15 is provided with an output amplifier which is used to amplify the signal derived from the emitter of VT_3. A direct coupling is employed between all the transistors, except for one a.c. path which is formed by the feedback capacitor $C_f = 5\mu\mathrm{F}$.

The biasing voltages of various points of the circuit are indicated on the diagram; these voltages were measured with the feedback loop disconnected and with $r = 4{\cdot}7\mathrm{k}\Omega$. It is to be noted that VT_1, which acts as the inverting amplifier, is supplied through a potential dropper $R_0 = 1\mathrm{k}\Omega$. This arrangement ensures that the amplifier output voltage cannot be greater than about 2·0V peak-to-peak; hence neither VT_2 nor VT_3 can be overdriven (i.e. they operate linearly).

The oscillator was primarily intended for operation at radio frequencies; hence, in order to ensure a fairly large working bandwidth, a comparatively low value of R_1 was chosen (440Ω in Fig. 15). The value of the emitter resistance of VT_2 was chosen as $R_{E1} = 100\Omega$, to reduce the attenuation of the phase-shift stage.

R_1 and R_2 were calculated approximately by using equations (22) and (23) with a nominal value of $B = 3$.

* *Imperial College of Science and Technology, London*

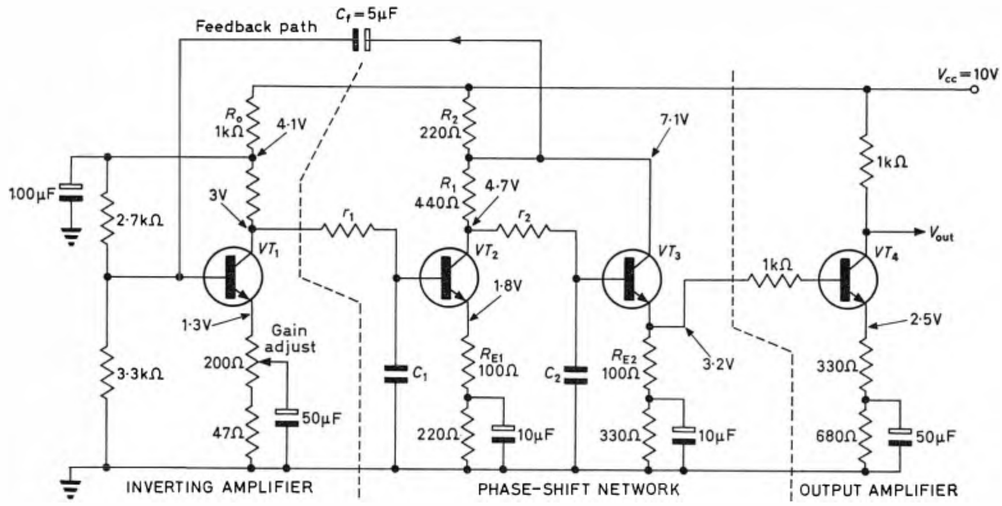

Fig. 15 *RC*-oscillator circuit for radio frequencies (all resistances are within 5% tolerance)

In the calculations, it was assumed that

(i) the r_2C_2 network did not load the output of VT_2

(ii) the input resistance of VT_3 could be neglected

(iii) the internal feedback in VT_2 and VT_3 could be disregarded.

The following values of the relevant small-signal parameters were assumed for VT_2 and VT_3:

(a) mutual conductances $g_{m2} = 200$mA/V and $g_{m3} = 280$mA/V

(b) output resistances $r_{02} = r_{03} = 5$kΩ

(c) current gain $\beta_3 = \beta_2 = 50$.

The calculations gave $R_2 = R_1/2 = 200\Omega$, and $R_{E2} = R_1/4 \simeq 100\Omega$.

Theoretically, for $B = 3$ the frequency of oscillation should be given by

$$f_0 = \sqrt{15}/2\pi Cr \quad \ldots\ldots\ldots\ldots\ldots\ldots (35)$$

In practice, it was found that, on the whole, this formula was inaccurate. This is not surprising if it is recalled that the calculations were based on rather gross simplifying assumptions. The main factors that make equation (35) inaccurate are:

(i) input resistances of VT_2 and VT_3, which are estimated to be about 5kΩ

(ii) input resistance of VT_1 which probably does not exceed 1kΩ.

The circuit could be made to oscillate by adjusting the setting of the gain-control potentiometer in the emitter of VT_1. If the gain was set only slightly above the critical value A_0, an undistorted sinusoidal waveform could be obtained at the emitter of VT_3. It appeared that the signal at this emitter contained less distortion than that at any other point of the circuit. However, since the signal level at the emitter of VT_3 was rather low, an amplifier based on VT_4 was used to produce an output of about 0·5V r.m.s.

The oscillation frequency f_0 was measured for two different values of $r_1 = r_2 = r$, for $C_1 = C_2 = C$ ranging from 0 to 2200pF. The circuit oscillated readily with $C = 0$, at a frequency which was determined primarily

TABLE 3

C, pF		2200	390	150	75	27	0
r=4·7kΩ	f_0, MHz	0·057	0·312	0·74	1·33	2·7	7·7
	V_{out}, V	0·8	0·8	0·8	0·9	0·9	0·7
r=1 kΩ	f_0, MHz	0·22	1·11		3·7	6·65	14·3
	V_{out}, V	1·0	1·0		1·7	1·6	1·1

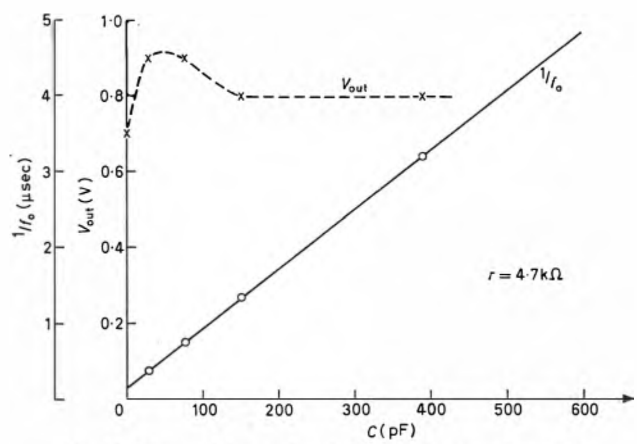

Fig. 16 V_{out} and $1/f_0$ as functions of tuning capacitances C

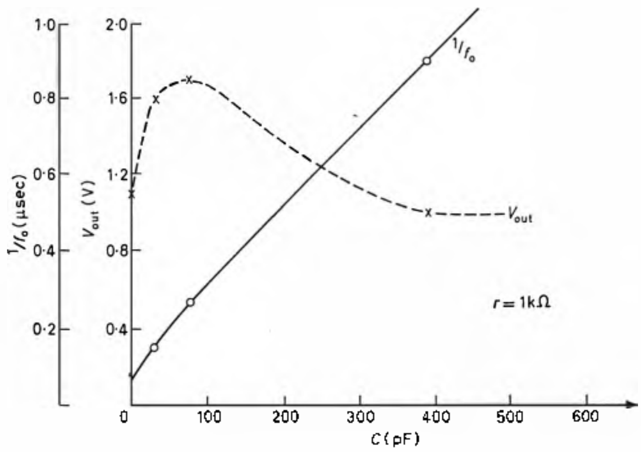

Fig. 17 V_{out} and $1/f_0$ as functions of tuning capacitances C

by the input capacitances of VT_2 and VT_3. The amplitude of the signal at the collector of VT_4 was also measured. The results are shown in Table 3 and plotted in Figs. 16 and 17 for $C < 400$pF.

Fig. 16 shows that the amplitude V_{out} of the output signal, for $r = 4{\cdot}7\text{k}\Omega$, is almost constant as a function of C. Amplitude stability of the oscillator can thus be regarded as satisfactory, especially in view of the fact that no special means of amplitude stabilization (such as thermistors) are employed. The graph of $1/f_0$ is a straight line except at low values of C. This implies that the frequency obeys the relationship $f_0 = d/2\pi Cr$, where d is a constant. The value of d can be found by measuring f_0 at a fairly large value of C, so that the input capacitances of VT_2 and VT_3 can be ignored. By taking $C = 2200$pF, it is found that $d = 3{\cdot}7$. This value of d, and f_0 corresponding to $C = 0$, can be used to estimate the input capacitances C_{in} of VT_2 and VT_3. It is found that $C_{in} = 16$pF.

Fig. 17 shows that the performance of the oscillator with $r = 1\text{k}\Omega$ is not very satisfactory. The variation of V_{out} is quite pronounced, and the effect of the transistor input capacitances on f_0 is more significant than in Fig. 16 (note the curved portion of the $1/f_0$ graph in Fig. 17). However, it should be possible to correct these defects by suitably modifying R_1, R_2 and R_{E2}.

It is worth mentioning that a special radio-frequency oscillator, identical to the circuit of Fig. 15, was also built. This had $r = 5{\cdot}6\text{k}\Omega$ and was tuned by means of a 2-gang cpacitor. Each gang had a maximum capacitance of 365pF. The frequency could be varied continuously from 0·29MHz to 3·8MHz. The amplitude variation over the whole frequency range did not exceed $\pm 8\%$. The circuit oscillated satisfactorily when the supply voltage was varied from 8·5 to 12V, though V_{out} was not constant.

Oscillator with one tuning element

The experiments described above indicate that the transistor phase-shift stage (Fig. 15) operates satisfactorily, even if it is not an ideal all-pass circuit. It should be possible, therefore, to construct an oscillator by employing two such stages and an inverting amplifier (in accordance with the scheme suggested in Fig. 7). If the two stages are identical, except for their rC networks, their transfer functions can be written as

$$f_1(\omega) = A_1 \frac{(B_1 - jX_1)}{(B_2 + jX_1)} \quad \ldots\ldots\ldots\ldots (36)$$

and

$$f_2(\omega) = A_1 \frac{(B_1 - jX_2)}{(B_2 + jX_2)} \quad \ldots\ldots\ldots\ldots (37)$$

where $X_1 = \omega C_1 r_1$ and $X_2 = \omega C_2 r_2$.

If the first stage does not load the amplifier and the second stage does not load the first, the transfer function of the whole circuit with feedback loop interrupted is

$$k(\omega) = -A_0 A_1^2 \frac{(B_1 - jX_1)(B_1 - jX_2)}{(B_2 + jX_1)(B_2 + jX_2)} \quad \ldots\ldots (38)$$

The circuit will oscillate if the feedback loop is closed and if $k(\omega) = 1$. Here, as in the analysis of the preceding oscillator, it is assumed that the input of the amplifier does not load the second phase-shift stage. The conditions of oscillation are given by

$$-A_0A_1^2(B_1 - jX_1)(B_1 - jX_2) = (B_2 + jX_1)(B_2 + jX_2) \quad \ldots\ldots (39)$$

or

$$\left.\begin{aligned} -A_0A_1^2(B_1^2 - X_1X_2) &= B_2^2 - X_1X_2 \\ A_0A_1^2(X_1 + X_2)B_1 &= B_2(X_1 + X_2) \end{aligned}\right\} \quad \ldots\ldots (40)$$

from which

$$A_0 = B_2/B_1A_1^2 \quad \ldots\ldots\ldots\ldots (41)$$

and

$$X_1X_2 = B_1B_2 \quad \ldots\ldots\ldots\ldots (42)$$

or

$$\omega_0^2 C_1C_2 r_1r_2 = B_1B_2$$

The final formula for the frequency of oscillation is

$$f_0 = 1/2\pi \frac{\sqrt{(B_1B_2)}}{\sqrt{(C_1C_2 r_1r_2)}} \quad \ldots\ldots\ldots\ldots (43)$$

If $C_1 = C_2 = C$ and $r_1 = r_2 = r$, this becomes

$$f_0 = \frac{\sqrt{(B_1B_2)}}{2\pi Cr} = d/2\pi Cr \quad \ldots\ldots\ldots\ldots (44)$$

The results obtained from equation (39) are rather surprising in at least one respect. Thus equation (41) shows that, even if the phase-shift stages are not ideal all-pass circuits, A_0 required for oscillation is independent of the C and r values. This implies that the oscillator can be tuned by varying only one of its frequency-determining elements (either C or r). Equation (43) indicates that, with

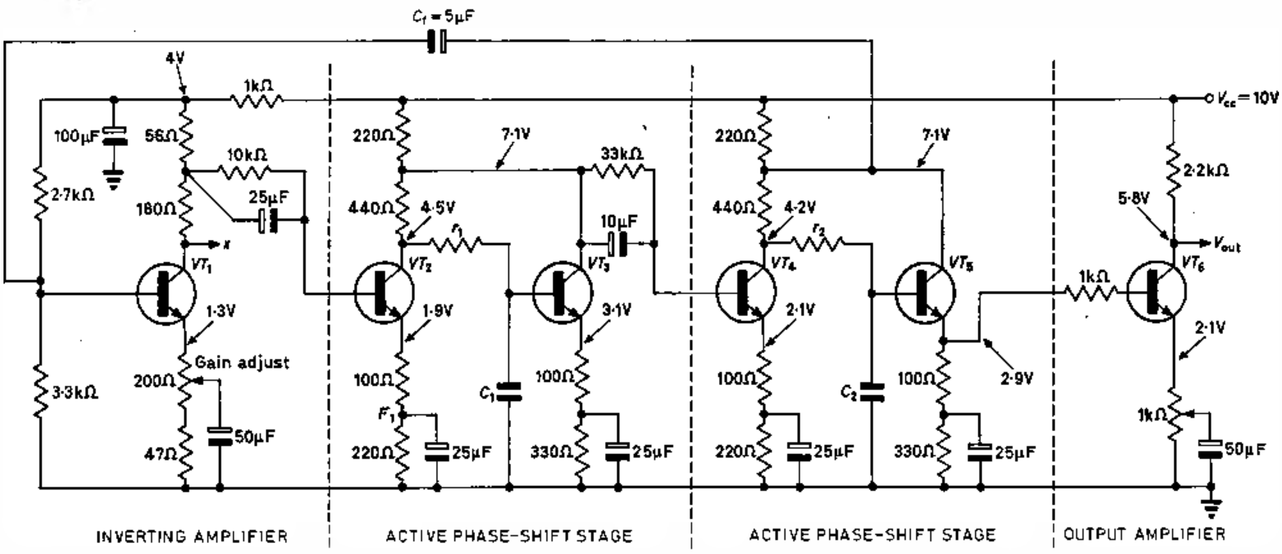

Fig. 18 Oscillator with two phase-shift stages (all resistances are within 5% tolerance)

this method of tuning, f_0 is inversely proportional to $\sqrt{(Cr)}$. On the other hand, if two resistors or two capacitors are varied simultaneously and if $C_1 = C_2 = C$ and $r_1 = r_2 = r$, then f_0 is inversely proportional to Cr.

An oscillator with two active phase-shift stages was built and investigated experimentally. A detailed circuit diagram of the oscillator is shown in Fig. 18. The phase shifters in this circuit are identical to that of Fig. 15, but the inverting amplifier is different in that only a fraction of its output is fed to the input of the first phase-shift stage. This arrangement ensures that the phase shifters operate linearly. A direct coupling is provided between the individual circuits of the oscillator, except for the feedback path which is formed by $C_f = 5\mu$F. The signal produced at the emitter of VT_5 is rather low; hence an output amplifier of adjustable gain is used. The amplifier can be connected directly to the collector of VT_1 instead of the emitter of VT_5.

The circuit of Fig. 18 may appear unduly complicated, in that the emitters of VT_2, VT_3, VT_4 and VT_5 are provided with separate biasing resistances and bypass capacitors. However, the situation can be simplified by providing common biases for the points F_1-F_3 and F_2-F_4 (Fig. 18). Such a simplified biasing arrangement was tried in practice and proved to be entirely satisfactory.

First, the oscillation frequency f_0 and the output signal V_{out} of the oscillator of Fig. 18 were measured when C_1 and C_2 were varied simultaneously (with $C_1 = C_2 = C$). The results are given in Table 4 for $r_1 = r_2 = 5{\cdot}6\text{k}\Omega$, and are plotted in Fig. 19.

TABLE 4

C, pF	2200	800	390	150	75	27	0
f_0, kHz	34	91	185	454	830	1820	6060
V_{out}, V	1·6	1·6	1·6	1·6	1·6	1·55	1·55

Table 4 and Fig. 19 show that V_{out} is almost constant over the whole frequency range (from 34kHz to 6·06MHz. It should be mentioned, however, that V_{out} tended to drop appreciably at frequencies above about 1MHz unless h.f. ceramic capacitors were added in parallel with the electrolytic emitter-bypass capacitors.

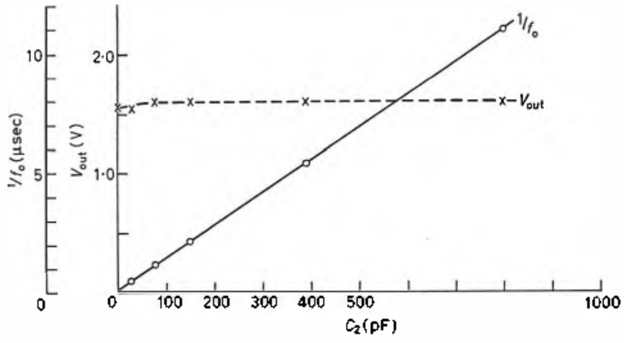

Fig. 19 V_{out} **and** $1/f_0$ **as functions of tuning capacitances** C **(for the oscillator in Fig. 18)**

The graph of $1/f_0$ in Fig. 19 is a straight line except at $C < 100$pF; this confirms the correctness of equation (44). Again, by adopting the procedure outlined in the preceding section, it is possible to calculate d for equation (44) and estimate the input capacitances C_{in} of VT_3 and VT_5. It was found that $d = 2{\cdot}64$ and $C_{in} = 12{\cdot}5$pF.

Next, with $r_1 = r_2 = r = 5{\cdot}6\text{k}\Omega$ and C_1 set at 200pF, C_2 was varied from 10 to 2200pF. In this case, the only points of the oscillator where a constant output could be expected were the collector of VT_1 and the collector of VT_5. The output amplifier was therefore coupled to the collector of VT_1. The variation of voltages at the emitters of VT_3 and VT_5 with C_1 constant and C_2 variable is caused by the impedance of C_1 decreasing with increasing f_0 and that of C_2 increasing; here, it has to be borne in mind that C_2 decreases faster than the rate of increase of f_0.

Results of the measurements of f_0 and V_{out} with C_2 tuning are given in Table 5 and plotted in Fig. 20.

TABLE 5

C_2,pF	2200	800	390	150	75	27	10
f_0, kHz	109	182	256	400	540	770	1040
V_{out}, V	1·7	1·7	1·7	1·7	1·7	1,65	1·5
$\sqrt{C_2}$	47	28·3	19·8	12·3	8·7	5·2	3·16

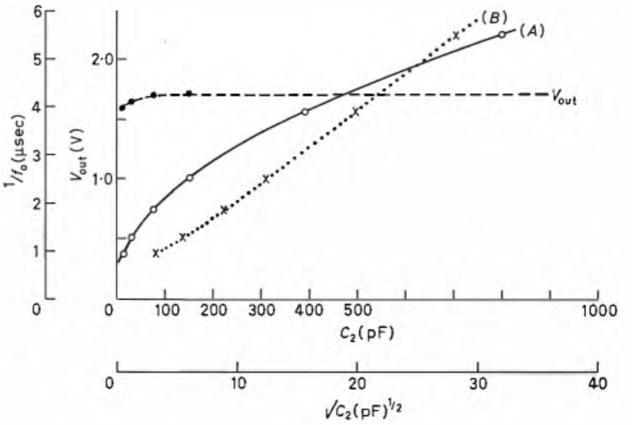

Fig. 20 V_{out} **and** $1/f_0$ **as functions of one tuning capacitance** C_2 **(for the oscillator in Fig. 18)**

Table 5 and Fig. 20 show that V_{out} remains almost constant when C_2 is varied from 10 to 2200 pF. Curve A in Fig. 20 illustrates the dependence of $1/f_0$ on C_2, while curve B shows $1/f_0$ as a function of $\sqrt{C_2}$. It is seen that this second 'curve' is effectively a straight line, except for $C_2 < 100$pF.

An additional oscillator, in which the relative positions of C and r were interchanged, was also built. A detailed diagram of this circuit is shown in Fig. 21. The emitter and collector resistances in the oscillator are identical to those of Fig. 18, but the transistors VT_3 and VT_5 are provided with independent biasing networks consisting of $R_x = 10\text{k}\Omega$ and $R_y = 5{\cdot}6\text{k}\Omega$. With $C_1 = C_2 = 150$pF, the circuit oscillated satisfactorily at a frequency of 145kHz.

In theory, it should be possible to tune this oscillator by connecting variable resistances in parallel with both of the R_y or with one of R_y only (as indicated by the chain-dash lines in Fig. 21). However, no practical investigation of these possibilities was undertaken. It may be added that the effective values of the tuning resistors r in the oscillator of Fig. 21 are determined by a parallel combination of R_x, R_y and the input resistances R_{in} of VT_3 or VT_5; i.e.

$$1/r = 1/R_x + 1/R_y + 1/R_{in}$$

The values of R_{in} are not known and cannot easily be

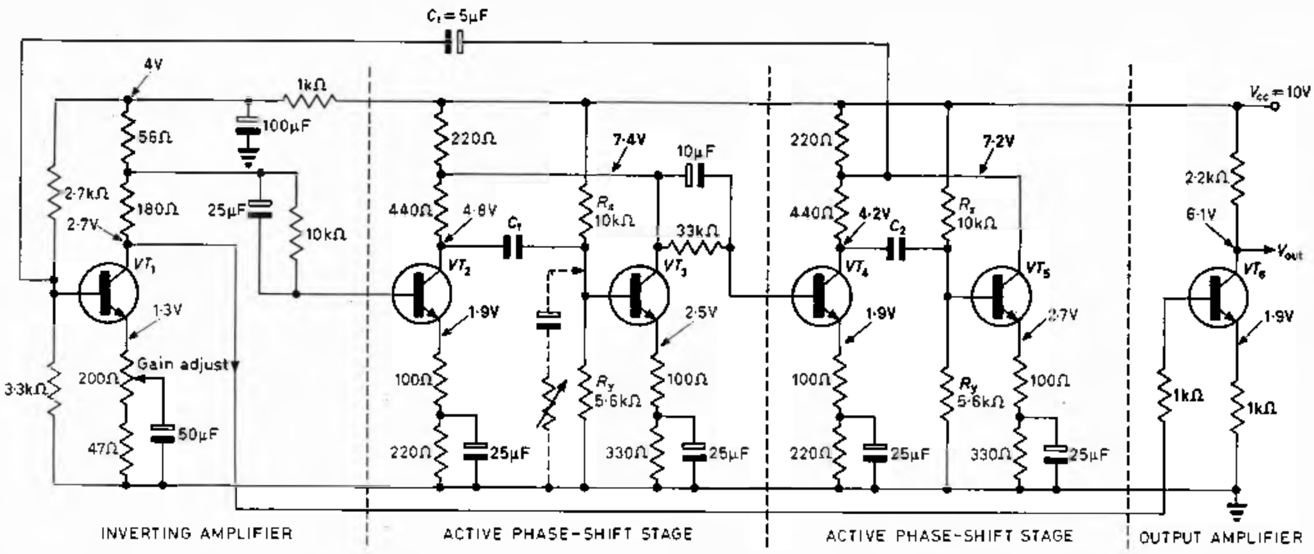

Fig. 21 Oscillator with two *CR* phase-shift stages (all resistances are within 5% tolerance)

measured directly. However, in the circuit of Fig. 21, it can be estimated that they are comparable in magnitude with R_x and R_y.

Conclusions

The two oscillators described (Figs. 15 and 18) can be regarded as successful, in that they can generate radio frequencies and are easily tuned. The upper frequency limit was not investigated, but with the circuit of Fig. 15 it was possible to generate frequencies of up to 25MHz, if values of r smaller than 500Ω were chosen. If the oscillator of Fig. 18 is tuned by simultaneously varying C_1 and C_2 (with $C_1 = C_2$), it can be used as a 2-phase oscillator. The 90° phase difference between the corresponding points of the two phase-shift stages would require that the stages be identical, but they do not have to be ideal all-pass circuits.

The oscillator of Fig. 15 is simpler than that of Fig. 18 in that it employs fewer transistors. On the other hand, it can only be tuned by varying two elements and is affected by tracking inaccuracies in the ganged capacitor.

The oscillator of Fig. 18 is notable for its amplitude stability, irrespective of whether it is tuned by varying one or two capacitors. The circuit may appear to be unduly complicated, since it requires at least five transistors; however, this is not a great disadvantage in view of the fact that the prices of some types of h.f. silicon transistors are comparable with those of certain passive components. Furthermore, the circuit can be simplified along the lines suggested in the preceding section.

Design of the active phase-shift stages used in the oscillators was based on the formulas which were derived for valve or field-effect-transistor circuits. Hence the calculations were approximate and it was not possible to determine optimum operating conditions for the transistors. Secondly, frequency stability of the oscillators was not investigated. It seems reasonable to expect that their stability should not be inferior to that of other RC oscillators of comparable performance. Thirdly, no special means were used to stabilize the amplitude of the oscillator output signals. It seems likely that stability and 'purity' of the waveforms generated by the oscillators could be substantially improved by the use of such simple stabilizing devices as thermistors or miniature lamps.

In the circuits of Figs. 15 and 18, all the biases and interstage couplings are arranged by means of suitable resistances with bypass capacitors. In theory, it should be possible to modify these biasing and coupling arrangements in such a way that they can be replaced by semiconductor diodes. Thus the resistance of 220Ω in the emitter of VT_2 should be replaceable by two forward-biased silicon diodes. Similarly, such biasing can be arranged for the emitters of VT_3, VT_4 and VT_5. The coupling between the collector of VT_3 and the base of VT_4 can be provided by a suitable Zener diode. If this type of biasing proved successful, it would be possible to construct the oscillator of Fig. 18 in the form of a solid-state circuit. However, the gain adjustment and feedback path for such a circuit would have to be provided 'externally'; also, the tuning would have to be done by an external capacitor.

At this stage, it is almost impossible to discuss adequately the applications of the two oscillators. Only a few suggestions will therefore be made. It is fairly clear that the oscillators have no particular advantages at audio frequencies. On the other hand, they may offer a possibility of extending the range of inexpensive *RC* signal generators into the medium- and short-wave frequencies. If the oscillator of Fig. 18 can be made as an integrated circuit with single-capacitor tuning, it may prove useful as the local oscillator in transistor radio receivers. Also, this oscillator is almost ideally suited to frequency modulation and should therefore prove useful in sweep-frequency generator or in various telemetering systems.

REFERENCES

1 Owens, J. H.: Audio Oscillator Uses New R-C Design. *Electronics 27*, 176-7 (1954).
2 Pasupathy, S.: A Transistor RC Oscillator Using Negative Impedances. *Electronic Engng. 38*, 808-9 (1966).
3 Sidorowicz, R. S: A Wideband Polyphase Frequency Changer. *ATE J. 13*, 210-26 (1957)

BIBLIOGRAPHY

1 Edson, W. A.: *Vacuum Tube Oscillators*. Wiley, 1953.
2 Chance, B., *et al.*: *Waveforms*. McGraw-Hill, 1949.
3 Kharkevich, A. A.: *Nonlinear and Parametric Phenomena in Radio Engineering*. Gos. Izd. Tekh. Teor. Lit., Moscow, 1956.
4 Reich H. J.: *Functional Circuits and Oscillators*. Van Nostrand, 1961.
5 Szerszen, J.: *Transistor Oscillators*. Generatory tranzystorowe, PWN, Warsaw, 1961.
6 Groszkowski, J.: *Frequency of Self-Oscillations*. Pergamon Press, 1964.

High-speed linear gate

by E. A. Faulkner* and J. B. Grimbleby*

This article describes a linear gate employing complementary silicon planar transistors. The circuit gives a switching time of 5ns with negligible spikes, linearity within 0·1% and a temperature coefficient of 0·04% per degK. The gate has particular applications in boxcar integrators and phase-sensitive detectors.

(Voir page 597 pour le résumé en français: Zusammenfassung in deutscher Sprache auf Seite 598)

A RECENT paper[1] has emphasized the advantages of current-switching configurations in the design of high-performance phase-sensitive detectors. The same points were, in fact, discussed in more detail in an earlier publication[2]. These simple unbalanced current-switching circuits are ideal in phase-detector applications where the reference mark/space ratio is known to be unity, i.e. where the reference voltage contains no even harmonics of its fundamental frequency. (In this context we use the term mark/space ratio to refer to the ratio of the intervals between the zero-crossing points, whatever the waveform.) However, in the output of the unbalanced gate, the switched signal is superimposed on a squarewave (Fig. 1) whose amplitude is greater than the maximum signal amplitude, and any departure from unity in the reference mark/space ratio will give rise to an offset in the d.c. output. This will cause noise to appear on the output if the reference signal fluctuates in amplitude or waveform (as can happen with mechanical choppers, for example).

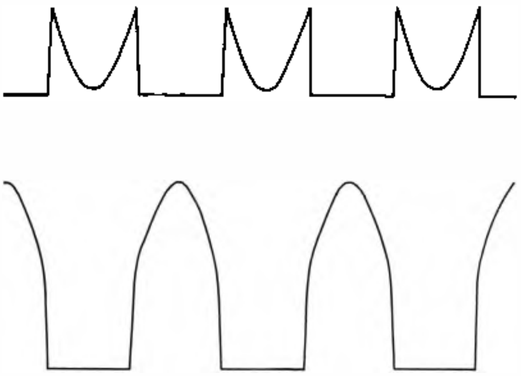

Fig. 1 Outputs of a simple unbalanced current-switching phase-sensitive detector

Also, phase shifters of the type which are commonly used in the reference channel change the mark/space ratio of any waveform containing even harmonics, thereby causing a shift in output which may make optimization difficult. An additional disadvantage of simple unbalanced current-switching circuits is that, at repetition frequencies below about 10Hz, it becomes increasingly difficult to filter the large a.c. component that appears in the output at the reference frequency.

These considerations have led some workers to prefer saturating transistor or diode gates in phase-sensitive detector and boxcar integrator circuits. However, neither of these systems has the advantages, in terms of speed, linearity and temperature coefficient, of the transistor current switch. In this article a symmetrical transistor current-switching gate is described, which was designed for boxcar integrators, phase-sensitive detectors and other applications requiring a very fast linear gate with negligible offset voltage.

Circuit description

The circuit is shown in Fig. 2; all transistors are assumed to be of the silicon planar type. It is symmetrical and consists of two sections: an *n-p-n* section and a *p-n-p* section, with nominally identical components. The reference voltage is applied in antiphase to the bases of transistors VT_2 and VT_5; the circuits used to provide these voltages (Figs. 3 and 4) will be discussed later. For use as a single-ended gate (in boxcar integrators, for example), the point A is connected to the zero rail and the output is taken from point B.

The a.c. signal voltage V_S is connected to the emitters

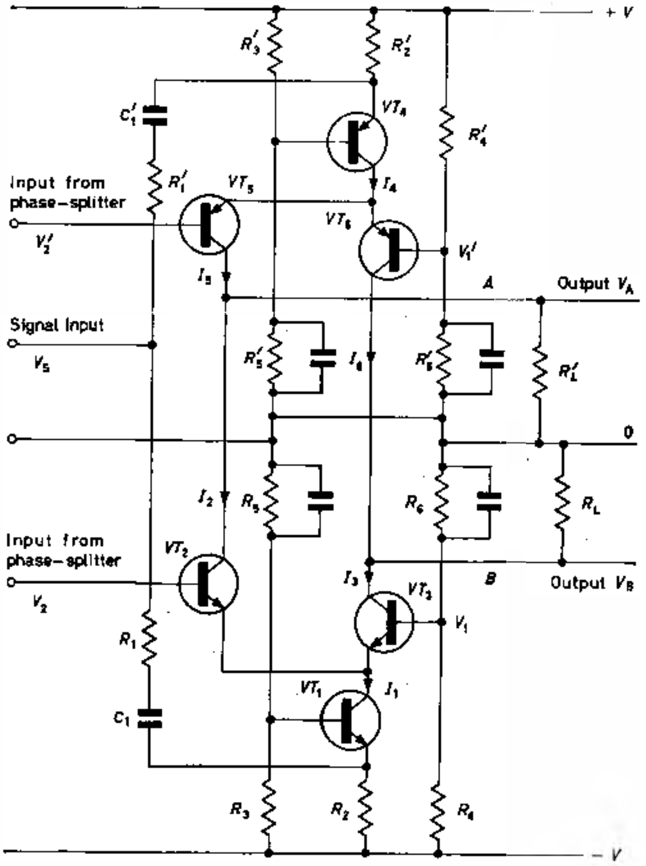

Fig. 2 Circuit diagram of the symmetrical current-switching gate

* J. J. Thomson Physical Laboratory, Reading, Berkshire

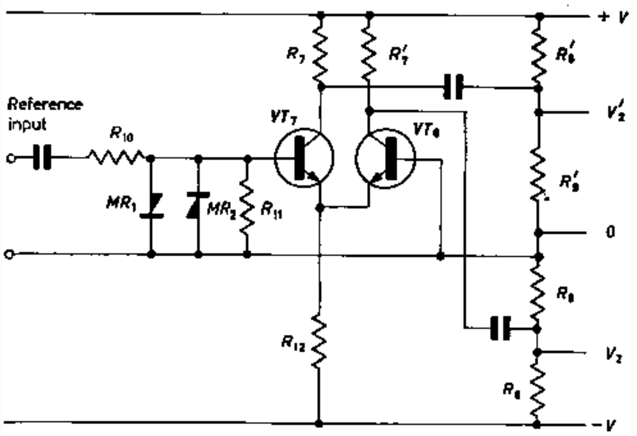

Fig. 3 Phase splitter for use with mark/space ratios close to unity

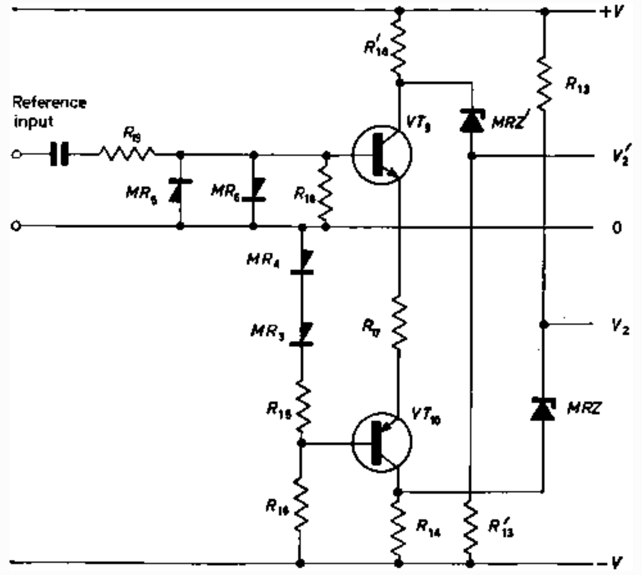

Fig. 4 Phase splitter for use with mark/space ratios differing greatly from unity

of transistors VT_1 and VT_4 via resistors R_1, R_1'; so that the collector currents (subject to the usual approximations) are given by

$$\left.\begin{aligned} I_1 &= (I_1)_0 - \alpha_1 V_S/R_1 \\ I_4 &= (I_4)_0 + \alpha_1 V_S/R_1' \end{aligned}\right\} \quad \ldots\ldots\ldots\ldots\ldots (1)$$

where $(I_1)_0$, $(I_4)_0$ are the standing currents in VT_1, VT_4, respectively, and α_1 is the common-base current gain of the transistors.

It will be assumed that the circuit has been adjusted so that, in the absence of any a.c. reference signal V_R, the voltages V_2 and V_2' have values of $(V_2)_0$ and $(V_2')_0$ such that each pair of switching transistors is balanced and $I_2 = I_3$ and $I_5 = I_6$. When a reference signal is applied, V_2 and V_2' have values given by

$$\left.\begin{aligned} V_2 &= (V_2)_0 + V_R \\ V_2' &= (V_2')_0 - V_R \end{aligned}\right\} \quad \ldots\ldots\ldots\ldots\ldots (2)$$

Assuming the usual exponential relationship between the collector current and base-emitter voltage in the switching transistors, we find that the ratios of their collector currents are given by

$$I_2/I_3 = I_5/I_6 = \exp{(V_R/V_t)} \quad \ldots\ldots\ldots (3)$$

where $V_t = kT/e$ and is equal to approximately 25mV at room temperature. The currents must also satisfy the relations

$$\begin{aligned} I_2 + I_3 &= \alpha_2 I_1 \\ I_5 + I_6 &= \alpha_2 I_4 \quad \ldots\ldots\ldots\ldots\ldots\ldots (4) \end{aligned}$$

where α_2 is the common-base current gain of the transistors $VT_{2,3,5,6}$, which are assumed identical.

Combining equations (3) and (4),

$$\left.\begin{aligned} I_2 &= \alpha_2 I_1 \frac{1}{1 + \exp{(-V_R/V_t)}} \\ I_5 &= \alpha_2 I_4 \frac{1}{1 + \exp{(-V_R/V_t)}} \end{aligned}\right\} \quad \ldots\ldots\ldots\ldots (5)$$

$$\left.\begin{aligned} I_3 &= \alpha_2 I_1 \frac{1}{1 + \exp{(V_R/V_t)}} \\ I_6 &= \alpha_2 I_4 \frac{1}{1 + \exp{(V_R/V_t)}} \end{aligned}\right\} \quad \ldots\ldots\ldots\ldots (6)$$

The output voltages V_A and V_B are given by

$$V_A = (I_5 - I_2)\, R_L' \quad \ldots\ldots\ldots\ldots\ldots\ldots (7)$$

$$V_B = (I_6 - I_3)\, R_L \quad \ldots\ldots\ldots\ldots\ldots\ldots (8)$$

and, assuming the circuit to be balanced at d.c., i.e. $(I_1)_0 = (I_4)_0$ and $R_1 = R_1'$, these may be written as

$$V_A = \frac{2\alpha_1\alpha_2 R_L'}{R_1} \, \frac{V_S}{1 + \exp{(-V_R/V_t)}} \quad \ldots\ldots (9)$$

$$V_B = \frac{2\alpha_1\alpha_2 R_L}{R_1} \, \frac{V_S}{1 + \exp{(V_R/V_t)}} \quad \ldots\ldots (10)$$

Equations (9) and (10) summarize the action of the circuit. Putting $V_t = 25$mV, it can be seen that a change in V_R from +170 to −170mV is sufficient to cause a change in the factor $1/[1+\exp{(-V_R/V_t)}]$ from 1/1·001 to 1/1000. Switching action therefore takes place during a change in V_R of the order of 350mV, provided that the speed is not limited by the characteristics of the switching transistors. In the case of generally available transistors ($f_t \simeq$ 400mHz), this limits the switching speed to about 5ns.

Two circuits are shown for the reference phase splitter, the first of which (Fig. 3) is designed for phase-sensitive detectors and other applications in which the reference mark/space ratio is close to unity. It consists of a long-tailed pair, the current being switched between VT_7 and VT_8 by a voltage on the base of VT_7. The voltage necessary for complete switching is about ±200mV; voltages greater than this have little further effect on the outputs. To prevent large voltages on the input causing base-emitter breakdown, a diode limiter is incorporated. The resistors R_8 and R_9 are, of course, equal to R_4 and R_6, respectively, and similarly with R_8', R_9', R_4', and R_6'.

The second circuit (Fig. 4) is designed for applications where the mark/space ratio differs greatly from unity, such as in boxcar integrators. Normally, the resistors R_{14}, R_{14}' and R_{17} are equal, thus giving a voltage gain of ±1. Temperature compensation is provided by the diodes MR_3, MR_4, forward bias is applied by R_{16} and diodes MR_5, MR_6 limit the input voltage to ±0·6V, thus giving an output of 1·2V peak-to-peak. The Zener diodes are chosen so that V_2 and V_2' are approximately equal to V_1 and V_1'.

Practical circuit

The list below shows the circuit values for a gate giving, before overload, a peak output of ±1V from an impedance of 1kΩ:

$V = 15$V

$R_1 = 1$	$R_4 = 2{\cdot}2$
$R_3 = 3{\cdot}9$	$R_5 = 2{\cdot}2$
$R_3 = 1$	$R_6 = 1$

Transistors: *n-p-n* MPS3646

p-n-p MPS3640

The circuit values for the phase splitters are given below:

$R_7 = 0{\cdot}22$ $R_{10} = 1$

$R_8 = 2{\cdot}2$ $R_{11} = 1$

$R_9 = 1$ $R_{12} = 3{\cdot}3$

Transistors as above

Diodes HS9008

$R_{13} = 4{\cdot}7$ $R_{17} = 0{\cdot}22$

$R_{14} = 0{\cdot}22$ $R_{18} = 1$

$R_{15} = 0{\cdot}1$ $R_{19} = 1$

$R_{16} = 2{\cdot}2$

$MRZ = 6{\cdot}2$V Zener diode

Transistors and diodes as above

All resistances are in kilohms.

The complete circuit (i.e. gate together with phase splitter) is set up initially so that, in the absence of any a.c. reference voltage, the currents in the switching pairs VT_2, VT_3 and VT_5, VT_6 are approximately equal. This is done for each section separately, as follows. To set up the *n-p-n* section, the base of the *p-n-p* transistor VT_4 is connected to the $+15$V rail, thus making I_4 (and therefore I_5, I_6) zero. R_4 is then adjusted to make V_A and V_B equal within a factor of 2. This procedure is repeated for the *p-n-p* section.

The d.c. balance $[(I_1)_0 = (I_4)_0]$ is then obtained as follows. A 1kHz sinusoidal voltage is applied at the reference input and the voltage V_A is monitored using an oscilloscope. The resulting squarewave voltage at V_A is removed by suitable adjustment of R_3 or R_3'.

Performance

The performance of the gate when used as a phase-sensitive detector is assessed in terms of the following parameters:

(i) linearity of response to in-phase signals

(ii) rejection of out-of-phase signals

(iii) d.c. drift of zero-signal output referred to full-scale output

(iv) temperature coefficient of the output with in-phase input.

These quantities depend on the signal level being considered; so that it is essential to refer them to the same specified input level. This will be termed the 0dB level.

The linearity of response to in-phase signals is determined by the intermodulation method, since departures from linearity of less than 1% are difficult to measure directly. The procedure adopted is as follows. A signal consisting of the sum of two sinusoids, each at the -6dB level, whose frequencies add up to that of the reference, is applied at the input. The beat at the output is measured by means of a voltmeter connected from *A* to *B*, and this is referred to the output obtained from a signal in phase with the reference at the 0dB level. Care must be taken to ensure that the low-order harmonics of the sinusoids do not coincide with the reference or harmonics of the reference.

In order to determine the rejection of out-of-phase signals, the output due to an in-phase signal at the -6dB level is measured. A -6dB voltage of frequency slightly greater than the reference is added to the input, and the change in output is expressed as a fraction. The d.c. output is measured as a function of temperature, with both zero signal and a 0dB in-phase signal. Typical results for the gate shown in Fig. 2 with the phase splitter of Fig. 3 are given below. The measurements are made at a 1 kHz reference frequency and the 0dB input level defined as the in-phase input necessary for an output of $\pm 0{\cdot}3$V:

Intermodulation product referred to full-scale output:	0·1%
Effect of out-of-phase signals referred to full-scale output:	$<$ 0·03%
D.C. drift of zero signal output referred to full-scale output:	0·02%
Temperature coefficient of output with in-phase input:	0·04%

The waveforms at output *B* with a 5MHz reference are shown in Fig. 5; the upper trace having an in-phase signal, the lower trace a quadrature signal.

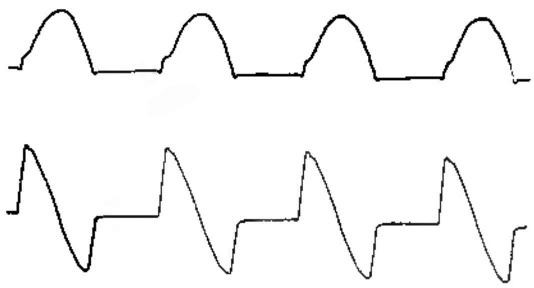

Fig. 5 Output of symmetrical current-switching gate when used as a phase-sensitive detector of 5MHz (the upper trace shows an in-phase signal, the lower trace a quadrature signal)

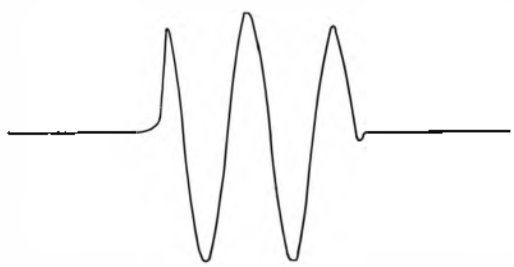

Fig. 6 Output of the gate with a 20MHz signal input, and a 4MHz squarewave (risetime $\simeq$ 7ns) on the reference input

An additional parameter which is of interest for applications requiring a short gate time is the switching speed. This is measured by applying fast-risetime pulses to the reference input (using the circuit of Fig. 4) and a synchronous sinewave at the 0dB level. The output of the gate is observed by means of a sampling oscilloscope connected across R_L, which, for purposes of this measurement, is reduced to 100Ω. A typical trace showing a 20MHz sinewave gated at a 4MHz rate is shown in Fig. 6, and this demonstrates the fast switching together with a notable absence of spikes. Switching speeds measured using a 2V reference pulse with 7ns rise and fall times are as follows:

Gate switch ON time : 4ns typical

Gate switch OFF time: 3ns typical

This circuit is the subject of a patent application.

REFERENCES

1 LACY, J. G.: A current switching phase-sensitive detector, *Electronic Engng*, *39*, 148 (1967).

2 FAULKNER, E. A., and HARDING, D. W.: A high performance phase-sensitive detector, *J. Sci. Instrum*, *43*, 97 (1966).

Accurate current-to-frequency convertor

by J. Korytkowski, M.Sc.*

An analogue-to-freqeuncy convertor having an output frequency proportional to the input current is described. The convertor produces a repetitive-pulse output, the frequency of which can be varied over the range 0-4kHz by an input-current range of 0-4mA; over the range 0-1mA, the accuracy is better than 0·1%. The convertor operation is based on the use of stable reference Zener diodes, an integrating capacitor and silicon transistors.

(Voir page 597 pour le résumé en français: Zusammenfassung in deutscher Sprache auf Seite 598)

THE convertor described uses the known technique of periodically charging and discharging the integrating device. Magnetically coupled multivibrators (i.e. solid-state voltage-to-frequency convertors using ferromagnetic inductors as integrating devices[1,2,3]) were developed more than ten years ago, and the quality of these convertors is continually improving[4,5]. It is impossible to achieve very good linearity with these convertors, since the magnetic properties of inductors change with wide-range frequency variations. Voltage-to-frequency convertors using special integrating amplifiers are also applied in digital voltmeters[6]; they have better accuracy than convertors using ferromagnetic inductors but they are not as simple. Simple transistorized analogue-to-frequency convertors previously described[7,8] have a poor accuracy.

When a signal is applied in the form of a current, it is possible to produce an accurately linear analogue-to-frequency convertor, since a simple but almost ideal current-integrating device—i.e. a capacitor—may be used. The integrating constant of such a device does not change practically over a wide frequency band.

Principle of operation

The basic circuit of the current-to-frequency convertor is shown in Fig. 1. The input current flows to a buffer amplifier *BA* which has a current gain nearly equal to unity. The amplifier provides a very high output resistance, so that the output current

$$I_{out} = k_B I_{in} \quad \ldots\ldots\ldots\ldots\ldots\ldots \quad (1)$$

does not depend in practice on the output voltage V_s. The output current charges an integrating capacitor C_5 through a compensating resistor R_6. The output voltage is fed to a transistorized switch *TS*; the characteristics of this switch are shown in Fig. 2. The switches S_1 and S_2 are opened when the input voltage V_s is lower than V_p (this voltage is the sum of V_r, the reference voltage, and V_t, the threshold voltage), and the leakage currents I_s' (comparator-input current) and I_s'' (a capacitor-discharge current) may be neglected.

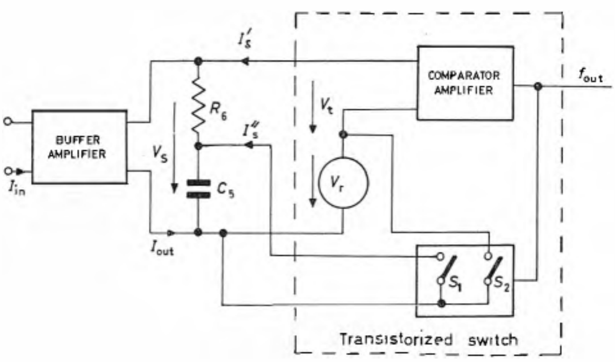

Fig. 1 Block diagram of convertor

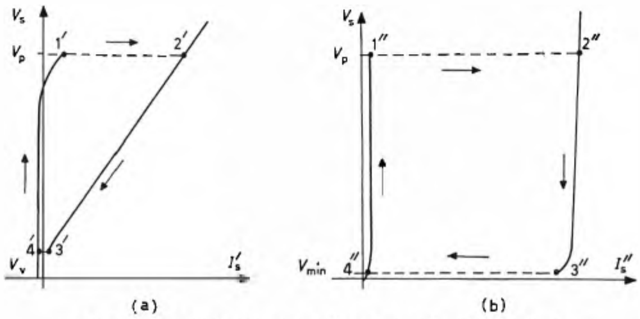

Fig. 2 Dynamic characteristic of transistorized switch

The voltage V_s across R_6 and C_5 is

$$V_s = R_6 I_{out} + 1/C_5 \int I_{out}\,dt \quad \ldots\ldots\ldots\ldots \quad (2)$$

When I_{out} is constant,

$$V_s = R_6 k_B I_{in} + V_{min} + \frac{k_B I_{in}}{C_5}\, t \quad \ldots\ldots\ldots\ldots \quad (3)$$

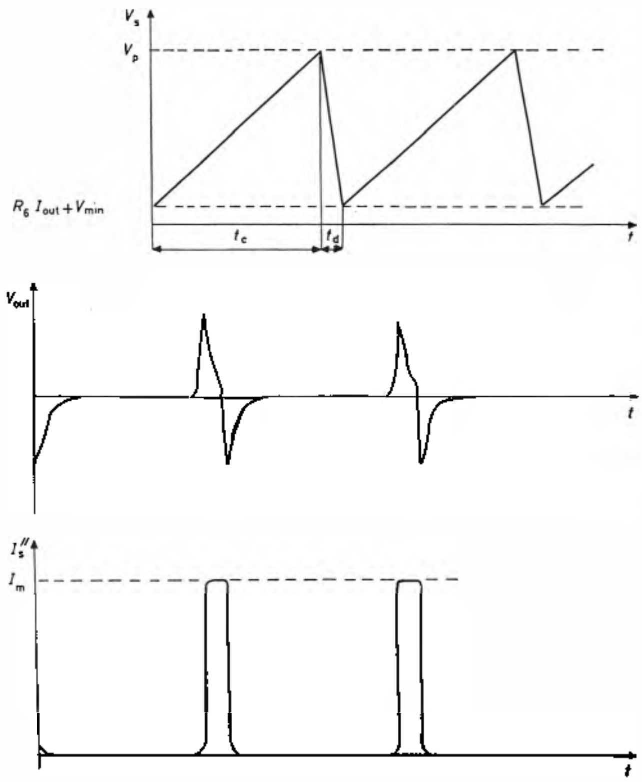

Fig. 3 Input and output voltage and current waveforms of transistorized switch

* *Instytut Elektrotechniki, Warsaw, Poland.*

so that V_s is a ramp voltage which rises linearly with time, as shown in Fig. 3.

When the output voltage V_s from the integrating circuit reaches a predetermined level V_p [points 1′ and 2′ on Fig. 2(a) and points 1″ and 2″ on Fig. 2(b)], it operates S_1 and S_2. These cause short-circuiting of reference-voltage source V_r and fast discharge of the integrating capacitor. Thus, if care is taken to ensure that discharge is at a constant large current, the discharge time t_d may be very short. When the input voltage V_s of the transistorized switch falls to a value equal to V_v, S_2 returns to the OFF state [points 3′ and 4′ on Fig. 2(a)], but if S_1 operates after a delay, the voltage across the capacitor drops to V_{min} [points 3″ and 4″ on Fig. 2(b)].

The frequency of the sawtooth waveform is

$$f_{out} = \frac{1}{t_c + t_d} \simeq 1/t_c - t_d/t_c^2 \quad \text{.......... (4)}$$

if $t_d \ll t_c$ .... (5)

where t_c is the charge time and t_d is the discharge time of the capacitor. The charge time t_c may be found from equation (3):

$$t_c = \frac{(V_p - V_{min} - R_6 k_B I_{in})\, C_5}{k_B I_{in}} = \frac{C_5}{k_B I_{in}}(V_p - V_{min}) - R_6 C_5 \quad \text{........ (6)}$$

and

$$f_{out} = \frac{1}{\dfrac{C_5(V_p - V_{min})}{k_B I_{in}} - R_6 C_5 + t_d} \quad \text{...... (7)}$$

When R_6 satisfies the equation

$$R_6 C_5 = t_d \quad \text{.................. (8)}$$

the frequency of the sawtooth wave is accurately proportional to the input current

$$f_{out} = \frac{k_B I_{in}}{C_5(V_p - V_{min})} \quad \text{.................. (9)}$$

The highest value of the input current when the circuit generates a sawtooth wave is limited to

$$I_{max} \simeq \frac{V_v - V_{min}}{R_6} \quad \text{........... (10)}$$

where V_v and V_{min} are the characteristic voltages of the transistorized switch (see Fig. 2).

The convertor

The circuit of the convertor is shown on Fig. 4.

Buffer amplifier

Two transistors VT_1 and VT_2 in Darlington configuration form a simple but accurate buffer amplifier fed from Zener diodes MRZ_{27} and MRZ_{28} working as a voltage source V_2. Thus, if care is taken to ensure a sufficient current gain from the Darlington pair and a very low residual current from the transistors, the amplifier non-linearity, temperature and supply errors are very small. The buffer-amplifier-fed integrating capacitor C_5 should have a very low leakage and a sufficiently low temperature capacitance coefficient.

Voltage reference source

Selected Zener diodes MRZ_{10} and MRZ_{11} produce a highly stable voltage drop V_0. The reference voltage V_r is the difference between V_0 and a compensating voltage drop V_k across silicon diodes MR_{38-40}. This arrangement gives a small increase of the reference voltage V_r due to the increase of the ambient temperature, and thus the temperature influence on the output frequency is compensated for. The temperature changes of k_B, V_{min} and t_d [equation (7)] are compensated for by a change of V_p, which depends on the reference voltage V_r and the threshold voltage V_t of the comparator amplifier.

The reference diodes MRZ_{10} and MRZ_{11} are fed from a constant-current source, which consists of a transistor VT_{22}, a Zener diode MRZ_{23}, a temperature-compensating diode MR_{24} and resistors R_{21}, and R_{25}. R_{21} is controlled to produce a supply current I_r at which the reference

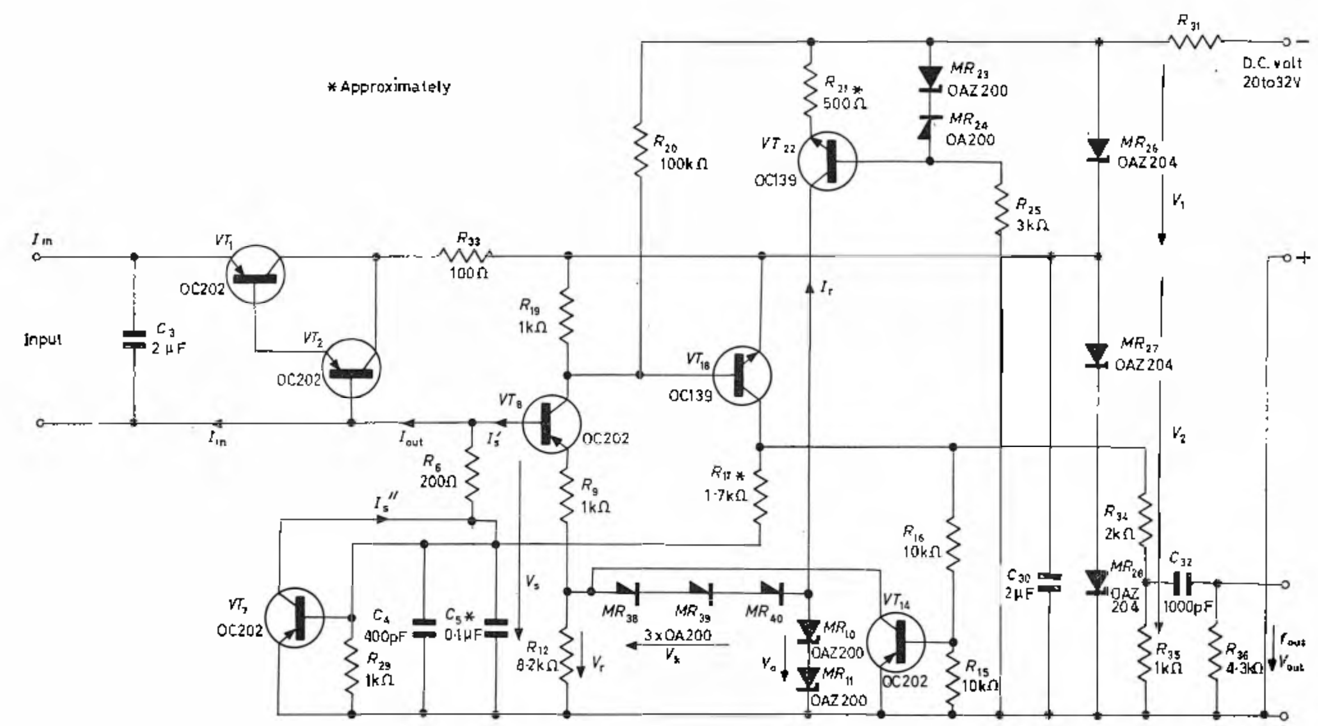

Fig. 4 Circuit diagram of convertor

diodes have a sufficiently small Zener voltage/temperature coefficient.

Comparator amplifier and transistor switches

Transistors VT_8 (*p-n-p* type) and VT_{18} (*n-p-n* type) form a simple comparator amplifier which controls transistor switches VT_7 and VT_{14}. When the emitter-base voltage on V_8 is greater than a particular threshold voltage, VT_{14} and VT_7 are switched on. These cause short-circuiting of the reference-voltage source V_r (by VT_{14}) and fast constant-current discharge of the integrating capacitor C_5 (by VT_7). The amplitude of the discharge current may be controlled by R_{17}. C_4 causes a delay action of switch VT_7, to ensure that the capacitor discharges to a very low collector-emitter saturating voltage.

The output voltage is taken from a voltage divider (R_{34} R_{35}) and a differentiating network (C_{32} R_{36}). This provides bidirectional voltage pulses of almost the same amplitude for positive and negative polarity (Fig. 3).

Adjustments

Four preset adjustments control:

(a) the current supplying the reference diodes
(b) the integrating-capacitor discharge current
(c) the temperature coefficient of output frequency
(d) the conversion ratio of the convertor.

(a) The current I_r supplying the reference diodes is adjusted by variation of R_{21}, so that the reference diodes have a sufficiently small Zener-voltage/temperature coefficient (approximately 12mA for OAZ200).

(b) The amplitude I_m of the discharge current I_s'' is controllable by R_{17} to a value rated for VT_7 (100mA for OC202).

(c) When the input current is constant, the output frequency of the convertor, according to equation (7), depends on the buffer-amplifier gain k_B, the voltages V_D and V_{min}, the discharge time t_d,the resistance R_6 and the capacitance C_5. The temperature change of the last two may be neglected if care is taken to choose the correct types of components. The approximate values of the temperature coefficients of the output frequency, as affected by different factors, are shown in Table 1.

TABLE 1

	Temperature coefficient	Conditions
$\frac{1}{f_n}\ \frac{\partial f}{\partial k_B}\ \frac{dk_B}{d\tau}$	+0·006% per degC	if transistor-Darlington-pair current gain is 500 (approximately), f_n = 1000Hz
$\frac{1}{f_n}\ \frac{\partial f}{\partial V_{min}}\ \frac{dV_{min}}{d\tau}$	+0·001 − 0·007% per degC	if $V_D \simeq 10V$
$\frac{1}{f_n}\ \frac{\partial f}{\partial t_d}\ \frac{dt_d}{d\tau}$	+0·015% per degC	if $I_d \simeq 100 I_{in}$

The temperature coefficient of the output frequency affected by the voltage V_D is negative and depends on the number of compensating diodes MR_{38-40} which are applied. In this way the coefficient may be reduced to a value not greater than ±0·007% per degC.

(d) The conversion ratio of the convertor is adjustable by variation of the value of the integrating capacitor C_5.

Convertor performance specification

Input

Input direct-current signal 0-1mA
Input voltage ⩽1·8V

Output

Output frequency of voltage pulses 0-1kHz
Output voltage: amplitude ⩾2V; pulse duration ⩾5μs
Load resistance ⩾20kΩ
Conversion ratio 1kHz/mA

Accuracy

Nonlinearity error ⩽0·1%
Temperature error ⩽0·1% for 10 degC temperature change
Supply error ⩽0·05% for 10% voltage change

Supply

Voltage 20-30V d.c.
Power consumption approximately 1W

An experimental convertor was built according to Fig. 4. Results of the investigations proved that the convertor performance was in accordance with the above specification. The errors of the convertor plotted against the input current for 19°C and 50°C are shown on Fig. 5.

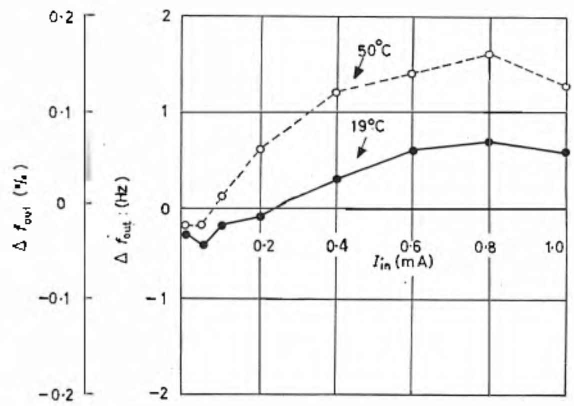

Fig. 5 Convertor errors plotted against input current for temperatures 19°C and 50°C

Conclusion

The current-to-frequency convertor described in this article has limited input-current and output-frequency ranges for high accuracy. The frequency and current ranges can be extended as better components become available. After modification, the current-to-frequency convertor may be a very useful measurement tool, in particular for analogue-current telemetering and control systems.

Acknowledgments

The work described was conducted while the author was visiting the University of Manchester Institute of Science and Technology and the author wishes to thank Prof. H. Rosenbrock and Dr. J. Rawcliffe for their assistance.

REFERENCES

1. Royer, G. H. A Switching Transistor D.C./A.C. Converter Having an Output Frequency Proportional to the D.C. Input Voltage. *Trans. Amer. Inst. Elect. Engrs. 74*, 332 (1955).
2. Van Allen, R. L. A Variable Frequency Magnetic Coupled Multivibrator. *ibid.*, 35 (1955).
3. Uchrin, G. C., Taylor, W. O. A New Self-Excited Square-Wave Transistor Power Oscillator. *Proc. Inst. Radio Engrs. 43*, 99 (1955).
4. Smiljanic, G. Operation of Magnetically Coupled Multivibrator with Square HB Loop Cores *Electronic Engng. 37*, 44 (1965).
5. Smiljanic, G. A Linear Voltage to Frequency Converter. *Industr. Electronics, 3*, 532 (1965).
6. Dance, J. B. Digital Voltmeters Basic Principles of Operation. *ibid.*, 332 (1965).
7. Walker, A. D. A Voltage Controlled Oscillator Using a Standard Integrated Circuit. *Electronic Engng. 38*, 21 (1966).
8. De Sa, A. A Digital Method of Measurement of Amplitude and Phase at Low Frequencies. *J. Sci. Instrum. 42*, 265 (1965).

Analysis of stub matching by scattering-matrix methods

by J. N. Saha, M.Tech., M.Sc.*

The use of a Smith chart in determining the frequency characteristics of a stub-matched radio-frequency transmission line involves considerable effort, particularly when determining the forward transmission of power on a very-high-frequency line supported by the large number of stubs encountered in practice. A digital computer can be usefully employed in solving such problems, by deriving expressions suitable for programming. In this article, for a transmission line consisting of 2-port network sections connected in cascade, the scattering matrixes of each section have been combined to yield an overall transfer matrix for both shunt and series stubs, and design equations for a perfect match have been derived. The frequency response of the line matched by a shunt stub, as well as by a series stub, has been calculated by a digital computer and plotted.

(Voir page 597 pour le résumé en français: Zusammenfassung in deutscher Sprache auf Seite 598)

In a stub-matching problem, the length of the stub and its point of insertion in the transmission line can be determined by the immittance method, as has been done by Wing and Eisenstein[1]. In this method, while the length of the stub and its location are determined in terms of normalized conductance and susceptance, the behaviour of the system outside the frequency of matching cannot be predicted. This can be done, however, with the help of a Smith chart; but then the calculation at frequencies at the regular intervals required for plotting the response becomes excessively laborious. For example, the forward transmission of r.f. power from the source to the load through a lossless line supported by the large number of stubs encountered in practice cannot be assessed readily by the immittance method, nor can it be conveniently determined using the Smith chart. While the analysis of matching by a single stub is described in this article, the transmission of r.f. power through a lossless line supported by several stubs will be dealt with separately.

The scattering-matrix technique adopted here leads to expressions that have been programmed on an Atlas digital computer, and the frequency response obtained has been plotted.

Symbols

a = incident parameter
b = reflected parameter
ρ = stub reflection coefficient with magnitude $|\rho|$ and angle θ_S
ρ_R = load reflection coefficient with magnitude $|\rho_R|$ and angle θ_R
ρ_{in} = input reflection coefficient with magnitude $|\rho_{in}|$
β = phase-change coefficient
l = line length
l_s = short-circuited stub length
l_o = open-circuited stub length
R = load impedance (resistive)
Z_0 = characteristic impedance
Z_3 = impedance terminating the stub of a 3-port network
$m = R/Z_o$
$t = 2\sqrt{m}/(m+1)$
b_S = normalized stub susceptance
x_S = normalized stub reactance
c, d = constants
f_0 = matched frequency (corresponding phase-change coefficient β_0)
f' = any other frequency (corresponding phase-change coefficient β')
$k = \beta'/\beta_0$
Subscript figures denote positions

Matching a transmission line by a shunt stub

The insertion of a stub in a transmission line gives rise to a 3-port network, with the line forming the main branches and the stub as the third branch. It has been shown recently[2] that such a network can be resolved effectively into a 2-port equivalent, with the help of the scattering-matrix formulation. For a shunt 3-port network,

$$\begin{bmatrix} a_i \\ b_i \end{bmatrix} = \frac{1}{2+2\rho}\begin{bmatrix} (3+\rho) & (1-\rho) \\ (\rho-1) & (1+3\rho) \end{bmatrix}\begin{bmatrix} b_o \\ a_o \end{bmatrix} \quad \ldots\ldots (1)$$

where a_i and b_i are the incident and reflected parameters at the input port and a_o and b_o those at the output port, respectively. ρ is given by

$$\rho = \frac{Z_3 - Z_0}{Z_3 + Z_0} \quad \ldots\ldots\ldots\ldots\ldots\ldots (2)$$

Z_3 being the terminating load of the shunting branch and Z_0 the characteristic impedance of the line and the stub.

The relationship between the input and output parameters of a lossless line of length l has been shown[3] to be

$$\begin{bmatrix} a_i \\ b_i \end{bmatrix} = \begin{bmatrix} e^{j\beta l} & 0 \\ 0 & e^{-j\beta l} \end{bmatrix}\begin{bmatrix} b_o \\ a_o \end{bmatrix} \quad \ldots\ldots\ldots\ldots (3)$$

For a transmission line of characteristic impedance Z_0 connected in cascade with another transmission line of characteristic impedance mZ_0, the transfer matrix of the step discontinuity can be worked out from elementary scattering-matrix methods. The relationship between the input and output parameters is given by

$$\begin{bmatrix} a_i \\ b_i \end{bmatrix} = \frac{1}{2\sqrt{m}}\begin{bmatrix} (m+1) & (m-1) \\ (m-1) & (m+1) \end{bmatrix}\begin{bmatrix} b_o \\ a_o \end{bmatrix} \quad \ldots (4)$$

If we introduce this concept of step discontinuity at the

* *Department of Communications, Government of India*

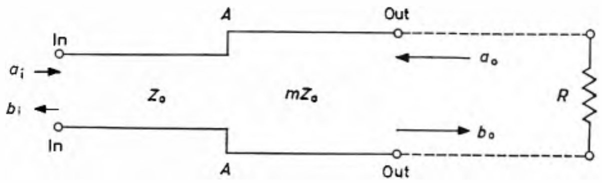

Fig. 1 Step discontinuity at the load end

load end of the transmission line (Fig. 1), we achieve, in fact, a matched condition at the OUT-OUT terminal. All the power flowing through the section between *A-A* and OUT-OUT is absorbed at *R*, and there is no reflection at the terminal OUT-OUT, i.e. $a_o = 0$. For the network of Fig. 1,

$$R/Z_0 = m \quad \text{(5)}$$

and the load reflexion coefficient $\rho_R(|\rho_R|\angle\theta_R)$ is given by

$$\rho_R = \frac{R - Z_0}{R + Z_0} = \frac{m-1}{m+1} \quad \text{(6)}$$

Equations (4) and (6) combine to give

$$\begin{bmatrix} a_i \\ b_i \end{bmatrix} = 1/t \begin{bmatrix} 1 & \rho_R \\ \rho_R & 1 \end{bmatrix} \begin{bmatrix} b_o \\ 0 \end{bmatrix} = b_o/t \begin{bmatrix} 1 & \rho_R \\ \rho_R & 1 \end{bmatrix} \quad \text{(7)}$$

where

$$t = \frac{2\sqrt{m}}{1+m} \quad \text{(8)}$$

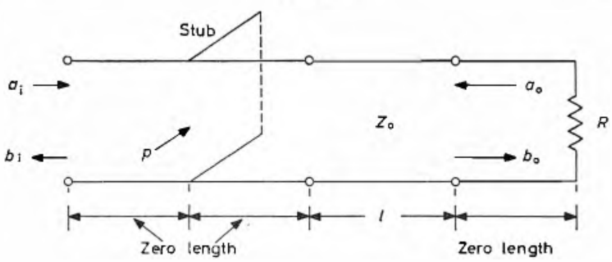

Fig. 2 Single stub configuration

If we connect a stub junction in cascade with a short section of a transmission line of length *l* terminated in a load *R* (Fig. 2), the overall transmission relationship can be obtained by merely combining their respective scattering matrixes. We then have, for the system shown in Fig. 2,

$$\begin{bmatrix} a_i \\ b_i \end{bmatrix} = \frac{1}{2+2\rho} \begin{bmatrix} (3+\rho) & (1-\rho) \\ (\rho-1) & (3\rho+1) \end{bmatrix} \begin{bmatrix} e^{j\beta l} & 0 \\ 0 & e^{j\beta l} \end{bmatrix} b_o/t \begin{bmatrix} 1 & \rho_R \\ \rho_R & 1 \end{bmatrix}$$

$$= \frac{b_o}{2t(1+\rho)} \begin{bmatrix} (3+\rho)\,e^{j\beta l} & (1-\rho)\,e^{-j\beta l} \\ (\rho-1)\,e^{j\beta l} & (1+3\rho)\,e^{-j\beta l} \end{bmatrix} \begin{bmatrix} 1 \\ \rho_R \end{bmatrix} \quad \text{(9)}$$

For a perfect match of the system,

$$b_i = 0 \quad \text{(10)}$$

Equations (9) and (10) yield

$$\rho_R\, e^{-j\beta l} = \frac{1-\rho}{1+3\rho} \quad \text{(11)}$$

With b_S as the normalized stub susceptance,

$$\rho = \frac{1 - jb_S}{1 + jb_S}$$

or

$$|\rho|\angle\theta_S = 1\angle\tan^{-1}[-2b_S/(1-b_S^2)] \quad \text{(12)}$$

Equations (11) and (12) combine to give

$$b_S = \frac{2|\rho_R|}{\sqrt{(1-|\rho_R|^2)}} \quad \text{(13)}$$

and

$$\theta_R - 2b\beta l = \tan^{-1}(2/b_S) \quad \text{(14)}$$

Since the reflection coefficient at a short-circuited termination is -1 and that at an open-circuited termination is $+1$, i.e.

$$\rho_{sc} = -1 = e^{j\pi} \quad \text{(15)}$$

$$\rho_{oc} = +1 = e^{j0} \quad \text{(16)}$$

we may write

$$\theta_S = \pi - 2\beta l_s \quad \text{(17)}$$

and

$$\theta_S = 0 - 2\beta l_o \quad \text{(18)}$$

where l_s and l_o are the lengths of the short- and open-circuited stub, respectively.

For each value of $|\rho_R|$ in equation (13), there are two roots of b_S, one positive and the other negative. If we denote one set of values by subscript 1, say, when the positive value of b_S is under consideration, and the other set by the subscript 2 when the negative value of b_S is under consideration, we may write

$$\theta_R - 2\beta l_1 = \tan^{-1}\frac{2}{-b_S} \quad \text{(19)}$$

$$\theta_{S1} = \tan^{-1}\frac{-2b_S}{1-b_S^2} \quad \text{(20)}$$

$$\theta_R - 2\beta l_2 = \tan^{-1}\frac{2}{b_S} \quad \text{(21)}$$

$$\theta_{S2} = \tan^{-1}\frac{2b_S}{1-b_S^2} \quad \text{(22)}$$

where l_1 and l_2 denote the corresponding stub distances from the load. Two cases deserve special treatment here:

Case 1: when $\theta_R = 0$

Since $\tan^{-1}(2/b_S)$ is a positive angle (less than 180°, i.e. lying in the second quadrant), in order to avoid a negative value for βl_1, we may put $\theta_R = 2\pi$ instead of zero in equation (19) without any loss of generality. Again, the angle θ_{S1} in equation (20) always lies in the third or fourth quadrant, e.g. $-135°$, $-50°$ etc.; so that βl_{s1} and βl_{o1} are obtained directly on substitution.

In equation (13), when for set 2 the negative value of b_S is considered, a negative value is automatically imposed on $|\rho_R|$, which must be taken into account by considering θ_R shifted by π radians because of this negative value of b_S. Thus equation (21) becomes

$$\pi - 2\beta l_2 = \tan^{-1} 2/b_S \quad \text{(23)}$$

whence βl_2 is calculated. The values of βl_{s2} and βl_{o2} for short- and open-circuited stubs at position 2 are readily obtained.

Case 2: when $\theta_R = \pi$

Putting $\theta_R = \pi$ in equation (19), βl_1 is obtained. For a short-circuited stub at position 1,

$$\beta l_{s1} = \frac{\pi - \theta_{S1}}{2} \quad \text{(24)}$$

where θ_{S1} is given by equation (20); βl_{o1} is obtained similarly.

When the negative value of b_S is considered, a shift in θ_R by π radians has to be considered, as before. Equation (21) then becomes

$$2\pi - 2\beta l_2 = \tan^{-1} 2/b_S \quad \text{(25)}$$

whence βl_2 is found. For a short-circuited stub at position 2,

$$\beta l_{s2} = \frac{\pi - \theta_{S2}}{2} \quad \ldots\ldots\ldots\ldots \quad (26)$$

For an open-circuited stub at position 2,

$$\theta_{S2} = 2\pi - 2\beta l_{o2} \quad \ldots\ldots\ldots\ldots\ldots \quad (27)$$

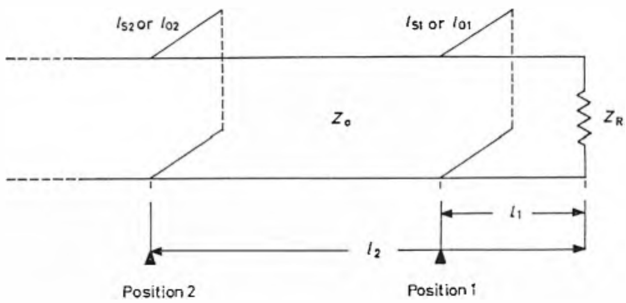

Fig. 3 Stub location in the transmission line

In equation (27), 2π has been substituted for zero to avoid a negative value of βl_{o2}. The possible stub configurations are shown in Fig. 3.

Matching a transmission line by a series stub

The relation between the input and output parameters in a shunt 3-port network has been stated in equation (1). The corresponding equation for the series 3-port network is obtained simply by replacing ρ by $-\rho$. The expression, equivalent to equation (9), can then be obtained as before, and the condition for a perfect match imposed and equations derived. Since

$$\rho = \frac{jx_S - 1}{jx_S + 1} = \exp(j\theta_S) \quad \ldots\ldots\ldots \quad (29)$$

where x_S is the normalized stub reactance, we may write

$$\theta_S = \tan^{-1}\frac{2x_S}{x_S^2 - 1} \quad \ldots\ldots\ldots\ldots \quad (30)$$

Proceeding as in the shunt stub, the design formulas can be worked out. The results for both shunt and series stubs are given Table 1.

TABLE 1

	Shunt Stub	Series Stub
	$b_S = 2\lvert\rho_R\rvert / \sqrt{(1-\lvert\rho_R\rvert^2)}$	$x_S = 2\lvert\rho_R\rvert / \sqrt{(1-\lvert\rho_R\rvert^2)}$
$\beta l_1 =$	$[c\pi - \tan^{-1}(2/b_S)]/2$	$[c\pi - \tan^{-1}(-2/x_S)]/2$
$\theta_{S1} =$	$\tan^{-1}[2b_S/(1-b_S^2)]$	$\tan^{-1}[2x_S/(x_S^2-1)]$
$\beta l_{s1} =$	$(\pi - \theta_{S1})/2$	$(\pi - \theta_{S1})/2$
$\beta l_{o1} =$	$-\theta_{S1}/2$	$(2\pi - \theta_{S2})/2$
$\beta l_2 =$	$[d\pi - \tan^{-1}(2/b_S)]/2$	$[d\pi - \tan^{-1}(-2/-x_S)]/2$
$\theta_{S2} =$	$\tan^{-1}[-2b_S/(1-b_S^2)]$	$\tan^{-1}[-2x_S/(x_S^2-1)]$
$\beta l_{s2} =$	$(\pi - \theta_{S2})/2$	$(\pi - \theta_{S_2})/2$
$\beta l_{o2} =$	$(2\pi - \theta_{S1})/2$	$-\theta_{S_2}/2$
when $\theta_R = 0$	$c = 2,\ d = 1$	$(\pi - \theta_{S2})/2$
when $\theta_R = \pi$	$c = 1,\ d = 2$	$-\theta_{S2}/2$

Frequency characteristics of a stub-matched transmission line

Table 1 gives the design formulas for the determination of the stub length (open- or short-circuited, shunt or series) and two possible locations nearest to the receiving end with a resistive termination. While there is full transmission of power at the matched frequency, reflection takes place at other frequencies, the determination of which will now be described.

From equation (9), the input reflection coefficient ρ_{in} is given by

$$\rho_{in} = b_i/a_i = \frac{(\rho - 1)e^{j\beta l} + \rho_R(3\rho + 1)e^{-j\beta l}}{(3 + \rho)e^{j\beta l} + \rho_R(1 - \rho)e^{-j\beta l}} \quad \ldots \quad (31)$$

Substituting $\rho = e^{j\theta_S}$ and $\rho_R = |\rho_R|e^{j\theta_R}$, and simplifying,

$$\frac{\{\cos\theta_S - 1 + |\rho_R|\cos(\theta_R - 2\beta l) + 3|\rho_R|\cos(\theta_S + \theta_R - 2\beta l) + j[\sin\theta_S + |\rho_R|\sin(\theta_R - 2\beta l) + 3|\rho_R|\sin(\theta_S + \theta_R - 2\beta l]\}}{\{3 + \cos\theta_S + |\rho_R|\cos(\theta_R - 2\beta l) - |\rho_R|\cos(\theta_S + \theta_R - 2\beta l) + j[\sin\theta_S + |\rho_R|\sin(\theta_R - 2\beta l) - |\rho_R|\sin(\theta_S + \theta_R - 2\beta l]\}} \quad \ldots\ldots\ldots \quad (32)$$

A transmission line of length l has an electrical length $\beta_0 l$ at a frequency f_0 corresponding to the phase-change coefficient β_0. At any other frequency f', the electrical length of the same line is $\beta' l$, or $(\beta'/\beta_0)\beta_0 l$. Denoting β'/β_0 by k, we may introduce this factor whenever a frequency-dependant term occurs, and thus generalize the expression.

The input reflection coefficient at position 1 is obtained by putting $l = l_1$, and $\theta_{S1} = \pi - 2k\beta l_{s1}$ for a short-circuited stub, and $\theta_{S1} = 2\pi - 2k\beta l_{o1}$ for an open-circuited stub, in equation (32). Those for position 2 can be obtained similarly.

The formulas given in Table 1 were programmed on an Atlas digital computer to determine the length of either open- or short-circuited stubs and their location for various load conditions. In the same program, the magnitude of ρ_{in}, as well as its angle given by equation (32) for all the stub configurations, were computed for the normalized frequency k ranging from 0 to 4, in steps of 0·05. The variation of the reflection coefficient with frequency for a few typical cases is shown in Figs. 4-7. For various values of $|\rho_R|$, the corresponding stub location and the stub length are shown in the figures.

For a short-circuited stub on the line, total reflection takes place at zero frequency, as shown in Figs. 4 and 6; because at this frequency the stub directly short-circuits the line, thereby preventing any power from reaching the load. For an open-circuited stub, at zero frequency, the input reflection coefficient has the same magnitude as the load reflection coefficient, as shown in Figs. 5 and 7. At the matched frequency, where $f/f_0 = 1$, there is no reflection. The variations are quite regular at frequencies about the matched frequency, but for frequencies further away from the matched frequency they are rather irregular. However, they agree with the results obtained on the Smith chart. The greater the degree of mismatch, i.e. the greater the value of $|\rho_R|$, the narrower is the frequency spectrum within a given magnitude of reflection coefficient.

For a particular load and a given reflection-coefficient maximum, it can be determined easily from these curves which stub configuration would allow the maximum bandwidth. As an example, for $|\rho_R| = 0{\cdot}50$, $\theta_R = 0$ and an input reflection coefficient not exceeding 0·40, the best choice would be the short-circuited stub at position 2, which allows a bandwidth of $0{\cdot}81\,f_0$ to $1{\cdot}30\,f_0$ (see Fig. 6).

The expression for the input reflection coefficient ρ_{in} for the system adopting a series stub can be derived as in the case of the shunt stub:

$$\rho_{in} = b_i/a_i = \frac{(\rho + 1)\,e^{j\beta l} + \rho_R(1 - 3\rho)\,e^{-j\beta l}}{(3 - \rho)\,e^{j\beta l} - \rho_R(\rho + 1)\,e^{-j\beta l}} \quad \ldots \quad (33)$$

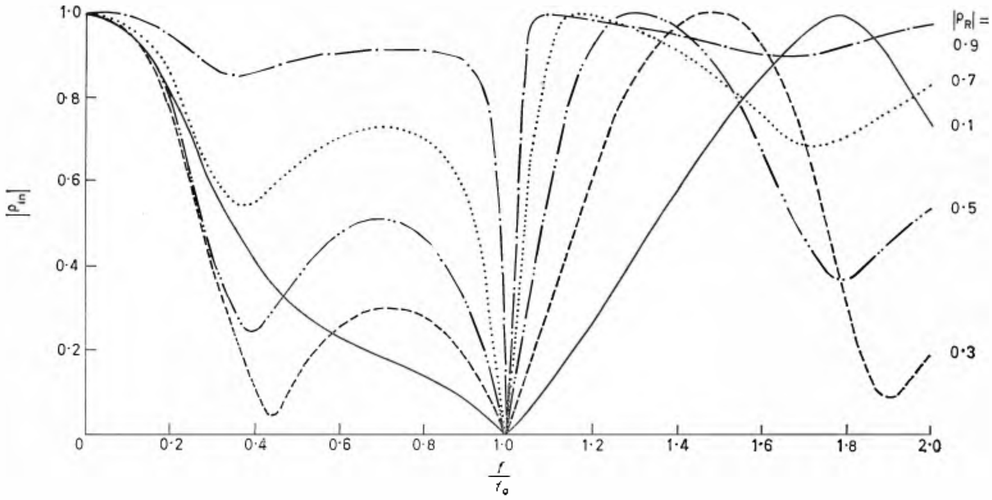

Fig. 4 Frequency response for s.c. shunt stub when $\theta_R = 0$, or for o.c. series stub when $\theta_R = \pi$, at position 1

$\lvert\rho_R\rvert$	$\beta_0 l_1$	Stub Length
0·1	132·1°	101·4°
0·3	126·3°	122·2°
0·5	120·0°	139·1°
0·7	112·8°	153·0°
0·9	102·9°	166·4°

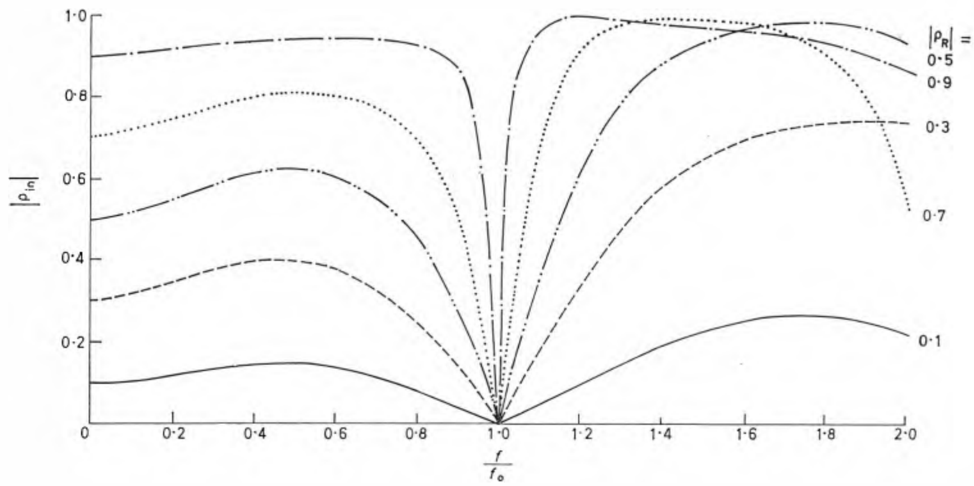

Fig. 5 Frequency response for o.c. shunt stub when $\theta_R = 0$, or for s.c. series stub when $\theta_R = \pi$, at position 1

$\lvert\rho_R\rvert$	$\beta_0 l_1$	Stub Length
0·1	132·1°	11·4°
0·3	126·3°	32·2°
0·5	120·0°	49·1°
0·7	112·8°	63·0°
0·9	102·9°	76,4°

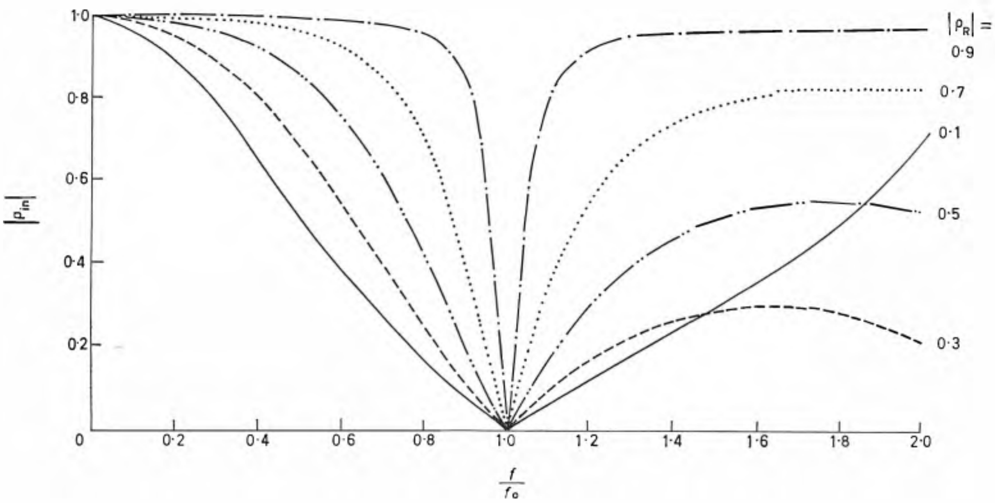

Fig. 6 Frequency response for s.c. shunt stub when $\theta_R = 0$, or for o.c. series stub when $\theta_R = \pi$, at position 2

$\lvert\rho_R\rvert$	$\beta_0 l_2$	Stub Length
0·1	47·9°	78·6°
0·3	53·7°	57·8°
0·5	60·0°	40·9°
0·7	67·2°	27·0°
0·9	77·1°	13·6°

The curves giving the variation of the input reflection coefficient with frequency for the series stub are shown, together with those for the shunt stub (Figs. 4 to 7).

On the Smith chart, the location of the admittance presented to a transmission line by a short-circuited shunt stub is directly opposite to that of the impedance of an open-circuited series stub of the same length, and hence their phases are separated by $\pi/2$ rad. Since the phase angle of the reflection coefficient is a function of the line length, the phase difference between the reflection coefficients in these two cases is π rad. Thus, a short-circuited shunt stub, when $\theta_R = 0$, inserted at position 1 has the

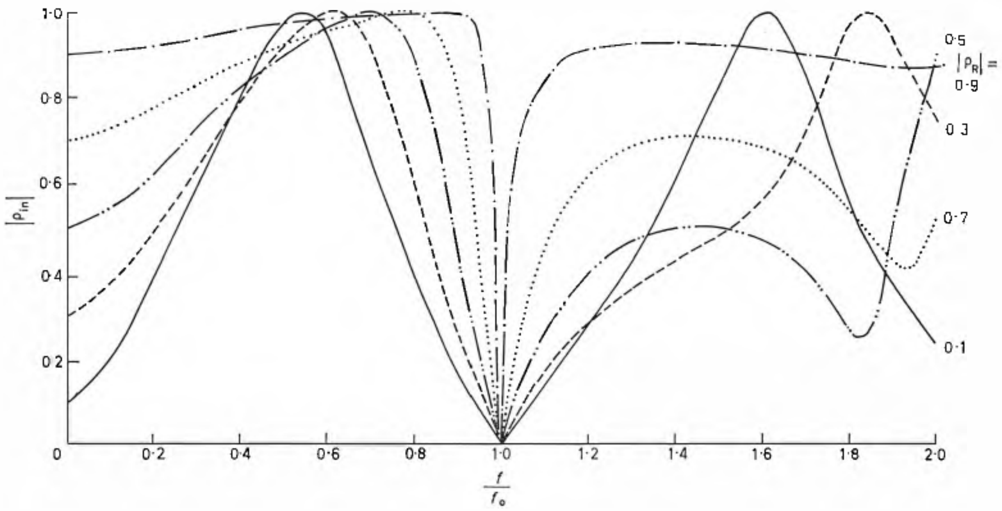

Fig. 7 Frequency response for o.c. shunt stub when $\theta_R = 0$, or for s.c. series stub when $\theta_R = \pi$, at position 2

$\lvert\rho_R\rvert$	$\beta_0 l_2$	Stub Length
0·1	47·9°	168·6°
0·3	53·7°	147·8°
0·5	60·0°	130·9°
0·7	67·2°	117·0°
0·9	77·1°	103·6°

same matching effect as an open-circuited series stub of the same length, when $\theta_R = \pi$, inserted at the same position. Fig. 4 testifies to this fact. Similarly, the frequency response of the system of an open-circuited shunt stub at position 1, when $\theta_R = 0$, is the same as that of a short-circuited series stub at the same position, when $\theta_R = \pi$, as illustrated in Fig. 7. The curves in other figures can be explained in the same way.

Conclusions

Formulas for shunt- and series-stub matching have been derived using the scattering-matrix approach. Frequency responses for different stub configurations have been computed and plotted. The results have been verified on the Smith chart and found to be correct. The scattering-matrix formulation can be extended to the case of a transmission line supported by a large number of stubs, and the transmission characteristics can be obtained by programming on a digital computer.

Acknowledgments

The author is grateful to the Government of India for financing the research and to Prof. C. Adamson for providing research facilities in the Department of Electrical Engineering and Electronics, the University of Manchester Institute of Science and Technology.

REFERENCES

1 Wing, A. H., Eisenstein, J.: Single- and Double-Stub Impedance Matching. *J. Appl. Phys.* *15*, 615 (1944).
2 Gledhill, C. S.: Resistor Transmission Line Circuits. *Proc. IEE*, *112*, 2046 (Nov. 1965).
3 Kuo, F. F.: *Network Analysis and Synthesis*, p. 365, Wiley, 1964.

Backfire meander-line antenna

by S. C. Loh† and J. Jacobsen*, Ph.D., A.Inst.P.

An experimental study of the radiation characteristics of the meander-line antenna operated under backfire conditions is described. Electrical performance is generally improved, particularly with regard to the halfpower bandwidth and the operating-frequency beamwidth.

(Voir page 597 pour le résumé en français: Zusammenfassung in deutscher Sprache auf Seite 598)

THE meander-line antenna first proposed by Maclean[1] is a linearly polarized antenna of the form shown in Fig. 1. It radiates in the endfire direction as the result of a travelling wave of current along the antenna structure. Its useful bandwidth has been found experimentally to be approximately $\pm 6\%$ of its centre frequency of operation, with a sidelobe level better than 6dB. It has also a rather large halfpower beamwidth, ranging from 20°-40° to 25°-80° for the *E*- and *H*-planes, respectively. Moreover, it is claimed by Maclean[1] that the meander-line antenna has

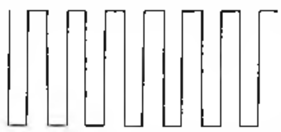

Fig. 1 Meander line

* *Laboratory of Electromagnetic Theory, Technical University of Denmark, Lyngby, Denmark.*

† *Formerly with the Technical University of Denmark; now with the Physics Department, Chinese University of Hong Kong.*

been shown to be an acceptable alternative to the Yagi and zigzag antennas. It gives a slightly better bandwidth (12%) than the Yagi (10%) and greater ease of construction than the zigzag, particularly for large conductor diameters.

The backfire meander-line antenna consists of an ordinary endfire meander-line structure, terminated at the open end, opposite to the feed end, by a large surface-wave plane reflector (the term surface-wave plane reflector was proposed by Ehrenspeck[2-7] to distinguish it from the ordinary plane reflector used in the antenna array). The

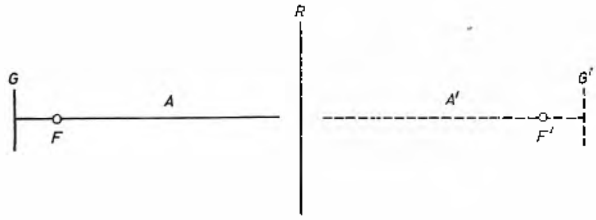

Fig. 3 Simplified version of backfire antenna

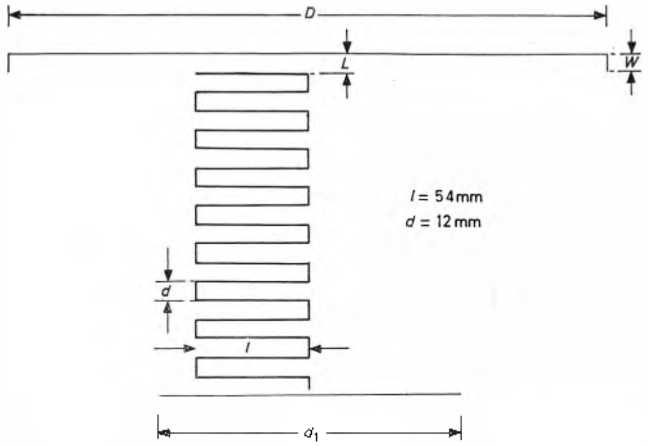

Fig. 2 Backfire meander-line antenna

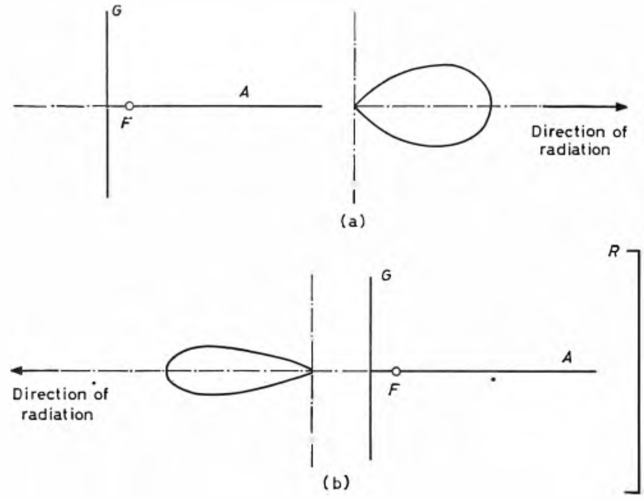

Fig. 4 Principle of (a) endfire and (b) backfire antennas

configuration of the antenna structure is shown in Fig. 2. Although the new antenna offers a similar sidelobe level and slightly better bandwidth (±10%), the halfpower beamwidth is greatly improved.

Principle of the backfire antenna

The direction of radiation of an ordinary endfire antenna may be reversed if a large surface-wave plane reflector is placed at the open end of the endfire structure *A* (shown in Fig. 3), opposite to the feed. Because of the reversed direction of radiation, the new antenna is thus called a backfire attenna.

The backfire principle was first applied by Ehrenspeck to the endfire (Yagi) antenna, and improved radiation properties were achieved. The present authors have also undertaken a detailed experimental study of the backfire helical and zigzag antennas[8-9] and found the results very promising. Although only detailed experimental studies of backfire antennas have been undertaken so far, a satisfactory theoretical analysis of the antenna is yet to be found. Nevertheless, a qualitative approach to the design has been proposed by Zucker[10].

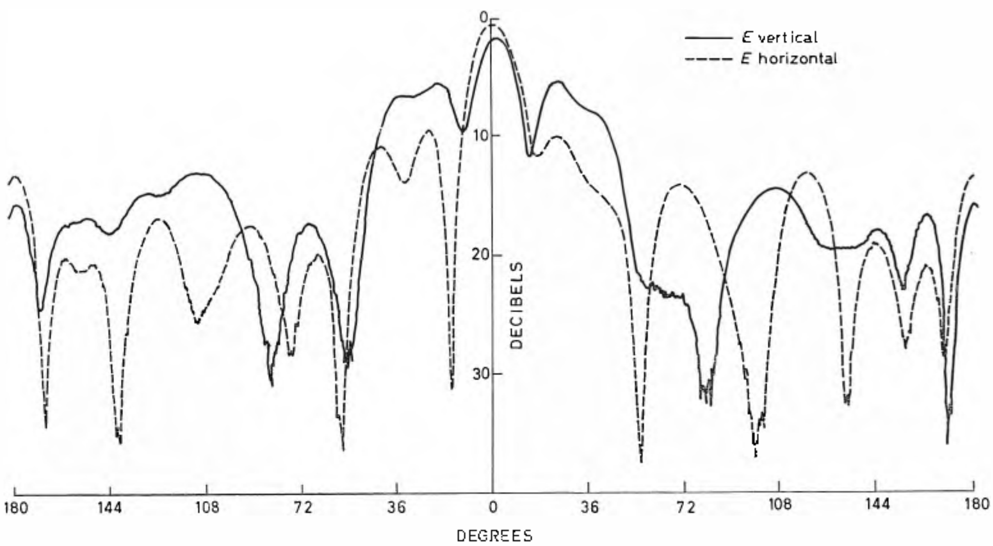

Fig. 5 Radiation pattern for backfire meander-line antenna

Construction

The antenna was tested in an anechoic chamber and the test frequency was chosen as 3GHz (S-band) for the sake of convenience in construction of the antenna. An 8-turn meander-line antenna was constructed with $l/d = 4{\cdot}5$, suggested by Maclean as the best dimension ratio. Three different sizes of plane reflector were used, namely $d_1 = 15$, 20 and 25cm. The circular plane reflector of diameter $d_1 = 20$cm ($d_1 = 2\lambda_0$, where λ_0 is the wavelength at the centre frequency, i.e. $f_0 = 3$GHz) gave the best result. It has been found that the circular surface-wave plane reflector of diameter $D = 40$cm, with a rim of width $W = 2{\cdot}5$cm, gave the best radiation patterns. The size of the plane reflector (d_1) and the width of the rim (W) have very little influence on the main lobe, but they do affect the sidelobe level slightly. The distance L between the open termination of the antenna and the surface-wave plane reflector varies between 0·1 and 0·25cm and has no effect on the radiation patterns taken.

Experimental results

The backfire meander-line antenna (end-fed) was used as a receiving antenna, and E- and H-plane radiation patterns were recorded. The best patterns, judged by the sidelobe level, are shown in Fig. 5. These were recorded at a frequency of 2·4GHz. At other frequencies in the operating

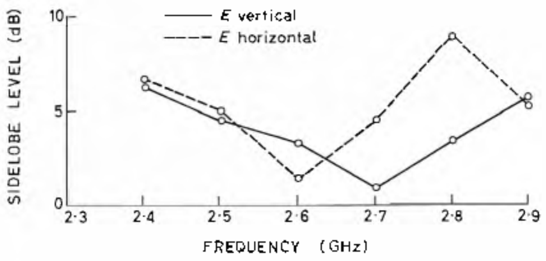

Fig. 6 Sidelobe level versus frequency for backfire meander-time antenna

range of the antenna, the sidelobes were in general rather high, and Fig. 6 shows the variations of the worst sidelobe levels with respect to the main lobe. Fig. 7 shows the halfpower beamwidth for the meander-line antenna against armlength l of the antenna, where the armlength is expressed in terms of free-space wavelength (λ_0). It shows a remarkable improvement over the ordinary endfire meander-line antenna. It varies between 14°-19° and 12°-16° for the two principal planes. The variation of the backlobe level (in dB) against frequency is shown in Fig. 8.

Conclusions

The backfire meander-line antenna has been shown to possess better radiation properties than the ordinary endfire meander-line antenna. It offers a slightly better bandwidth and also much better halfpower beamwidth with the same sidelobe level.

Acknowledgments

This work was carried out at the Laboratory of Electromagnetic Theory, The Technical University of Denmark, and one of the authors (S.C.L.) is grateful to Prof. L. H. Knudsen for the invitation to work in the laboratory. The authors wish to thank R. F. Millar for his interest and suggestions concerning the material in this paper.

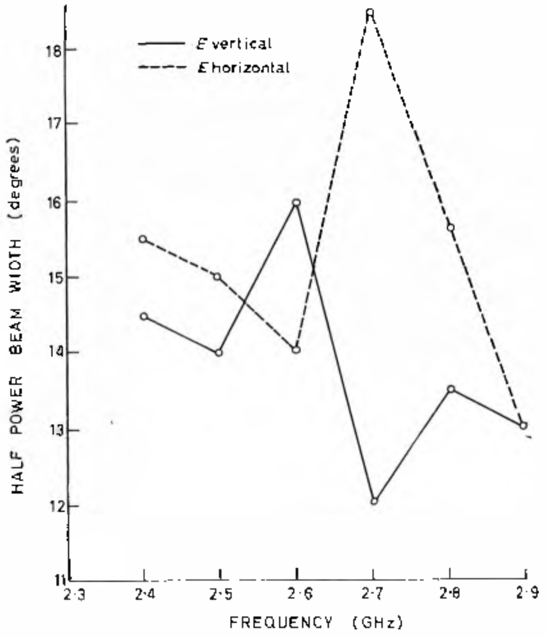

Fig. 7 Halfpower beamwidth versus frequency for backfire meander-line antenna

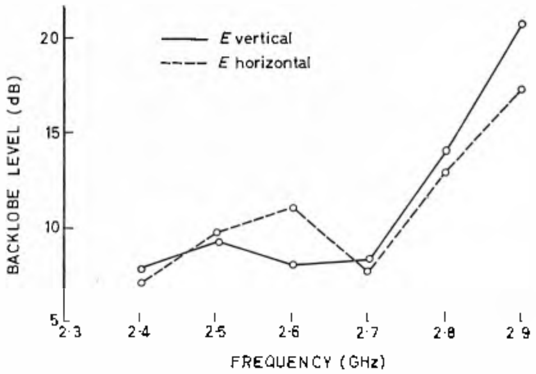

Fig. 8 Backlobe level versus frequency for backfire meander-line antenna

REFERENCES

1 MACLEAN, T. S. M.: The meander-line aerial. *Electronic Engng*, *37*, 667-669 (Oct. 1965).

2 EHRENSPECK, H. W.: The backfire antenna, a new type of directional line source. *Proc. Inst. Radio Engrs*, *48*, 109-110 (Jan. 1960).

3 EHRENSPECK, H. W.: The backfire antenna, a new type of directional line source. AFCRL Report 722, Air Force Cambridge Research Laboratories, Bedford, Mass., USA (Aug. 1961).

4 EHRENSPECK, H. W.: Reflection antenna employing multiple director elements and multiple reflection of energy to effect increased gain. US Patent 3 122 745 (Feb. 1964).

5 STORM, J. A., EHRENSPECK, H. W.: Backfire antennas for SHF, UHF and VHF bands. AFCRL 63-114, Air Force Cambridge Research Laboratories (April 1963).

6 EHRENSPECK, H. W.: The backfire antenna: new results. *Proc. Inst. Elect. Electronic Engrs*, *53*, 639-641 (June 1965).

7 EHRENSPECK, H. W.: The short backfire antenna. *ibid.*, *53*, 1138-1140 (Aug. 1965).

8 LOH, S. C., JACOBSEN, J.: The radiation characteristics of the backfire helical and zigzag antenna (to be published by the Institute of Electronics and Radio Engineers).

9 LOH, S. C., JACOBSEN, J.: An experimental study of the radiation characteristics of some backfire antennas. Report IR36, Laboratory of Electromagnetic Theory, The Technical University of Denmark (May 1966).

10 ZUCKER, F. J.: The backfire antenna: a qualitative approach to its design. *Proc. Inst. Elect. Electronics Engrs*, *53*, 764-747 (July 1965).

Directivity of an array of slots on the surface of a cylinder

by J. Ricardi*

General expressions for the directivity of arrays of axial and circumferential slots on an infinite conducting cylinder are derived. The optimum spacing for 2- to 7-slot arrays on an infinite cylinder between 1 and 4 wavelengths in diameter is presented, and the minimum number of slots required to produce a uniform pattern in the equatorial plane is determined.

(Voir page 597 pour le résumé en français: Zusammenfassung in deutscher Sprache auf Seite 598)

IT is generally understood that the electric dipole and the slot are the two fundamental radiators which serve as a building block for the array-antenna designer. A great deal of theoretical analysis has been carried out in order to understand the properties and performance characteristics of these elements when they are operated in free space or in the immediate vicinity of a flat plane, an infinite circular cylinder, a sphere or an oblate spheroid. Although the literature contains much information on axial or circumferential slots located on the surface of a conducting right-circular cylinder[1-4], an expression for the directivity of the array has not been presented. In this article, the results previously derived are used to develop an expression for the directivity of an array of axial and circumferential slots. Curves are presented showing the variation in directivity as a function of the number of slots, the angular spacing between them and the radius of the cylinder, with two modes of excitation.

General expressions

Figs. 1(a) and (b) represent a slot on a section of an infinitely long right-circular conducting cylinder coaxial with the z-axis. A cylindrical-co-ordinate system (ρ, ϕ, z) specifies the locations of the slots, which are separated from one another by an angle τ. The vector ρ makes an angle ϕ with the reference direction through the 0th slot. The vector r, whose direction is determined by the angles θ and ψ locates the observation point. The length, L or α, and the width, W or α, are symmetrically distributed about the radius which determines the location of the centre of each slot.

Using the common expressions for the field of a single slot on a cylinder[5] and applying the principle of superposition, one obtains the field of an array of axial or circumferential slots:

$$E_{\phi a}(\theta, \phi) = M_1 f_1(\theta) \sum_{n=0}^{\infty} \sum_{p=0}^{N-1} \epsilon_n \frac{j^n b_p \exp(j\psi_p) \cos n(\phi - p\tau)}{H_n^{(2)\prime}(ka \sin\theta)} \quad \ldots\ldots\ldots (1)$$

and

$$E_{\theta a}(\theta, \phi) = 0 \quad \ldots\ldots\ldots\ldots\ldots\ldots (2)$$

for an axial slot array, where $\epsilon_n = 1$ ($n=0$), $\epsilon_n = 2$ ($n \neq 0$),

$$M_1 = \frac{\exp(-jkr)\, L}{\pi^3 a r} \quad \ldots\ldots\ldots\ldots (3)$$

and

$$f_1(\theta) = \left\{ \frac{\cos[(kL/2)\cos\theta]}{1 - [(kL/\pi)\cos\theta]^2} \right\} \quad \ldots\ldots\ldots (4)$$

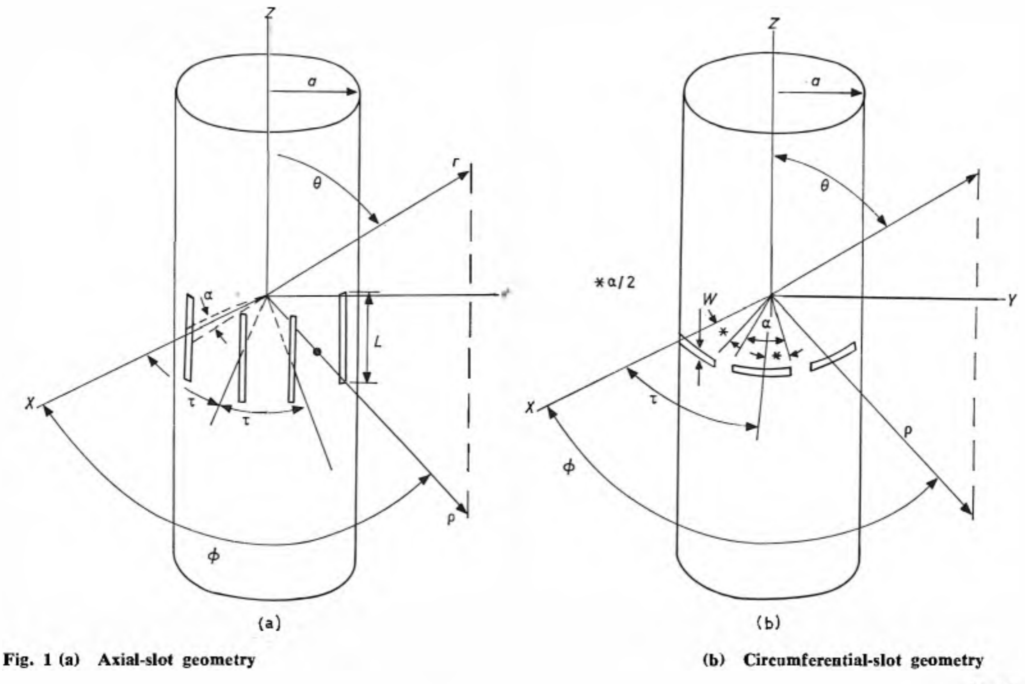

Fig. 1 (a) Axial-slot geometry **(b) Circumferential-slot geometry**

* *Massachusetts Institute of Technology, Lexington, Massachusetts, USA (operated with support from the USAF)*

For a circumferential slot array,

$$E_{\phi c}(\theta, \phi) = j\frac{M_2 f_2(\theta)}{\sin\theta}$$

$$\sum_{n=0}^{\infty}\sum_{p=0}^{N-1} \times \epsilon_n \frac{nj^n \cos(n\alpha/2) b_p \exp(j\psi_p) \sin n(\phi - p\tau)}{[\pi^2 - (n\alpha)^2] H_n^{(2)\prime}(ka\sin\theta)} \quad (5)$$

$$E_{\theta c}(\theta, \phi) = \frac{M_2}{\sin\theta}$$

$$\sum_{n=0}^{\infty}\sum_{p=0}^{N-1} \times \epsilon_n \frac{j^n \cos(n\alpha/2) b_p \exp(j\psi_p) \cos n(\phi - p\tau)}{[\pi^2 - (n\alpha)^2] H_n^{(2)}(ka\sin\theta)} \quad (6)$$

where $$M_2 = \frac{\alpha \exp(-jkr)}{j\pi r} \quad (7)$$

$$f_2(\theta) = \frac{\cot\theta}{jka} \quad (8)$$

n is an integer; $H_n^{(2)}$ and $H_n^{(2)\prime}$ are the Hankel function of the second kind and its first derivative (with respect to the argument), respectively; $k = 2\pi/\lambda$ and λ is the wavelength of operation. The subscripts ϕ and θ, whenever they are used, indicate the positive direction of the associated electric field; the subscripts a and c indicate whether the variable is associated with an axial or a circumferential array of slots, respectively. The constants b_p and ψ_p are the amplitude and phase of the voltage exciting the pth slot.

The directivity D of any antenna is defined[6] as

$$D(\theta_0, \phi_0) = \frac{4\pi|E(\theta_0, \phi_0)|^2}{\int_0^{2\pi} d\phi \int_0^{\pi} d\theta \, |E(\theta, \phi)|^2 \sin\theta} \quad (9)$$

where $E(\theta, \phi)$ is the total field intensity in the direction θ and ϕ. Substituting equation (1) into equation (9) and performing the ϕ integration gives

$$D_{\phi a}(\theta_0, \phi_0) = \frac{\left| f_1(\theta_0) \sum_{n=0}^{\infty}\sum_{p=0}^{N-1} \epsilon_n \frac{j^n b_p \exp(j\psi_p) \cos n(\phi_0 - p\tau)}{H_n^{(2)\prime}(ka\sin\theta_0)} \right|^2}{\sum_{n=0}^{\infty} \epsilon_n \left(\sum_{p=0}^{N-1} b_p^2 + 2\sum_{p=0}^{N-2}\sum_{q=p+1}^{N-1} b_p b_q \xi_{pq} \right) Q_n} \quad (10)$$

where $$\xi_{pq} = \cos n(p-q)\tau \cos(\psi_p - \psi_q)$$

and $$Q_n = \int_0^{\pi/2} \frac{f_1^2(\theta)\sin\theta d\theta}{|H_n^{(2)\prime}(ka\sin\theta)|^2}$$

Similarly, the use of equations (5), (6) and (9) results in $D_{\theta c}(\theta_0, \phi_0) =$

$$\frac{\left| \frac{M_2}{\sin\theta_0} \sum_{n=0}^{\infty}\sum_{p=0}^{N-1} \epsilon_n \frac{j^n \cos(n\alpha/2) b_p \exp j\psi_p) \cos n(\phi_0 - p\tau)}{[\pi^2 - (n\alpha)^2] H_n^{(2)}(ka\sin\theta_0)} \right|^2}{\sum_{n=0}^{\infty} \cos^2(n\alpha/2) \left(\sum_{p=0}^{N-1} b_p^2 + 2\sum_{p=0}^{N-2}\sum_{q=p+1}^{N-1} b_p b_q \xi_{pq} \right) R_n} \quad (11)$$

where

$$R_n = \int_0^{\pi/2} \left\{ \frac{\epsilon_n}{|H_n^{(2)}(ka\sin\theta)|^2} + \left[\frac{\sqrt{2}\, n\cot\theta}{ka|H_n^{(2)\prime}(ka\sin\theta)|} \right]^2 \right\} \frac{M_2^2 d\theta}{\sin\theta}$$

It is appropriate to point out that these expressions have been derived by assuming that the voltage is sinusoidally distributed along the slot, that the cylinder is a perfect conductor infinitely long, that the slot length is much larger than its width and that the observation point is located in the far field.

Uniform excitation

These results can be simplified by specializing to a particular configuration and excitation distribution. For example, if all the slots are excited in phase and with the same amplitude, equations (10) and (11) become

$$D_{\phi a}[(\pi/2), (N-1)\tau/2] = \frac{\left| \sum_{n=0}^{\infty}\sum_{p=0}^{N_0} \frac{\epsilon_n \epsilon_p j^n \cos(n\beta_p\tau/2) f_1(\pi/2)}{H_n^{(2)\prime}(ka)} \right|^2}{\sum_{n=0}^{\infty}\sum_{p=0}^{N_0} \epsilon_n \{\epsilon_p \cos n\beta_p\tau/2\}^2 Q_n} \quad (12)$$

$$D_{\theta c}[(\pi/2), (N-1)\tau/2] = \frac{\left| \sum_{n=0}^{\infty}\sum_{p=0}^{N_0} \frac{\epsilon_n \epsilon_p j^n \cos(n\beta_p\tau/2)\cos(n\alpha/2) M_2}{[\pi^2 - (n\alpha)^2] H_n^{(2)}(ka)} \right|^2}{\sum_{n=0}^{\infty}\sum_{p=0}^{N_0} \epsilon_n \cos^2(\alpha/2)\{\epsilon_p \cos(n\beta_p\tau_2)\}^2 N_n} \quad (13)$$

where $N_0 = (N-1)/2$, $\beta_p = 2p$

for N an odd integer, and

$N_0 = N/2$, $\beta_p = 2p + 1$

for N an even integer.

The values $\theta_0 = \pi/2$ and $\phi_0 = (N-1)\tau/2$ were chosen because, with many practical antennas, the maximum directivity is in this direction.

Still further simplification of the field equations can be made if the array of slots extends *completely round* the cylinder, and the slots are equally spaced and are excited in phase and with equal amplitude. Referring to equations (1), (5) and (6), these conditions require that $b_p = 1$, $\psi_p = 0$ and $N\tau = 2\pi$. Making these substitutions,

$$E_{\phi a} = M_1 f_1(\theta) N \sum_{n=0}^{\infty} \epsilon_n \frac{j^{nN} \cos nN\phi}{H_{nN}^{(2)\prime}(ka\sin\theta)} \quad (14)$$

$$E_{\phi c} = \frac{jM_2 f_2(\theta) N}{\sin\theta} \sum_{n=0}^{\infty} \epsilon_n \frac{j^{nN} nN \cos(nN\alpha/2) \sin nN\phi}{[\pi^2 - (nN\alpha)^2] H_{nN}^{(2)\prime}(ka\sin\theta)} \quad (15)$$

$$E_{\theta c} = \frac{M_2 N}{\sin\theta} \sum_{n=0}^{\infty} \epsilon_n \frac{j^{nN} \cos(nN\alpha/2) \cos nN\phi}{[\pi^2 - (nN\alpha)^2] H_{nN}^{(2)}(ka\sin\theta)} \quad (16)$$

and the directivity becomes

$$D_{\phi a}(\theta_0, \phi_0) = \frac{\left| f_1(\theta_0) \sum_{n=0}^{\infty} \epsilon_n \frac{j^{nN} \cos nN\phi_0}{H_{nN}^{(2)\prime}(ka\sin\theta)_0} \right|}{\sum_{n=0}^{\infty} \epsilon_n Q_{nN}} \quad (17)$$

$$D_{\theta c}(\theta_0, \phi_0) = \frac{\left| \frac{M_2}{\sin\theta_0} \sum_{n=0}^{\infty} \epsilon_n \frac{j^{nN} \cos(nN\alpha/2) \cos(nN\phi_0)}{H_{nN}^{(2)}(ka\sin\theta_0)[\pi^2 - (n\alpha N)^2]} \right|^2}{\sum_{n=0}^{\infty} \left[\frac{\cos(nN\alpha/2)}{\pi^2 - (nN\alpha)^2} \right]^2 R_{nN}} \quad (18)$$

An array of this type is normally used to generate an omnidirectional or beacon beam which is uniform in the plane $\theta = \pi/2$. Referring to equations (14) and (16), it is evident that the magnitude of the terms with $n \geqslant 1$ must be small compared to the $n = 0$ term, otherwise the 'ripple' in the radiation pattern for $\theta = \pi/2$ would be objectionable. If the $n \geqslant 1$ terms are small compared with the $n = 0$ term, equations (17) and (18) reduce to

$$D_{\phi a}(\theta_0, \phi_0) = \frac{\left| f_1(\theta)\, \dfrac{1}{H_0^{(2)\prime}(ka \sin \theta_0)} \right|^2}{\displaystyle\int_0^{\pi/2} \frac{f_1^2(\theta) \sin \theta \, d\theta}{|H_0^{(2)\prime}(ka \sin \theta)|^2}} \quad \ldots\ldots\ (19)$$

$$D_{\theta c}(\theta_0, \phi_0) = \frac{\left| \dfrac{M_2}{\sin \theta_0 H_0^{(2)}(ka \sin \theta_0)} \right|^2}{\displaystyle\int_0^{\pi/2} \frac{M_2^2 d\theta}{|H_0^{(2)}(ka \sin \theta)|^2 \sin \theta}} \quad \ldots\ (20)$$

Setting $\theta_0 = \pi/2$ and defining the maximum variation in the field intensity ΔE as

$$\Delta E \left| \frac{\text{maximum value } E(\pi/2, \phi)}{\text{minimum value } E(\pi/2, \phi)} \right|$$

and applying the assumption used to obtain equations (19) and (20),

$$\Delta E_{\phi a} \simeq \left| \frac{H_N^{(2)\prime}(ka) + 2j^N H_0^{(2)\prime}(ka)}{H_N^{(2)\prime}(ka) - 2j^N H_0^{(2)\prime}(ka)} \right| \quad \ldots.\ (21)$$

$$\Delta E_{\theta c} \simeq \left| \frac{3H_N^{(2)}(ka) - 2j^N H_0^{(2)}(ka)}{3H_N^{(2)}(ka) + 2j^N H_0^{(2)}(ka)} \right| \quad \ldots.\ (22)$$

In using equation (21) or (22), ΔE may be less than unity. In this case, the correct result is obtained by inverting the right-hand side of these equations. This is necessary because of the inability to predict the vectorial combination of the terms in the general use of these equations.

Calculated results

A practical application of many of the directivity equations is probably not possible without the use of a high-speed computer; consequently, it may be argued that the directivity can be computed using the field equations and integrating entirely with the computer. However, the use of the directivity equations presented here will result in a considerable reduction in the time required to compute the desired results, since the integration on ϕ has already been carried out. It is also true that, in some instances, these equations can be used to obtain results without the use of a high-speed computer.

When one studies the properties of array antennas, it is important to determine the relationship between the directivity of the array and the number of elements and the spacing between them. Towards this end, the directivity in the broadside direction [i.e. $\theta = \pi/2$, $\phi = (N - 1)\tau/2$] was computed with uniform excitation ($b_p = 1 \psi_p = 0$) and several configurations. These data are summarized in Figs. 2 and 3, where directivity is given as a function of the length of arc $a\tau$ between the centres of adjacent slots. These results were obtained with the slot length equal to $0{\cdot}7\lambda$ and with $a/\lambda = 0{\cdot}5$, 1 and 2. In some of the cases considered, the array results in circumferential slots which overlap one another. This could be considered as an array with alternate slots offset by a small amount each side of a circumferential centre line. It should be remembered that the data shown in Figs. 2 and 3 were obtained with arrays of slots which do not extend completely around the cylinder.

The beacon (or doughnut-shaped) radiation pattern is quite often produced by a slotted cylinder antenna. The array of slots extends completely around the cylinder and the amplitude and phase of the excitation voltages are

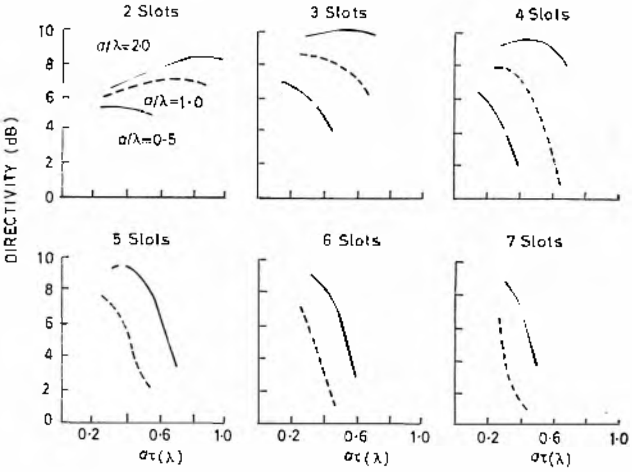

Fig. 3 Directivity as a function of slot spacing (circumferential slots)

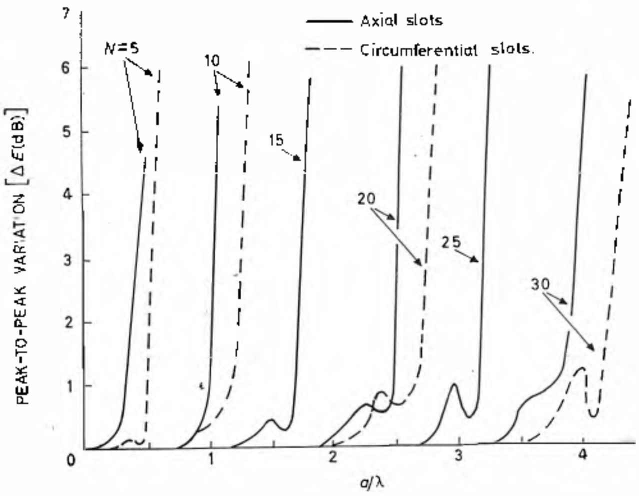

Fig. 4 Variation of slot-array radiation patterns ($\theta = \pi/2$)

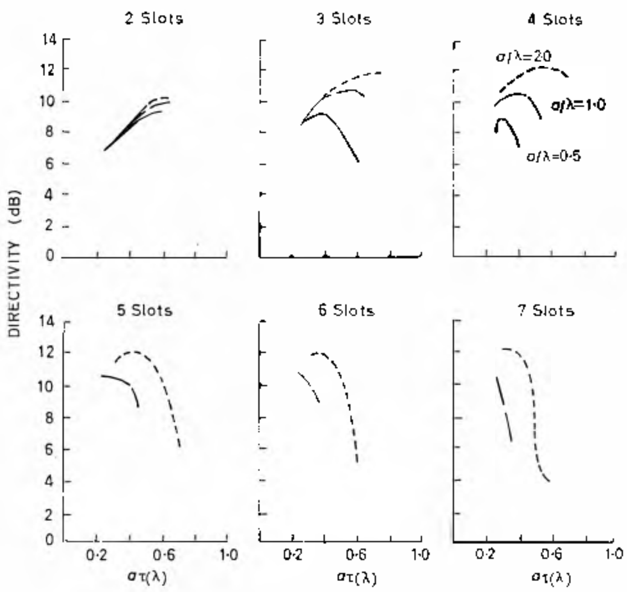

Fig. 2 Directivity as a function of slot spacing (axial slots)

equal. In this case, $\tau = 2\pi/N$ and the designer wishes to know how large N must be in order to obtain a negligible ripple in the radiation pattern. Using equations (14) and (16), the ripple $\Delta E_{\varphi a}$ and $\Delta E_{\theta c}$ was computed for 5, 10, 15, 20, 25 and 30-element arrays for $0{\cdot}2\lambda < a < 4{\cdot}5\lambda$. The results are shown in Fig. 4. Referring to these results, one can deduce that, if

$$N \geqslant (6/5)\ (ka + 1) \quad \ldots\ldots\ldots\ldots \quad (23)$$

for axial slots, and

$$N \geqslant (6/5)\ (ka + 1) - 1 \quad \ldots\ldots\ldots \quad (24)$$

for circumferential slots, ΔE will be less than 1dB.

Conclusions

The formulas for calculating the directivity of general arrays of both axial and circumferential slots on a cylinder are presented, together with some special cases, where the expressions are somewhat simpler. The calculated directivity of several arrays indicates that maximum directivity occurs for slot spacings betweens 0·3 and 0·6λ. Formulas indicating the minimum number of slots required to produce a doughnut-shaped pattern with less than 1dB ripple were deduced from calculated data.

Acknowledgment

The author wishes to thank M. Burrows for his discussion and review of the contents of this article. Both he and R. Crane gave many suggestions which facilitated obtaining the results presented.

REFERENCES

1 Sinclair, G.: The patterns of slotted-cylinder antennas, *Proc. Inst. Radio Engrs.*, *36*, 1487-1492 (Dec. 1948).
2 Wait, J. R.: *Electromagnetic radiation from cylindrical structures*, Pergamon, NY, 61-75 (1950).
3 Knudsen, H. L.: *Radiation from slots in circular cylinders*, Physics Engineering and Chemical Corporation, 12 April 1958.
4 Bailin, L. L.: The radiation field produced by a slot in large circular cylinder, *IRE Trans. AP-3*, 128-137 (July 1955).
5 Harrington, R. F.: *Time-harmonic electromagnetic fields*, McGraw-Hill, 245-250 (1961).
6 Kraus, J. D.: *Antennas*, McGraw-Hill, 24 (1950).

Large-scale integration of microcircuits

A new approach to the production of large-scale integrated microcircuits has been made at the Standard Telecommunications Laboratories at Harlow. Such circuits may be of the standard type, where large numbers of identical units are produced, or small-production types where only a few (or even one) are made. It is to the latter type that S.T.L. have applied themselves and have evolved a cellular substrate structure, each cell of which is identical; interconnexions between cells are machined with a gas laser and a micropositioner. The whole process is controlled by punched tape.

The cellular substrate is essentially a two-dimensional matrix of electrically isolated units. Unlike the common concept of small units, S.T.L. have sought to standardize on the components and not their functions so that a standard cell may contain, for example, a p-type base diffused planar transistor. Capacitance or diode functions can be obtained by using one of the pn junctions, high resistance values can be formed by connecting cells in series, and so on. Larger power dissipations can be handled by parallel connexion. A cell containing an active and passive unit may be less than 0·005in square (0·127mm square), with a yield of 40 000 cells in a slice. More complex cells would obviously be larger with less yield.

Cell interconnexions

The interconnexion pattern may be formed in several ways; whichever method is used the work to be machined is attached to the table of a micropositioner which has a 5cm travel in two orthogonal co-ordinates. Instructions to the table are fed from the punched tape to control speed, length and dictation. The laser employed at S.T.L. is a He-Ne device

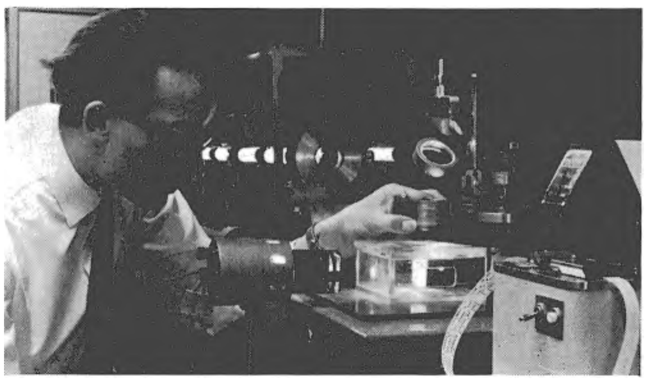

The helium-neon laser in use with the co-ordinate table and tape-recorder

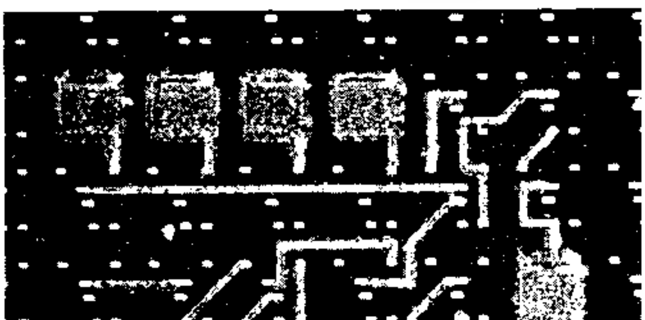

An example of local deposition, where the metal connexion film is deposited directly on to the slice

operating at a recurrence frequency of 2kHz and with 200W peak power. In a focused 10μm spot the power density laid down is about 200MW/cm². The output is in the infra-red at 1·15μm. On-off instructions for the laser are produced by the tape and the target film is cut in lines formed by overlapping dots.

Several methods of forming interconnexions have been used at Harlow. A photolithographic mask may be cut and an aluminium film then evaporated on the surface of the processed silicon slice, followed by a photoresist layer. The latter is then exposed to ultraviolet light through the mask in the ordinary way. Alternatively, the slice can first be covered with a graphite mask which is then machined with the laser to give an interconnexion pattern. Thereafter aluminium is evaporated over the whole slice and chemical etching of the underlying mask leaves the aluminium interconnexions in place.

A method which S.T.L. regard as particularly useful is that of local deposition. Here a glass plate, covered on its underside with a thin metallic film, is placed on the slice. The laser is focused through the glass on to the film which evaporates and is deposited as an interconnexion pattern directly on the slice. The importance of local deposition is in the direct connexion between the punched tape, produced by a computer, and the layout; no intermediate etching is necessary. The method is in the early development stages but already a minimum line-width of 25μm has been achieved.

Distortion in *RC* bridge feedback oscillators

By Vijay B. Mehta, M.Sc. Tech., B.Sc.(Eng.), Ph.D., A.M.I.E.(India)

Of the two methods of analysis for distortion in RC bridge feedback oscillators, that where the feedback attenuator (frequency-independent feedback path) is considered as part of the feedback network is shown to have many advantages. Different RC networks—the Wien network, RC bridged-T and balanced symmetrical twin-T—are compared for distortion in oscillators for a given amplifier system.

(Voir page 597 pour le résumé en français: Zusammenfassung in deutscher Sprache auf Seite 598)

An *RC* oscillator comprises an amplifier system and an associated feedback circuit, usually incorporating both positive and negative feedback paths. One of these contains a frequency-selective *RC* network, while the other, providing uniform feedback at all frequencies, invariably comprises a resistive attenuator which includes a thermistor or similar amplitude-stabilizing element in one or both of its arms. The total feedback is the difference between the outputs from the *RC* network and the resistive attenuator, generally obtained by feeding them to the differential inputs of an amplifier.

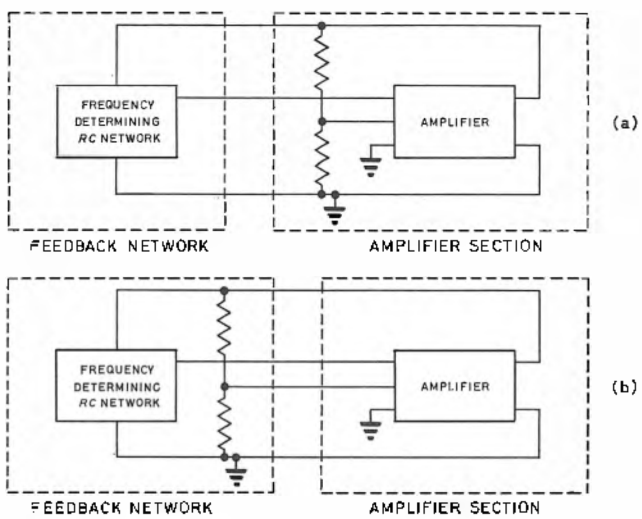

Fig. 1 Alternative analyses of *RC*-bridge feedback oscillators
(a) Resistive attenuator as part of the amplifier section
(b) Resistive attenuator as part of the feedback network

In the analysis of these *RC* bridge feedback oscillators for frequency stability or harmonic distortion, the feedback path consisting of the resistive attenuator can be interpreted either as a part of the amplifier section or as a part of the passive frequency-determining network[1,2] (Fig. 1b). Both these methods ar equally valid for the analysis of a particular oscillator. However, it has been shown[3] that, in order to get correct interpretation of the relative merits of different *RC* networks for frequency stability in an oscillator circuit with a given amplifier system, it is necessary that the frequency-independent path (resistive attenuator) is considered in conjunction with the *RC* network (dual feedback paths). The same argument also applies to the comparison of different *RC* networks for distortion in an oscillator circuit for a given amplifier system. The purpose of this paper is to show the advantages of this method of analysis over the other.

Recently, an attempt has been made by Ridler[4] to show that the analysis considering both feedback paths does not show, as clearly as might be desirable, the relationship between the oscillator waveform distortion and the distortion in the amplifier section alone, and that generally the analysis using the feedback path through the frequency selective network alone is clearer and simpler. He prefers the analysis based on the three-terminal frequency selective part of the Wien bridge to that considering the Wien bridge as a whole and derives an expression, on this basis, relating the distortion in the oscillator to the distortion in the amplifier section. Consider the Wien network with equal resistances and capacitances in both the arms ($u = v = 1$ in Fig. 2a). From the measurement of the distortion in the amplifier section and a knowledge of the transfer-function of the network, the distortion in the oscillator is predicted. However, if the parameters (u and v) of the Wien network are varied so that the loss in the network at the resonant frequency changes, this prediction no longer holds good as the amplifier gain has to be altered by changing the feedback through the second feedback path to maintain oscillations. This will necessitate a further measurement of the distortion in the amplifier section, whose feedback has been changed as the alteration in feedback varies the distortion as well. Thus, an analysis based on a single feedback path is restricted to predicting the distortion in the oscillator for one particular network only.

The Wien network, being a maximum-transmission network (at the resonant frequency), requires negative feedback through the frequency-independent path (resistive attenuator). This makes it possible to measure the distortion in the amplifier section including the resistive attenuator. However, minimum-transmission networks such as bridged-*T* (Fig. 3) or twin-*T* (Fig. 5) require positive feedback through the resistive attenuator; this might make it difficult to measure the distortion in the amplifier section, including the resistive attenuator, because of unwanted oscillations that could occur from positive feedback through this path.

Consideration of the resistive attenuator as a part of the feedback network rather than as a part of the amplifier section makes it possible to predict distortion in the oscillator (using any *RC* network) in terms of the distortion in the amplifier section (without feedback). This allows the evaluation of the relative merits of different *RC* networks in this regard without any measurement. Only one measurement of the distortion in the amplifier section (without feedback) is necessary in order to predict the distortion in the oscillator, using any RC network. Further, the analysis based on a single feedback path becomes a special case of that based on dual feedback paths. The latter method of analysis is not new[5] but no attempt to show its advantanges over the former seems to have been made hitherto. If the total feedback through both feedback paths is denoted by T,

$$T = \beta - k \quad \dots\dots\dots\dots\dots\dots \quad (1)$$

where β is the feedback through the RC network and k that through the resistive attenuator (frequency-independent) circuit. The feedback reduces the harmonic distortion produced in the amplifier section by a factor:

$$H = H_o/H_a = \frac{1}{|1 - AT|} \quad \dots\dots\dots \quad (2)$$

where H_o is the harmonic distortion in the oscillator, H_a the harmonic distortion in the amplifier system and A the gain of the amplifier section. Throughout, the amplifier is assumed to be ideal, in that its gain is independent of the frequency of the input signal and has no phase shift. It also has infinite input and zero output impedance. Further, it is also assumed that the amplifier is linear enough to render the intermodulation terms negligible in comparison with the harmonic distortion. This assumption is valid, for all practical purposes, because the bridge stabilization of the oscillators makes the amplifier operate in class A conditions.

For stable oscillation at the resonant frequency ω_o

$$(AT)_{\omega_0} = 1 \quad \dots\dots\dots\dots\dots\dots \quad (3)$$

Therefore, from equation (1):

$$k = \beta_o - (1/A) \quad \dots\dots\dots\dots\dots \quad (4)$$

where β_o is the transmission of the network at ω_o.
From equations (1), (2) and (4):

$$H = \frac{1}{A\,|\beta_o - \beta|} \quad \dots\dots\dots\dots\dots \quad (5)$$

Equation (5) shows that for lower harmonic distortion in the oscillator a higher gain in the amplifier system is desirable, provided this is not accompanied by excessive distortion. For a given gain of the amplifier system, a better waveform is obtained in the oscillator, the higher the value of the expression $|\beta_o - \beta|$. The relative merits of different RC networks can now be obtained from the standpoint of harmonic distortion in the oscillator for a given amplifier system.

Wien network

The generalized form of the Wien network is given in Fig. 2a. This network, being the maximum-transmission network, is usually employed in the positive feedback path of an RC oscillator as shown in Fig. 2b. The transmission, β, of the network at any angular frequency, ω, is given by[6,7]

$$\beta = E_o/E_i = \frac{yx^2 + jx(1 - x^2)}{(1 - x^2)^2 + x^2y^2}\, uv \quad \dots\dots \quad (6)$$

where E_o is the output of the network, E_i the input to the network, ω_o is the resonant frequency of the network given by $\omega_o = 1/RC$, $x = \omega/\omega_o$ and

$$y = \frac{u^2 + v^2 + u^2v^2}{uv}$$

At the resonant frequency ω_o, the transmission of the network is real and has a maximum of uv/y, so that

$$\beta_o = uv/y \text{ at } \omega = \omega_o,\ x = 1 \quad \dots\dots\dots \quad (7)$$

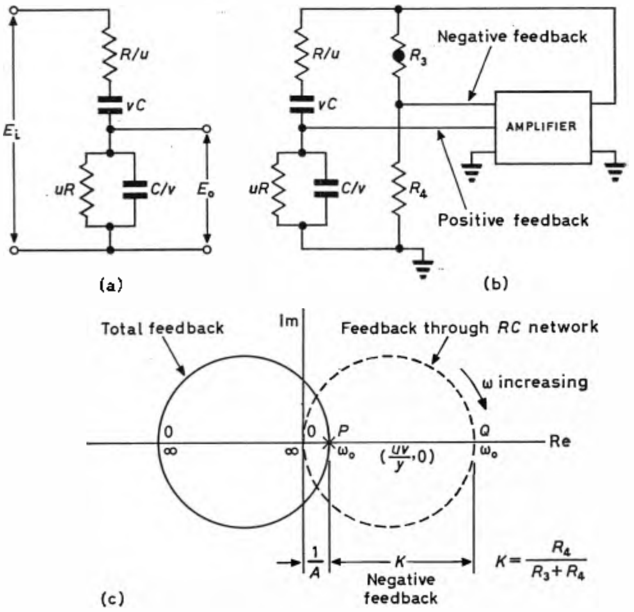

Fig. 2 Wien network
(a) Generalized Wien network
(b) Wien network in oscillator
(c) Feedback locus diagrams

From equations (5), (6) and (7)

$$1/H = \frac{Auv\,(1 - x^2)}{y\sqrt{[(1 - x^2)^2 + x^2y^2]}} \quad \dots\dots\dots\dots \quad (8)$$

The second harmonic ratio H_2 is obtained by substituting $x = 2$ in equation (8)

$$1/H_2 = \frac{3\,Auv}{y\sqrt{(9 + 4y^2)}} \quad \dots\dots\dots \quad (9)$$

Similarly, the third harmonic distortion ratio H_3 is

$$1/H_3 = \frac{8\,Auv}{y\sqrt{(64 + 9y^2)}} \quad \dots\dots\dots \quad (10)$$

Table 1 shows the values of $1/H_2$ and $1/H_3$ for the Wien network for different values of network parameters u and v.

TABLE 1

Wien network	$1/H_2$	$1/H_3$
$u = v = 1$	$0{\cdot}15A$	$0{\cdot}22A$
$u = \sqrt{(3/2)},\ v = 1$	$0{\cdot}157A$	$0{\cdot}238A$
$u = \sqrt{} = v2$	$0{\cdot}176A$	$0{\cdot}278A$

Substituting the value of $A = 3$, for the Wien network ($u = v = 1$) with equal resistances and capacitances in both the arms, the results derived by Ridler can be obtained. The advantages of this method of analysis can thus be appreciated.

Bridged-T network

Two common forms of the RC bridged-T network, which can be employed in an oscillator, are indicated in Figs. 3a and b. It can be shown that the properties of both networks are the same. These, being minimum transmission networks, are usually employed in the negative feedback

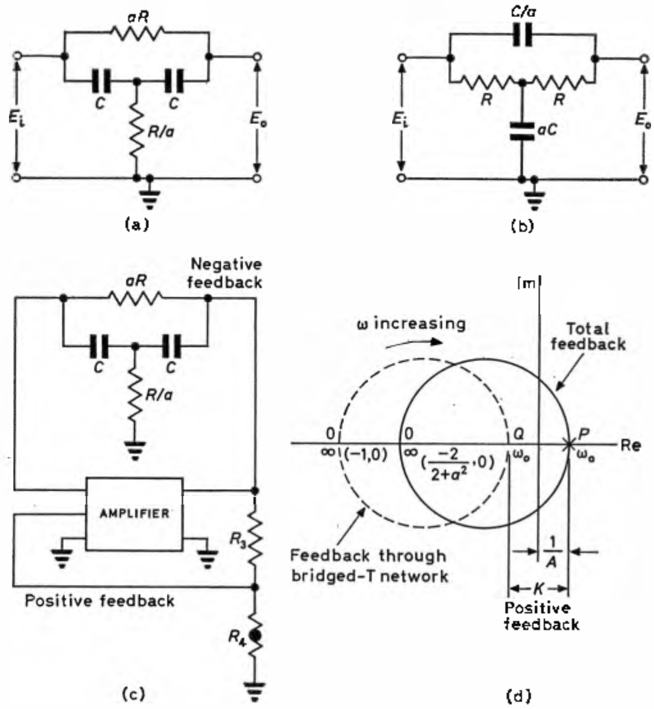

Fig. 3 Bridged-T network
(a), (b) Two commonly used forms of bridged-T network
(c) Bridged-T network in oscillator
(d) Feedback locus diagrams

path of an oscillator as shown in Fig. 3c, while the resistive attenuator provides the necessary positive feedback, required for oscillation (Fig. 3d). The transmission of the network at any frequency, ω, is given by[8]

$$\beta = \frac{a(1-x^2) + 2jx}{a(1-x^2) + jx(a^2+2)} \quad \dots\dots\dots (11)$$

At the resonant frequency $\omega_o = 1/RC$, the transmission of the network is real and has a minimum of $2/(a^2+2)$, i.e.

$$\beta_o = 2/(a^2+2) \text{ at } \omega = \omega_o,\ x = 1 \quad \dots\dots (12)$$

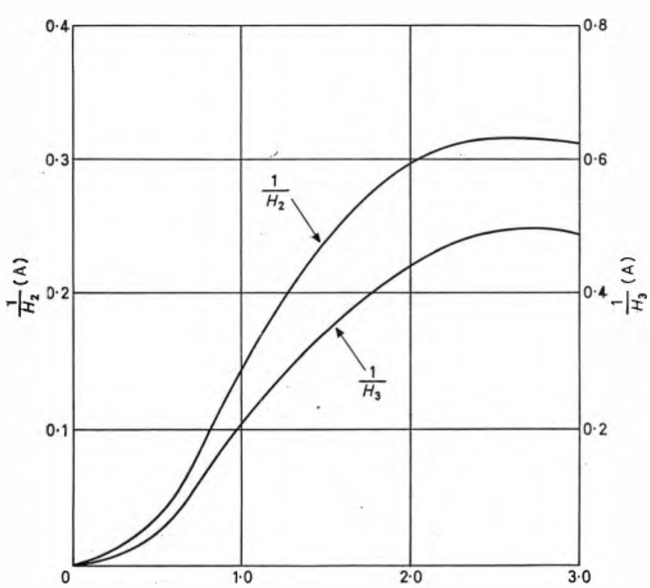

Fig. 4 Variation of $1/H_2$ and $1/H_3$ with *a* for bridged-T network

From equations (5), (11) and (12)

$$1/H = \frac{Aa^3(1-x^2)}{(2+a^2)\sqrt{[a^2(1-x^2)^2 + x^2(a^2+2)^2]}} \quad \dots\dots (13)$$

The second and third harmonic ratios are respectively given by

$$1/H_2 = \frac{3Aa^3}{(2+a^2)\sqrt{[9a^2 + 4(a^2+2)^2]}} \quad \dots\dots (14)$$

$$1/H_3 = \frac{8Aa^3}{(2+a^2)\sqrt{[64a^2 + 9(a^2+2)^2]}} \quad \dots\dots (15)$$

Fig. 4 shows the variation of $1/H_2$ and $1/H_3$ with a for the bridged-T network. The maxima for $1/H_2$ occurs at $a \simeq 2{\cdot}6$, while the maxima for $1/H_3$ occurs at $a \simeq 2{\cdot}87$.

Balanced symmetrical twin-T network

The balanced form of the symmetrical twin-*T* network, commonly employed in oscillator circuits, is shown in Fig. 5a. This has null transmission at the resonant frequency $\omega_o = 1/RC$ (Fig. 5c) and is therefore used in the negative feedback path of an oscillator as shown in Fig. 5b. Here

$$\beta = \frac{(x^2-1)}{(x^2-1) - 4jx} \quad \dots\dots\dots (16)$$

and

$$\beta_o = 0 \text{ at } \omega = \omega_o,\ x = 1 \quad \dots\dots\dots (17)$$

From equations (15), (16) and (17)

$$1/H = \frac{(x^2-1)}{\sqrt{[(x^2-1)^2 + 16x^2]}} \quad \dots\dots\dots (18)$$

The second and third harmonic ratios are respectively given by

$$1/H_2 = 3A/\sqrt{73} \simeq 0{\cdot}35A \quad \dots\dots\dots (19)$$

$$1/H_3 = 2A/\sqrt{13} \simeq 0{\cdot}55A \quad \dots\dots\dots (20)$$

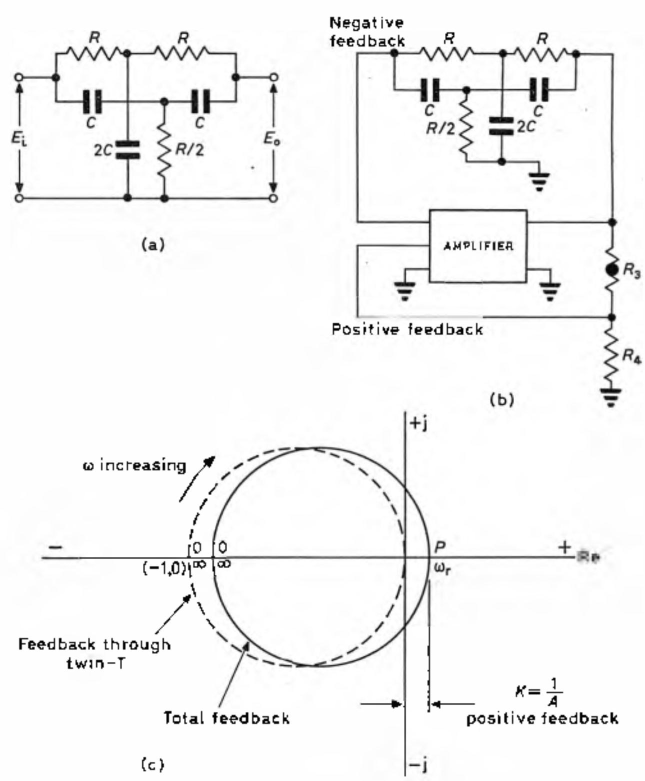

Fig. 5 Balanced symmetrical twin-T network
(a) Balanced symmetrical twin-T network
(b) Network in the oscillator
(c) Feedback locus diagrams

Conclusion

It has been shown that in the analysis for harmonic distortion in *RC* bridge feedback oscillators the method in which both feedback paths are considered offers many advantages over the other, which merely becomes a special case of the former.

Of the three *RC* networks considered, the twin-*T* seems to provide the best oscillator output waveform for a given amplifier system. Following this is the bridged-*T* network and finally the Wien network.

Acknowledgements

The investigation was conducted in the department of Electrical Engineering and Electronics in the University of Manchester Institute of Science and Technology during a research project sponsored by the Paul Instrument Fund and directed by Professor C. Adamson and Dr. J. Rawcliffe. The author's thanks are due to R. R. Sarma, Dr. M. K. Khanijo, K. K. Dasgupta, Dr. S. K. Datta and Miss S. Tate for their help.

REFERENCES

1. Post, F. J., Pit, H. F. Alternate Ways in the Analysis of a Feedback Oscillator and its Applications. *Proc. Instn. Radio Engrs.*, *39*, 169 (1951).
2. Lynch, A. C., Tillman, J. R. The Principles and Design of Valve Oscillators. *Electronic Engng.*, *17*, 414 (1945).
3. Mehta, V. B. Comparison of RC Networks for Frequency Stability in Oscillators. *Proc. Instn. Elect. Engrs.*, *112*, 296 (1965).
4. Ridler, P. F. Distortion in Feedback Oscillators. *Electronic Engng.*, *37*, 604 (1965).
5. Chance, B. *et al.* Waveforms. (McGraw-Hill Book Co., 1949).
6. Whale, H. A. Optimum Conditions for an RC Oscillator. *Electronics*, *21*, 178 (Feb. 1948).
7. Brown, D. A. H. The Equivalent Q of RC Networks. *Electronic Engng.*, *25*, 294 (1953).
8. Sulzer, P. G. A Note on a Bridged-T Network. *Proc. Instn. Radio Engrs.*, *39*, 819 (1951).

Transistorized colour television receiver

The completely transistorized colour television receiver, type 2000, recently announced by Thorn Industries, has 90 silicon transistors with their associated circuits, made up in ten plug-in printed boards and seven other units. The tuner unit employs four transistors and gang tuning; channel operation is by pushbutton and a Varicap diode operates automatic frequency control on the u.h.f. band. There is no common i.f. stage and the vision amplifier is wideband with separate shaping circuits for the two line systems. In the chrominance channel an automatic control reduces the effect of the level differences between luminance and chrominance signals, and is derived ultimately from the burst signal. The result is that a useful signal is always present at the output of the decoder.

Colour killer

So that compatible monochrome operation is not degraded by colour noise a killer circuit is employed which, on monochrome, switches off the first chrominance i.f. amplifier and at the same time switches out a 4·35MHz rejector circuit in the luminance channel. This rejector circuit, activated during colour reception, reduces sub-carrier patterning on the c.r.t. and avoids the build-up of a d.c. component (from non-linear c.r.t. characteristics) which would increase luminance at the expense of colour saturation. Control voltage for the killer circuit is derived, as with the automatic chrominance control, from the burst signal *via* the colour decoder.

Video stages

There are separate video stages for red, blue and green, each in the form of cascode pairs, with luminance signals driving the bases and colour difference signals the emitters. This method of matrixing luminance and chrominance signals outside the c.r.t. leaves the grid of the latter free for line and frame blanking and has other advantages. Transistor feed to the cathode implies that protection from the high voltage transients has to be included; a spark gap returned to the c.r.t. Aquadag coating lowers the energy of the transistors very quickly and currents flowing back into the transistor circuits are limited by series resistors.

E.H.T. generator and power supplies

The e.h.t. generator is a Cockroft-Walton tripler circuit, the final capacitance of which is the c.r.t. itself and the voltage reached is 24kV. A feedback amplifier ensures that the regulation at the final anode is maintained at about 1mA in 1MΩ. The e.h.t. input is synchronized from the line scan transformer secondary so that pulse feedback is avoided. As transistors are used in the high voltage generator no hard radiation is produced as with some valve rectifier circuits.

Line scanning

Line deflexion coils are fed from two identical parallel output transformers driving series-connected output transistors. To avoid unequal sharing of the flyback voltage the centre tap of the transformer is fed through the RC network to the junction of the transistors; the network is such that its impedance is low during flyback and very much higher at scan frequency.

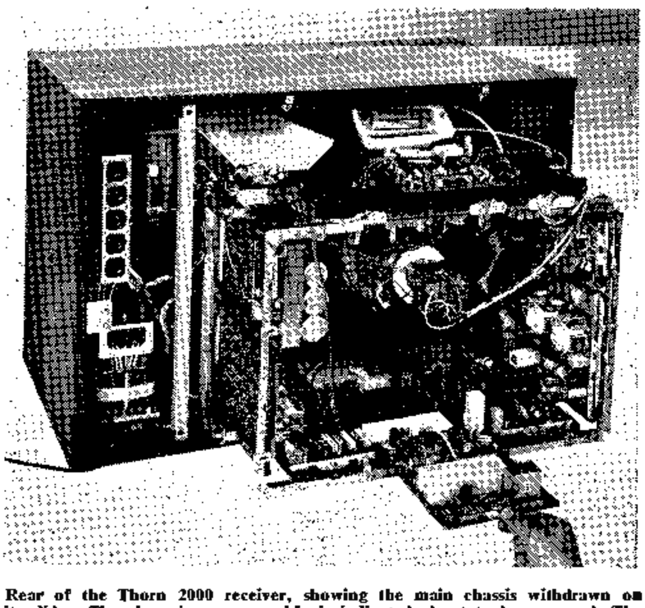

Rear of the Thorn 2000 receiver, showing the main chassis withdrawn on its slides. The chrominance assembly is indicated about to be removed. The e.h.t. rectifier assembly is mounted on top of the shadow-mask tube. All of the ten circuit boards are plugged in and can be withdrawn in the same way as the chrominance board

Maintenance

The servicing and maintenance of colour receivers in the field is largely a problem for the future. The design of the Thorn 2000 receiver has minimized the effect of circuit faults by using printed board and modular assemblies which may all be easily changed. This facility, combined with instruction in fault finding, should ensure that servicing and maintenance are at least as good as that with monochrome receivers.

LETTERS TO THE EDITOR

(We do not hold ourselves responsible for the opinions of our correspondents)

A second-order active filter circuit for tuned amplifiers and sinusoidal oscillators

SIR,—The authors of this article discussed their circuit principally with regard to its performance in the region of resonance. I believe that its performance at frequencies remote from resonance merits a little further discussion, since a slight modification can provide a markedly better attenuation at low frequency.

In the circuit in Fig. 2 of this article the only component ensuring that the filter response has a zero at d.c. is the input blocking capacitor. This is highly unsatisfactory for the following reason.

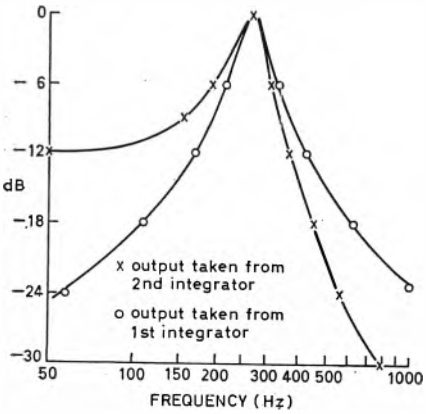

Suppose a filter is required for a range of centre frequencies, then the input blocking capacitor either has to be switched or has to be chosen so that it does not affect the filter response on the lowest frequency setting. If the latter is so, then for the higher centre frequencies the maximum attenuation on the lower side of the centre frequency will tend to be equal to Q_0 over an appreciable range of frequency. This disadvantage may be overcome by taking the output from the first integrator not the second one. The diagram above illustrates the differences in responses which are obtained experimentally with a filter having a Q_0 of 4.

K. F. KNOTT,
University of Salford

The authors reply

SIR,—Referring to Fig. 1 in the original paper, the virtual-earth analysis gives transfer functions of the following forms:

$V_2/V_s \propto j\omega_0/\omega\,[1+jQ_0(\omega/\omega_0-\omega_0/\omega)]\ldots(1)$
$V_1/V_s \propto 1/[1+jQ_0(\omega/\omega_0-\omega_0/\omega)]\ \ldots.\ (2)$

where the constants of proportionality are real and positive.

With a change of sign, equation (1) is the voltage transfer function of a series *LCR* circuit with the output taken across *C*, while equation (2) represents the same circuit with the output taken across *R*. The latter type of response, as Knott points out, is likely to be much more satisfactory in the case of a low-*Q* filter; out discussion was in fact restricted to the high-*Q* case where the difference between the two transfer functions is likely to be negligible.

In cases where transfer function, equation (1) is acceptable, there are considerable practical advantages in the arrangement described in our paper; these arise from the fact that the lowest possible temperature coefficient is obtained by running the two integrating transistors at different collector currents. In this situation, the best combination of input impedance and output impedance (for a given voltage gain at resonance) is obtained when the input is fed into the lower-current integrator and the output taken from the higher-current integrator, as is the case with the circuit values given in Table 1.

This letter gives us an opportunity of referring to a difficulty which has arisen during commercial production of these filters. Where an integrating transistor is run with a d.c. collector current substantially above 1mA it may go into high-frequency oscillation, the only symptom of which is that the circuit gives a *Q* very much lower than the calculated value. This oscillation can be prevented by inserting a resistor of about 10Ω in the base lead.

E. A. FAULKNER,
VISCOUNT DOWNE,
J. J. Thomson Laboratory,
University of Reading

Which international colour system?

SIR,—Since there is still no international agreement on a system of colour television, perhaps it is not too late to say a few words in favour of the older systems, namely, line sequential (l.s.) and field sequential (f.s.) transmission. While they do not share the enormous ingenuity which has gone into NTSC, Pal and Secam, they have certain advantages which should not be dismissed out of hand:

1 they work without ifs, ands, or buts;
2 they can use any colour display tube yet invented, or to be invented. Nevertheless, if f.s. should be adopted, some manufacturer would doubtless come along with a rotating-disk set which would offer a better picture at lower cost than any set using a colour tube. An acceptable projection tube would even remove the clumsiness of this arrangement;
3 they are simple; the receiver is hardly more complicated than a b.w. (black and white) set;
4 f.s. has long been used in closed-circuit work—a testimonial to its practicability.

Now a few remarks about the well-advertised disadvantages of these systems:

5 first, as to compatibility, that is the ability to receive colour transmissions in b.w. on a b.w. receiver: from the viewpoint of the set owner this is inconsequential, as long as the programme is also transmitted in b.w. on his usual channel. The overall cost of double transmission would have to be balanced against the lower cost of millions of l.s. or f.s. sets, when compared with NTSC etc. sets;
6 as to reverse compatibility, that is the ability to receive ordinary b.w. transmissions in b.w. on a colour set (as opposed to b.w. signals sent over a colour channel, which presents no problem in any case), this cannot be taken very seriously, because:
(a) everybody has a b.w. set already
(b) no colour tube will produce even as good a b.w. picture as a mediocre b.w. tube
(c) this sort of compatibility could also be provided in l.s. or f.s. sets using colour tubes without too much difficulty (switching of sweep rates etc.)
(d) an f.s. set equipped as in (c) and using a rotating disk, could provide a better b.w. picture on b.w. transmissions than any other kind of colour set, since it uses a b.w. tube;
7 bandwidth: since f.s. and l.s. cannot take advantage of the low colour bandwidth of the eye, they require more bandwidth for the same rendition of detail (although I believe that in the final Columbia Broadcasting f.s. system, the bandwidth was brought down to six megacycles, with what sacrifice of detail I cannot say). And of course the double transmission mentioned above would require extra bandwidth. But why shouldn't this bandwidth be provided, for example, on u.h.f.? It is a question of values, and is a valid political question;
8 f.s., but not l.s., suffers from colour break-up, that is colour fringes which accompany fast-moving objects. This is true, and is probably the most valid objection to f.s. But how great is this disadvantage? It could certainly be minimized by appropriate camera work and intelligent direction;
9 l.s. is said to suffer from an annoying moiré effect known as line crawl. I cannot testify to this, but it may be noted that a Japanese manufacturer has gone to the trouble of converting NTSC to l.s. in the receiver, the result being displayed on a Chromatron.

J. M. DIAMOND,
Roskilde,
Denmark

SHORT NEWS ITEMS

As part of the multimillion-pound Post Office plan to develop and modernize Britain's telephone system, a contract worth £1 217 000 for improvements and extensions at Bristol has been placed with the Plessey Telecommunications Group. The contract calls for the provision of additional trunk switching and signalling equipment, together with the necessary power plant at the Bristol trunk exchange.

A new airfield-visibility-measurement system was recently demonstrated in Luton by Kent Industrial Instruments Ltd (George Kent Group). First orders (for ten sets of equipment) have come from the British Meteorological Office, to whose specification the equipment is being made. These are for installation at civil and RAF establishments in different parts of the country where they are to be used in the assessment of meteorological visibility as an aid both in the operation of airports and for research. Demand for automatic continuous assessment of conditions, not just at the airfield and approaches, but right along each operational runway from landing to roll-out area is met easily by the Kent system, it is claimed, providing the air-traffic controller with a vital up-to-the-moment record of visibility hazards and variations. The system comprises, basically, a light transmitter and a photoelectric-cell receiver mounted on 10ft towers sited 200yd apart, with a control unit, a stabilized lamp power unit and an electronic strip-chart recorder. The transmitter produces a steady beam which is monitored by the receiver, and visibility measurements are stripchart recorded once every 20s, or at shorter intervals, as required. The measuring range is 100 to 4000yd when used on this 200yd baseline.

The introduction of colour on Independent Television early in 1970 was forecast recently by the Postmaster General. In order to prepare for colour, the ITA's duplicated 625-line service will begin in monochrome from four main transmitters in London, the Midlands, Lancashire and Yorkshire, during the late summer of 1969. When the colour service is introduced, it will begin simultaneously on Independent Television and BBC1, and will be broadcast from the same transmitting sites; the ITA and the BBC will be sharing transmitter sites and masts for all u.h.f. colour transmissions throughout the country. When the ITA starts transmitting its colour programmes, they will be within reach of 28 700 000 people (52% of the population). By the end of 1971, 43 400 000 people (79%) will be within reach. It is likely that, from the outset, more than half of the ITA's programme output will be in colour.

The Institution of Electronic and Radio Engineers intends to seek permission to amend its Bylaws so that existing Members can be regarded as Fellows and Associate Members as Members. This is in line with current thinking among the constituent members of the Council of Engineering Institutions towards standardizing their corporate-membership designations. It is also intended that the grade of Associate, which is limited at present to those persons who have the requisite experience but not the formal academic qualifications for corporate membership, will be broadened to include holders of the HNC or the City and Guilds Full Technological Certificate in Telecommunications. The purpose of this change is to enable senior technicians to be associated with, and partake in the same Institutional activities as, the professional engineers with whom they work so closely. It is hoped that these changes in structure will become effective before the end of this year.

The 22nd (1967) Electronics, Instruments, Controls and Components Exhibition and Convention will be held in the Exhibition Hall at Belle Vue, Manchester, from Tuesday, 26th September to Friday 29th, both dates inclusive.

The organizers report that the move to Belle Vue has materially benefited the exhibitors and themselves. The 1966 show was 30% bigger in size than that of 1965, while the 1967 exhibition already has 54 more exhibitors booking space than in 1966.

The British Calibration Service has now published information about the BCS approval scheme for calibration laboratories. The first BCS publications give information on the procedure for applying for BCS approval, the conditions regulating the operation of BCS-approved laboratories, the charge payable by the laboratories, and the detailed technical requirements for approval for certain types of measurement. The procedure is that an interested laboratory should first notify BCS Headquarters that it would like to offer an approved calibration service for particular measurements, which are named. The laboratory will then be notified for which of the measurements named it is possible at the time to undertake an approval investigation. Any organisation wishing to receive the publications may apply to the BCS Headquarters in the Ministry of Technology, Millbank Tower, London SW1, or to its local regional office of the Ministry.

First results from experiments carried by *Ariel III*, the first all-British satellite launched successfully by the US National Aeronautics & Space Administration (NASA) for the Science Research Council on the 5th May, indicate that the satellite and its experiments are continuing to operate satisfactorily.

The SRC Radio & Space Research Station terrestrial-noise experiment has already provided information about noise levels over the equatorial regions and also recorded intense storms over Western Europe during the first few days after launch. The voltage levels due to this terrestrial noise were on occasion greater than 100 times the galactic noise. Birmingham University has two experiments on board *Ariel III* which measure local electron density and temperature along the orbital path; measurements received so far indicate that both experiments are functioning correctly, and variations in the measurements made throughout the orbits reflect the higher level of solar activity which is occurring as sunspot maximum is approached. The Manchester University experiment to measure the intensity of cosmic radio waves at frequencies lower than those which normally penetrate the ionosphere, and in particular to find the variation in intensity from different parts of the sky, has been functioning well. The Sheffield University apparatus for the study of the nature, intensity and world-wide occurrence of radio waves at frequencies below 20kHz has been completely successful. Signals have been recorded on every orbit with intensities up to 10 million times the minimum detectable level.

Telephone subcribers in Australia's outback will soon be able to dial their own calls instead of having to go through an operator. Under a contract worth £39 000, the Plessey Telecommunications Group at Beeston (incorporating Ericsson Telephone Ltd), will supply advanced telecommunication equipment to the Australian Post Office, which will provide subscribers in remote parts of the country with a faster, more efficient service. Plessey is to supply 20 line connectors incorporating RC101-type rural carriers for open wires, which are also made at Beeston by the Transmission Division of the Plessey Electronics Group. Each line connector will provide automatic switching for up to 20 subscribers in a small rural area and is linked to the parent exchange by up to four junctions. These four junctions operate over a single pair of wires by using the RC101 subscriber carrier which has a capacity equal to 10 pairs of lines. It is intended that this equipment will be used by the Australian Post Office to replace gradually the old magneto exchanges in the outback which have previously been manned by part-time operators on a similar basis to the radio stations linked to the flying-doctor service.

G. & E. Bradley Ltd has been successful in obtaining a further order for X-band solid-state sources from Lockhead Electronics Inc. of Plainfield NJ, USA. The sources are used as local oscillators in a Doppler-radar system being manufactured by Lockheed for the US Army. The latest order brings the total value to $5 000 000, and it is expected that further orders will follow. Bradley has obtained these orders in the face of direct competition from 18 American companies. Special features of these solid-state sources are their high stability and reliability under adverse environmental conditions, and very low noise, which constitutes a major contribution to the present state of the art.

An experimental radar equipment under development at the Mullard Research Laboratories, named AVOID (airfield-vehicle obstacle indication device), is intended to aid the navigation of vehicles in conditions of zero or very poor visibility. AVOID would be of extreme value in emergency conditions where, for example, rescue or fire-fighting vehicles are attempting to reach a crashed aircraft in thick fog on an airfield. The radar is simple, compact, and could be powered from the vehicle electrical system. It has no moving parts (the aerial being a fixed unit with electronic scan) and is of all-solid-state construction, possibly using Gunn-effect devices. It operates in the f.m. c.w. mode in X-band, and the range is 100yd maximum, 3yd minimum, with a resolution of 2yd. In the present development stage, the equipment is very much in experimental form, and consideration is now being given to the most suitable method of display to the driver or navigator of the vehicle. Rather than a conventional p.p.i. display, for example, it would be feasible to provide a perspective display which would need no interpretation; there is also the possibility of exploiting head-up display systems, in which the display would be observed through the windscreen.

Electronic Engineering will be exhibiting at the Northern Electronics Exhibition at Belle Vue, Manchester, on the 26th-29th September inclusive. The Editor will be there on Tuesday and Wednesday, the 26th and 27th, and will be pleased to meet visitors.

Siemens closed-circuit television systems are being used by the firm of Wuppermann of Leverkusen, West Germany, for observing the feeding of slab ingots to the pusher-type furnace of a rolling mill for preheating to about 1500°C, followed by their removal. Observation is made with the aid of television cameras with special probe objectives and water-cooled protective casings that are built into the wall of the furnace. The feeding of slab ingots may be localized in this way to an accuracy of within a few centimeters. A slide is inserted in the probe objective to aid view-finding. Seven reference lines on the slide are associated with seven different slab widths.

The European Organization for Nuclear Research (CERN) have awarded Pye-Ling Ltd a contract worth £54 000 for the supply of four pulse modulators. Each modulator will deliver 20MW of peak r.f. power with a pulse duration of 8μs at a repetition rate of 10 pulses/s. The equipment will form a major part of a new 25 GeV r.f. particle separator for fundamental research. High-energy particles are passed successively through three r.f. deflection fields, the relative phase of each being adjusted so that the final deflection of one type of particle is made zero with respect to another type of particle. The modulators are designed to be able to deliver their r.f. power either to a proton synchrotron or to a hydrogen-bubble chamber of the fast-cycling type.

A new government publicity service for British firms exhibiting in selected overseas trade fairs was launched by the Central Office of Information in July. The service—known as Trade Fair Bulletins—produces single-sheet illustrated technical descriptions of products to be shown; these are also translated into appropriate languages. The bulletins are issued by Britain's Overseas Information Service well in advance of an exhibition's opening date to the trade and technical press, buying organizations, chambers of commerce and individual buyers in the country in which the fair is staged. The first 16 fairs to receive this service are all among those for which the Board of Trade is sponsoring participation by British industry; these include the Third International Trade Fair, Wellington, the Display of British Scientific Instruments, Mexico City, the International Trade Fair, Brno, the Marine Equipment Exhibition, Helsinki, and other international trade fairs at Sydney, Lima, and Tripoli.

Yorkshire Television Ltd, one of the new independent-television programme contractors, has ordered Marconi colour television cameras, telecine equipment and outside-broadcast units worth nearly £650 000. This is the first equipment to be ordered by one of the new programme contractors created in the reshuffle of independent television earlier this year, and it will give Yorkshire the first studio centre in the country to be designed for full colour capability from the outset. A total of 16 of the latest mark-VII colour cameras have been ordered. These will be used in a new studio centre at Kirkstall Road, Leeds, and two 4-camera colour outside broadcast units to be built by Marconi. The studio centre will contain a 4-camera studio, a 3-camera studio and a remotely controlled presentation studio with a single camera. The very high stability of the camera, which can be operated for long periods without adjustment, will be of particular importance in this last application. Three colour-telecine channels will also be supplied; these new units, which will be introduced later this year, employ a modified version of the mark-VII camera, and provide similar advantages in terms of stability and high-quality performance.

Corrigendum

In Part 1 of the article 'New shutdown amplifier (s.d.a.) for nuclear reactors' by I. G. Morris, the author wishes to point out the following errors:

p. 487, col. 2, l. 8: 'circuits' should read 'currents'

l. 28: the ratio should be 15/25kΩ

l. 39: the equation should read $1/R_{10}[R_{10}+RV_1(R \text{ to } Y) \times 1/R_8]$ volts/ampere

p. 488, col. 1, l.33: the voltage range should be 0 to 10V

p. 489, col. 2: the gain expression should be $R_4/(R_1 \times R_5)$

p. 489: the final sentences of the penultimate paragraph should be

'This is amplified and rectified by a circuit similar to that described for the z.m.t. The output and input choppers are driven by the same rectangular waveforms used for the main d.c. amplifier and the z.m.t., but synchronization of its waveform with that used in the other cases is not essential.'

NEW EQUIPMENT

A description, compiled from information supplied by the manufacturers, of new components, accessories and test instruments.

DIFFERENTIAL VOLTMETER

Honeywell Controls Ltd, Brentford, Middlesex

Honeywell have introduced a model-1000 differential voltmeter which can also be used as a differential ratiometer, a decade voltage divider, a precision voltage-reference source and an electronic null detector. As a differential voltmeter, the model-1000 gives ±0·0025% accuracy for measurement of d.c. signals, with six digits of numerical readout. 10% overrange on each range provides the seventh digit of resolution,

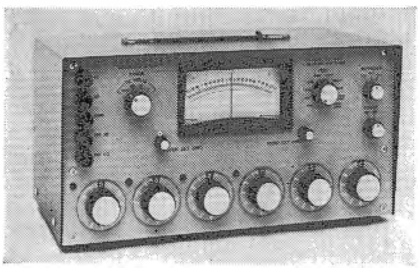

while an additional eighth digit may be read from the panel meter. This overrange eliminates dial manipulations and loss of resolution when the measured value is near a range-change point. 10μV null sensitivity is maintained on both the 1 and 10V ranges; potentiometric input impedance up to 11V provides errorless measurements of signals with high source impedances. Polarity is reversible from the front panel.

As a decade voltage divider, use is made of the model-1000 precision 6-decade Kelvin Varley divider network. Accurate voltage-level divisions can be made within ±0·001%. This instrument does not require a.c. power to operate in this model. Ratiometer operation gives precise d.c. ratio within ±0·001% accuracy. The external-reference-signal level may range up to ±100V d.c. Calibrated voltage levels of 6-digit resolution are available when the model-1000 is used as a calibrated reference source. This operation utilizes a Zener-diode reference and voltage divider. Output levels are selected by setting the desired voltage on the front-panel controls. The levels, accurate to ±0·0025%, vary from 0 to 11V d.c. and may be used for the calibration of potentiometric instruments. Electronic null-detector operation provides a high-sensitivity null indicator for general use. Drift-free operation and maximum reliability are achieved by the use of silicon field-effect transistors, which eliminate conventional electromechanical choppers. Input changes as small as 10nV or an input current of 10-15A may be detected.

For more information circle **No. 281**

MICROWAVE TUNING UNIT

Polarad Electronic Instruments, 34-02 Queens Boulevard, Long Island City, NY 11101, USA

The model-T-RW microwave tuning unit available from Polarad Electronic Instruments spans the 2-75GHz frequency range. It plugs into the model-TR general-purpose antenna-pattern receiver. Two features of the tuning unit which give maximum sensitivity are variable local-oscillator injection and a 1kHz modulated first local oscillator operating

with a 1kHz video-output filter. A large dynamic range permits uninterrupted direct reading of measurements. The first mixer is mounted externally, to give direct connexion to the receiving antenna at distances up to 100ft from the receiver. Operating modes include a.m., f.m., c.w., pulse and m.c.w.; there are three impulse bandwidths: 1MHz, 5MHz and wideband.

The model-T-RW operates from either 115/230V a.c. at 50-1000Hz or 12V d.c. for use in the field or laboratory.

For more information circle **No. 282**

MICROVOLTMETER FOR SIGNALS IN NOISE

Hewlett Packard Ltd, 224 Bath Road, Slough, Buckinghamshire

A new a.c. microvoltmeter is capable of measuring with full-rated accuracy signals as small as 300nV r.m.s. in a frequency range between 25Hz and 60kHz (or 1μV between 60 and 600kHz). The instrument has 13 sensitivity ranges, from 3μV to 3V full-scale in a 1-3-10 sequence. It also measures signals in a frequency range 5-25Hz with full-scale ranges of 30μV-3V. Basic accuracy is ±3% of full scale up to 60kHz, and ±5% above 60kHz. Input impedance is 10MΩ shunted by 20pF.

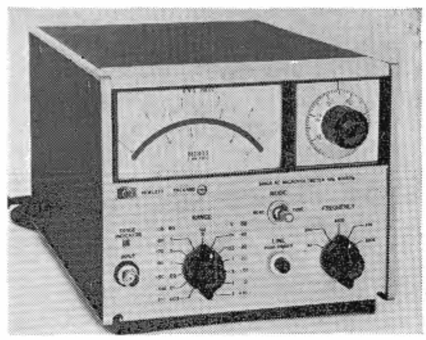

The high sensitivity is made practicable by the ability of the new microvoltmeter (model-3410A) to tolerate large amounts of noise with the signal. Noise r.m.s. voltages up to 20dB above full scale do not affect the accuracy of the reading down to signal levels that are only 1/10 of full scale (40dB below noise, i.e. 20dB above full scale).

The microvoltmeter uses a phase-locked synchronous detector rather than narrow-band filters to separate the effects of noise from the signal. The detector is an electronic gate controlled by an oscillator phase-locked to the input signal. Alternate halfcycles of the input signal are passed by the gate, and the output of the latter is smoothed by a low-pass filter to obtain a direct voltage proportional to the average value of the input waveform. Since both the positive and the negative excursions of noise and other randomly varying signals pass through the gate when open, these average to zero and do not affect the reading. Even though broadband noise has a frequency component that is the same as the signal frequency, it does not affect the reading as its phase varies randomly.

For more information circle **No. 283**

MAGNETIC REED SWITCHES AND RELAY UNITS

Kappa Electronics Ltd, 159 Hammersmith Road, London W6

Kappa Electronics introduce their range of type-WM10 reed switches and associated WR10 relay units. Three types of reed switches are available, each comprising a glass-encapsulated dry-reed switch mounted in a protective case

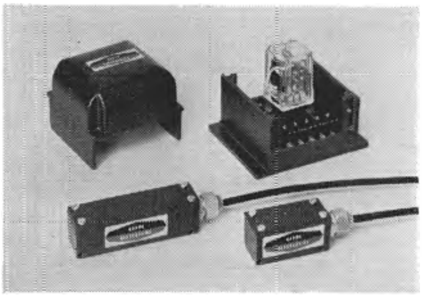

(either a plastics moulding or a robust cast-alloy housing). Each type is also available with normally-open or normally-closed contacts. Contact ratings are long-life 150mA, maximum 500mA, or long-life 250mA, maximum 1A; breakdown voltages are in excess of 500V d.c.; and operating times are in the region of 1ms. These switches can easily be installed and are not affected by normal vibration levels. They are actuated by the proximity of a permanent magnet supplied with the switch. Where it is required to switch loads in excess of the switch ratings, they can be used to energize the type-WR10 relay units. These comprise a plug-in relay and connexion base mounted into a cast-aluminium housing for protection. Versions available include 2- and 3-changeovers, rated at 5A, 250V r.m.s., together with a 4-pole contactor rated at 15A a.c. per pole. Standard coil voltage is 230V a.c., although other voltages are available.

For more information circle **No. 284**

INSTRUMENT CATHODE-RAY TUBES

Mullard Ltd, Torrington Place, London WC1

Seven types of instrument cathode-ray tube marketed by Mullard form the nucleus of a new range that will provide tubes for applications extending from simple work-bench oscilloscopes and data-display systems to the most sophisticated wideband instruments now used. Round-faced tubes types D7-19GH, D10-16GH and D13-48GH have screen diameters of 7, 10 and 13cm, respectively. These are intended for inexpensive oscilloscopes and data-display systems. Two new tubes for transistor

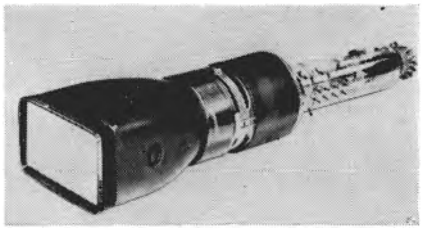

oscilloscopes are the D10-17GH and D14-12GH; both have frequency responses of up to 30MHz. The first tube is round-faced, has a useful scan area of 80 × 60mm and is 315mm long; the other tube has a rectangular face, a useful scan area of 100 × 80mm and is 365mm long. A tube designed for use in oscilloscopes with frequency responses up to 250MHz is the D13-45GH/01. This is a mesh p.d.a. tube that has an internal aluminized graticule and correction coils for picture rotation and orthogonality correction.

Wideband oscilloscopes are catered for by the tube type D13-50GH/01, (illustrated) which has a bandwidth of 800MHz. The sensitivity of this tube is increased in the vertical direction by means of a quadrupole electrostatic lens between the vertical deflection system and the horizontal deflection plates, and wideband operation is obtained by using a built-in delayline system instead of conventional deflection plates. Under typical operating conditions, the vertical and horizontal deflection sensitivities are 2V/cm and 15V/cm, respectively. The tube has a rectangular face that presents a display area 60 × 100mm, and incorporates an internal aluminized graticule.

For more information circle **No. 285**

SINGLE-TRACE UNIT FOR INCREASED SENSITIVITY

Marconi Instruments Ltd, St Albans, Hertfordshire

The sensitivity of the Marconi Instruments TF 2201 solid-state oscilloscope can be increased by a factor of ten with the introduction of the Single Trace Unit TM 6970A; this unit supersedes the

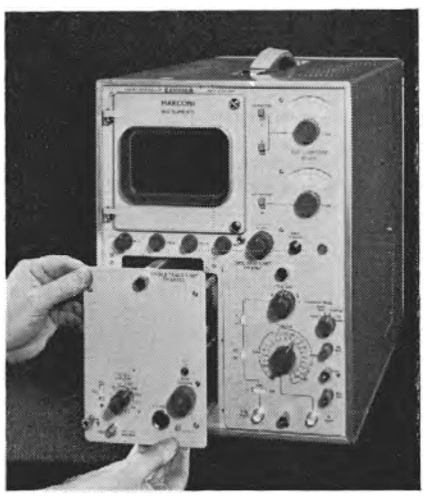

TM 6970. The plug-in unit has a maximum sensitivity of 5mV/cm and a 3dB bandwidth of at least 30MHz when used with the TF 2201. The sensitivity is selected by an 11-position high-impedance attenuator from 5mV/cm to 10V/cm in a 1-2-5 sequence, with a continuous control which varies the gain of the amplifier by at least 2·5:1. Minimum sensitivity is 25V/cm. The CAL position on the attenuator switch provides a reference 50Hz, 25mV, squarewave with which the gain of the amplifier may be standardized.

For more information circle **No. 286**

TRANSISTORIZED INDUCTANCE BRIDGE

Nombrex Ltd, Exmouth, Devon

The model-33 inductance bridge introduced by Nombrex comprises a source oscillator and amplifier coupled to a bridge which follows the Hay or Maxwell configurations, selectable by panel control, and has a miniature moving-coil meter for balance indication.

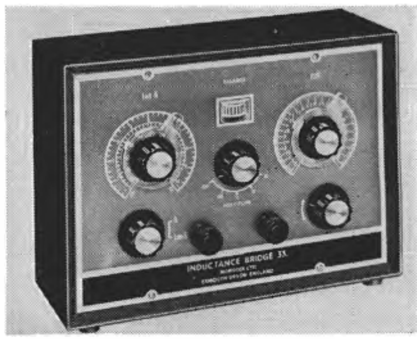

Among several special circuit features is selective negative feedback in the amplifier, to ensure positive and accurate indications. The instrument is transistorized and employs a printed-circuit assembly. The ranges of inductance are: 1-100μH, 100μH-10mH, 10mH-1H and 1-100H, with a tan δ range of 10 to 0·001. The instrument is 7·5in wide × 5·75in high by 3·75in deep and weighs about 1kg.

For more information circle **No. 287**

PLUG-IN LOGIC MODULES

West Hyde Developments Ltd, 30 High Street, Northwood, Middlesex

Plug-in logic modules introduced by West Hyde Developments Ltd reduce design time and allow simple breadboards of a system to be connected in minutes, the final units only requiring links onto a standard board for the finished equipment. The 16 modules of the new PIDAM (plug-in digital and analogue modules) system each carry out well defined functions and are easy to combine. Each module has a simple description printed on top showing its function, i.e. AND is a 4-input AND gate and BI (illustrated) is a bistable;

with the aid of simple rules all units can be connected directly. To make the system easier, the manufacturers supply all accessories (from an oscilloscope to a photocell), including printed-circuit

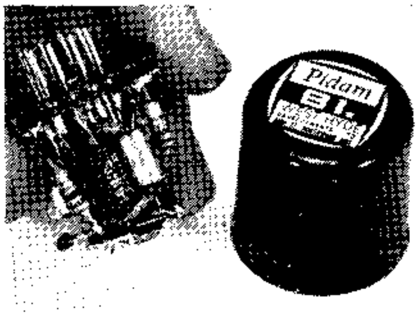

boards and chasses with thermistors, meters and reed switches, and special Letraset sheets showing all the modules. An illustrated booklet describes the whole system and many examples of use are explained in detail. The modules are not sealed and, if required, kits of parts are sold separately.

For more information circle **No. 288**

TABULATOR KEY

STC Electromechanical Division, Footscray, Sidcup, Kent

A tabulator-key switch announced by STC Electromechanical Division (the type-PM 21) has a claimed mechanical life of more than 10^9 operations; electrical life (at 24V d.c. 10mA) is over 20 million operations. This reliability has been achieved through a unique switching mechanism, believed to be the only one of its kind commercially available. It employs a hermetically-sealed dry-reed switch element actuated by a current ring magnet attached to the plunger mechanism. To ensure dependable operation, the reed has pivoted twin contacts; the mechanism is housed in a self-lubricating nylon mounting that eliminates the possibility of malfunction from dust adhesion. Another functional feature of the PM 21 is its very low contact bounce—less than 1·5ms. Total button travel is 6·35mm (0·25in), the operating force required being 90g/cm. These are typical characteristics favoured by most keyboard operators, but they can be altered to suit customer requirements. The PM21 is easily fitted *via* nonslip single-screw fixing; groups can be quickly installed side by side in adjacent rows.

For more information circle **No. 289**

POWER PACKS

Highland Electronics Ltd, 26-28 Underwood Street, London N1

Highland Electronics announce a new range of power packs with power relays, for use in 24V d.c. systems. They are suitable for alarm-annunciator systems, solenoids, relays etc. The power packs have a 24V d.c. full-wave unsmoothed output, using silicon rectifiers. A number of units may be connected in parallel to give larger output powers or in series to give higher voltages. All units have input-voltage taps at 110/115V, 200/220V, 220/235V and 235/250V. at 50/60Hz. The regulation from no load to full load is 12·15%. The power packs are available for maximum output currents ranging from 4 to 20A, with 1 or 2 power relays. All units are $7\frac{1}{2}$in × 5in × 5in with one 12-way terminal block for input, output and fuse-failure alarm and another for the power relay.

For more information circle **No. 290**

TRACKING PRESELECTOR

Hewlett Packard Ltd, 244 Bath Road, Slough, Buckinghamshire

A new tracking preselector from Hewlett Packard enhances the usefulness of wide-sweeping spectrum analyzers by simplifying the spectrum display. The new preselector reduces intermodulation products and spurious image and multiple responses that would otherwise clutter the spectrum analyzer c.r.t. display. Designed primarily for use with HP 8551/851 spectrum analzers, model-8441A preselector is a voltage-tunable narrowband filter that functions as a sweep-tuned r.f. stage over a frequency range from 1·8 to 12·4GHz. It automatically tracks the analyzer scan, passing signals to which the analyzer is tuned while rejecting others. Undesired responses are reduced by at least 35dB. The preselector uses a y.i.g. crystal that functions as a high-Q bandpass filter tuned to a magnetic field. The signal that controls the magnetic field, and hence the y.i.g. resonant frequency, can originate in an external source or in the preselector internal sweep circuits. When the control signal is supplied by the spectrum analyzer, the preselector is synchronized with the spectrum analyzer to serve as a sweep-tuned r.f. stage. Used independently, the preselector has special usefulness as a bandpass filter that is tuned electrically over a range from 1·8 to 12·4GHz. The passband is typically 20MHz at the low end of the band and about 70MHz at the high end. Internal sweep is provided (60Hz rate) and the sweep width is adjustable from 0 to 10GHz. Since the centre frequency can also be controlled by an external voltage, the unit will function as a programmed filter capable of changing frequency within 20ms. The wide-sweeping spectrum analyzer has proved useful in such applications as spectrum surveillance and electromagnetic-interference analysis. Presenting the whole of a broad frequency spectrum on the c.r.t. speeds measurements considersiderably. However, multiple signals often exist which can increase the difficulty of display interpretation. Using the preselector with the analyzer to 'unclutter' the display enables the operator to appraise the spectral environment more easily.

For more information circle **No. 291**

STATIC CONVERTORS

Nimbus Electronics Ltd, 60 Hilary Crescent, Rayleigh, Essex

A new range of 400Hz static convertors is introduced by Nimbus Electronics. They are transistorized and provide a

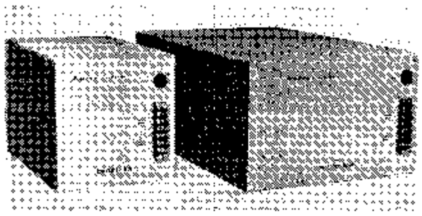

stable source of power for driving 400Hz equipment, mainly used in the aircraft industry. The range of convertors extends from the N050, rated at 50VA, to the N500, rated at 500VA. All have electronic cutout protection should the unit be overloaded. An all-silicon-transistor oscillator generates the 400Hz, and the frequency stability can be maintained to within ±1% over the ambient-temperature range up to 45°C. The oscillator and associated circuits are mounted on a printed board. The frequency and output voltage can be varied by preset potentiometers to ±10% of nominal. The output voltage is normally 115V r.m.s. at ±2% regulation, but can be varied on request. A 24V d.c. input unit can be supplied as an alternative to the normal mains input.

For more information circle **No. 292**

F.E.T. OPERATIONAL AMPLIFIER

Analog Devices Ltd, 38-40 Fife Road, Kingston-on-Thames, Surrey

Analog Devices model-147B/C is a differential operational amplifier with f.e.t. inputs. Featuring an order-of-magnitude improved performance in key parameters over conventional f.e.t. amplifiers, the model-147 is comparable in performance with most chopper-stabilized amplifiers. However, low noise, high common-mode rejection and differential operation allow the amplifier to perform better than chopper-stabilized

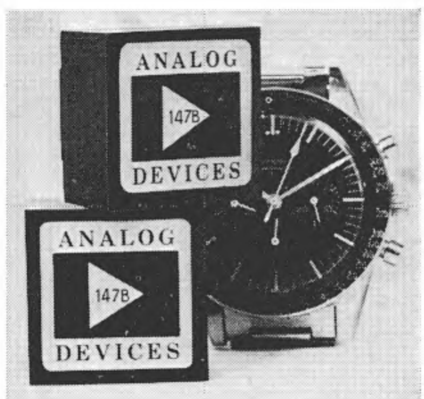

amplifiers in many applications. This amplifier may be used as a building block in circuits which amplify the outputs from photomultiplier tubes, ionization gauges and piezoelectric transducers. The high common-mode rejection ratio and low leakage current will ensure that the amplifier will give good performance in sample-and-hold circuits analogue-to-digital and digital-to-analogue convertors, and electrometer applications. Principle features of the specification are: open-loop gain 10^6V/V; leakage current 15×10^{-12}A, leakage-current drift $1{\cdot}5 \times 10^{-12}$A/degC; input impedance $10^{11}\Omega$, common-mode impedance $10^{12}\Omega$, common-mode rejection ratio 300 000:1; voltage drift 2μV/degC (model C), current noise 10^{13}A (d.c. to 1MHz); output 20V peak-to-peak, 10mA.

For more information circle **No. 293**

MAGNETIC RECORDING BELTS

Mastertape (Magnetic) Ltd, Colnbrook, Buckinghamshire

Mastertape (Magnetic) offer a rectangular-section magnetic-recording belt for in-contact recording and playback applications. The belt is basically of rubber loaded with magnetic iron oxide, similar in principle to those developed by the Bell Telephone Laboratories for recorded-announcement applications. Each is cast individually (not cut from an extended tube), thus ensuring good surface quality as well as dimensional accuracy and stability. The belts are normally used stretched round the edges of drums, and in such conditions their life appears to be unlimited, provided that they are kept clean and surface lubrication is maintained. Wear of belts is undetectable at reasonable head-contact pressures, and the life of heads is many times that expected from use with conventional magnetic tape. Either surface of the belt can be used, since the material is homogeneous, so accidental damage to one side does not necessarily make it useless. Practicable sizes for belts are in the range 2-12in in diameter, ¼-2in in width and 1/16-¼in thick.

With suitable recording conditions, a useful frequency range up to 2kHz per in/s belt speed can be achieved with a signal/noise ratio more than adequate for most applications. At 4in/s, for example, the frequency range can extend to 8kHz, with at least 40dB dynamic range on a track width of 0·1in, and, at this speed, a drum of 6in diameter will give a useful playing or delay time of 4½s per track.

For more information circle **No. 294**

INFRARED-SOURCE DIODES

Mullard Ltd, Torrington Place, London WC1

Two new gallium-arsenide diodes available from Mullard emit near-infrared radiation when subjected to about 1·5V. The radiation from the diodes (types CAY12 and 101CAY, right and left respectively in illustration) is coherent and can be easily modulated by varying the diode current. Maximum radiation from the diodes occurs at a wavelength of $0{\cdot}9\mu$m, which is also near the peak of the response curve of the type-BPX phototransistor. Hence one of the diodes and the phototransistor can be used in a simple compact communications system. A range of 100ft can be achieved and this can be extended by improving the lens system. This com-

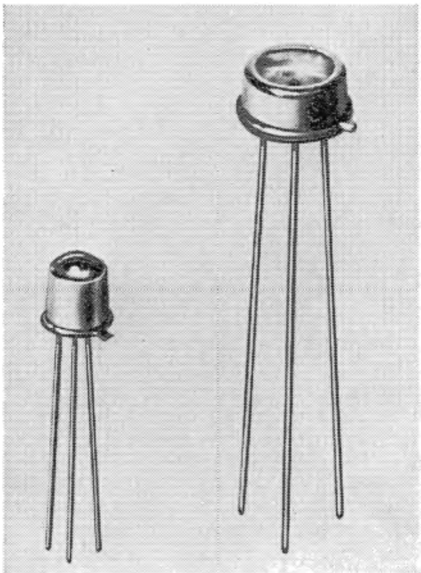

munication system could be used on noisy building sites to form a link between the cabins of tall cranes and the ground, or in crowded places where rapid secret communication free from interference is needed between two points.

The high-frequency performance and high switching speed of these diodes make them suitable for use in a.m. or pulsed communication links. Because the emitted radiation is coherent, the diodes can also be used to start laser actions in other devices.

For more information circle **No. 295**

HIGH-POWER SILICON DIODE

Westinghouse Brake and Signal Co. Ltd, 82 York Way, London N1

The Semiconductor Division of Westinghouse Brake and Signal have introduced

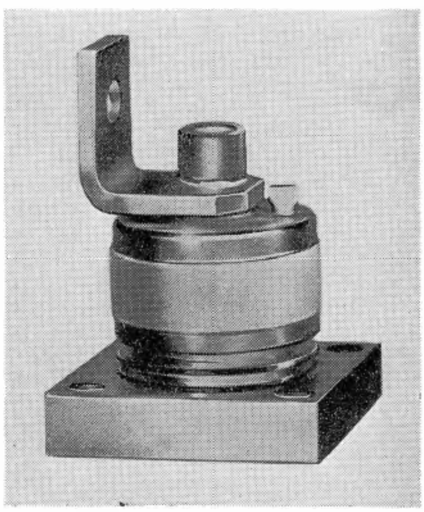

a new high-power silicon diode to their range; it is designated AR500. The AR500 is available with mean-forward-current ratings of up to 620A and voltage ratings up to 3kV. Compression-bond encapsulation is employed with a ceramic/metal housing on a square flat base with solid-top termination.

For more information circle **No. 296**

ACCELEROMETERS

Vibro-meter, Haletop Civic Centre, Wythenshawe, Manchester 22

The quartz-crystal accelerometers marketed by the UK office of Vibro-Meter SA, Switzerland, are now available in a new form of construction. The types 16QA 1000F and 16QA 10000F can be bolted to the vibrating specimen and can be calibrated *in situ*, by removing the protective cover and loading the sensing element with weights proportional to the seismic mass. When the static calibration is achieved, the associated piezoamplifier is switched to

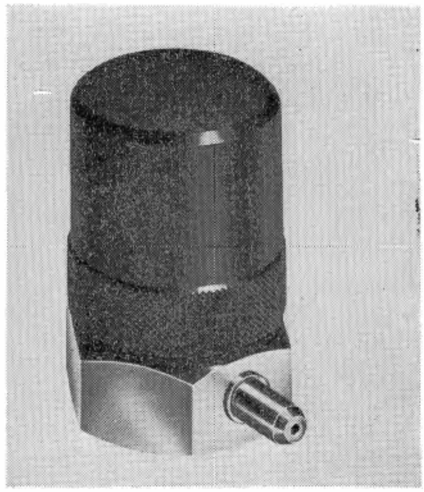

dynamic operation, and a frequency response from 2Hz upwards is available. The natural frequency of the accelerometer is 35kHz or 65kHz, respectively, for a sensitivity range from 0·05-1000g or 1-10000g. Sensitivity variation with temperature is 0·01% per degC over the range −60°C to +200C°. Special versions of the quartz-crystal accelerometer have been adopted by European airlines for the monitoring of jet-engine vibration and can be used up to 480°C.

For more information circle **No. 297**

CAPACITIVE MOVEMENT TRANSDUCER

Grunther Industrial Developments Ltd, 142-146 Old Street, London EC1

Now available to industrial users is the military-style capacitance transducer, joint-service reference 1120-99-961-5885, from Grunther Industrial Development. This device has found application in the services particularly as a tachometry pick-off. The transducer functions by detecting the change in electrical capacitance that occurs as an object moves in relation to a fixed probe, and operation is unaffected by large temperature variations, ambient lighting, surrounding magnetic materials, dust and oil. There is no physical contact between the transducer and the the object or shaft under measurement, and therefore no wear or loading effects. It is self-contained and encapsulated in a solid epoxy moulding approximately 1in cube. It gives an output voltage which varies directly with

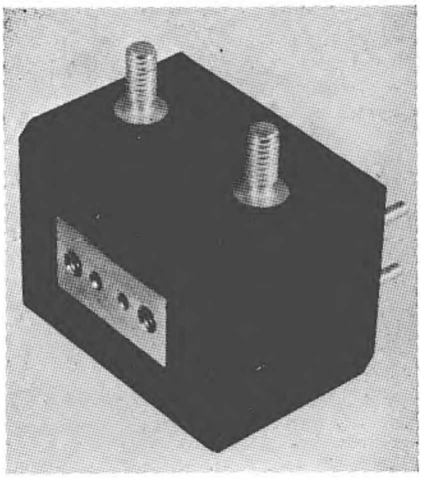

probe-capacitance changes, sensitivity being flat between zero and several kilohertz. The energizing supply required is nominally 12V d.c., consumption approximately 8mA, and the device exhibits a typical output variation of 0·7VpF change in probe capacitance.

For more information circle **No. 298**

ANALOGUE CONTROLLER

The English Electric Co. Ltd, English Electric House, Strand, London WC2

A new 3-term solid-state analogue controller has been added to the 'Modulectric' electronic-process-instrumentation range manufactured by English Electric. The controller is suitable for the closed-loop control of variables such as temperature, pressure, flow or level in a wide variety of industries, to an accuracy within better than ½%. The 'Modulectric' range includes transmitters combining direct-reading indicators with analogue d.c. output, power-supply units, remote indicators and other ancillary control devices capable of being built up to form a complete process instrumentation scheme. The new controller accepts an input from a 'Modulectric' transmitter (or other device) measuring the quantity to be controlled. It provides a p.i.d. output, suitable for feeding (after suitable amplification) to a valve actuator or other control element, thus forming a closed-loop control system. The characteristics of the controller can be varied over wide limits by means of preset controls, so that the optimum performance in terms of accuracy, speed of response, overshoot and drift is obtained from the control loop as a whole.

The controller is flush-panel or rack mounted; on the front panel are: deviation indicator scaled 20% of measured value, high or low; 10-turn desired-value potentiometer; auto/manual switch; remote manual-control potentiometer; and output indicator. The unit incorporates a built-in power supply from a.c. mains or 24V d.c. and utilizes all-silicon-transistor modular circuits. It has an accuracy of 0·5% f.s.d. and stability of ±0·1% f.s.d. Input (measured variable) ranges are 0-10mA, 4-20mA or 0-5V d.c., and output (controller signal)) 0-10mA d.c., direct or reverse acting. Weighing 14lb (6·4kg), the controller front panel is to DIN standard, measuring 144mm × 72mm wide.

For more information circle **No. 299**

SWEPT OSCILLATOR

Microwave & Electronic Systems Ltd, Lochend Industrial Estate, Newbridge, Midlothian, Scotland

The M1000-series swept oscillator, with M990 r.f. plug-ins, introduced by MESL, allows any r.f. plug-in to be used in the M1000 basic frame without any adjustment other than 'snapping in' the appropriate frequency scale. Frequency-band adjustments are thus effected in a matter of seconds. Two independently adjustable broadband sweeps F_1 and F_2 and M_1 and M_2 are provided and indicated on a linear frequency-readout scale. The sweep end-points are set by the front-panel F_1, F_2, M_1 and M_2 controls. Pushbuttons select the desired sweep mode. Controls M_1 and M_2 are used as frequency markers when the F_1 and F_2 sweep mode is operating, and similarly, controls F_1 and

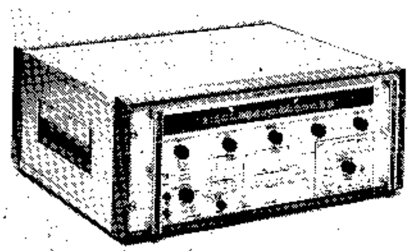

F_2 are used as markers when sweep is switched to the M_1-M_2 mode. The markers appear when the MARKER pushbutton is operated. FAST (recurrent), SLOW (single) and MANUAL sweeps can be button selected. Sweep-rates are variable from 0·01 to 100s and recurrent sweeps can be synchronized to the line frequency. Symmetrical ΔF sweep about either F_1, F_2 M_1 or M_2 can be chosen; the four ΔF pushbuttons on the r.f. plug-in can be used in any combination, to produce 15 ΔF widths in discreet and accurate steps. Modulation functions are selected by pushbutton; internal square-wave modulation is provided with a range of 800 to 1200Hz plus external a.m. and f.m. facilities. The r.f. output power level can be varied continuously over a 20dB range.

For more information circle **No. 300**

CORE-SWITCHING DIODE

Mullard Ltd, Torrington Place, London WC1

A new core-switching diode announced by Mullard can switch up to 400mA at 55V with a reverse recovery time of 20ns, and is therefore suitable for use with the most advanced ferrite-core memory matrixes produced today. The diode (type-BAX78) has a forward voltage drop of not more than 1·25V at 500mA and a reverse current of 100nA. The diode has a planar epitaxial construction and is enclosed within a JEDEC D0-7

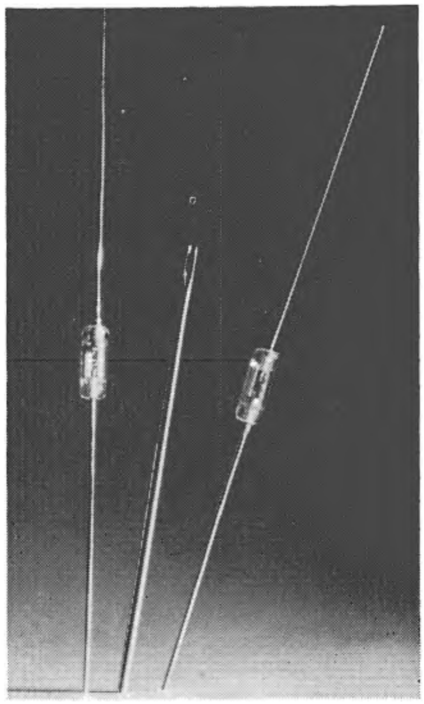

encapsulation. This small envelope (2·5mm diameter, 7·6mm long) allows many diodes to be packed into a small space, so that the minimum lead length required in high-speed core-switching circuits can be achieved.

For more information circle **No. 301**

ENCAPSULATED STABILIZED POWER SUPPLIES

Roband Electronics Ltd, Lowfield Heath Road, Charlwood, Horley, Surrey

The new range of encapsulated power supplies (e.p.s.) from Roband Electronics

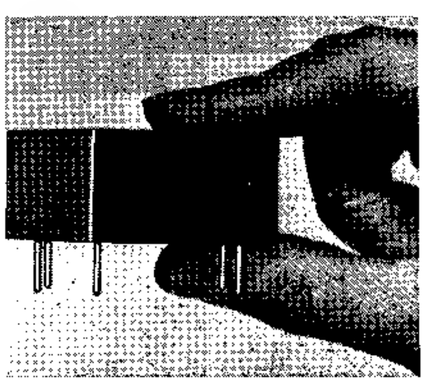

offers preset voltages of 3-8V, 5-30V and 30-60V, with current ratings of 2 and 5A. These units, while able to withstand considerable amounts of rough treatment, are small enough to be wired directly to circuit boards. Any number of units may be operated from a single source to provide multiple outputs. Any voltage or current in the range may be preselected by means of single external resistors. There are 12 units, covering the three voltage and two current ranges mentioned, with positive or negative common rail.

For more information circle **No. 302**

7-CHANNEL GALVANOMETER AMPLIFIER

Honeywell Controls Ltd, Brentford, Middlesex

Introduced by Honeywell Controls is the Accudata-107 d.c. amplifier, which has been specially designed for coupling high-impedance signal sources into their fluid-damped miniature galvanometers. Up to seven plug-in amplifiers can be accommodated in the complete unit, each being supplied from a common power source. Any number of amplifiers up to the maximum can be ordered in one assembly, and extra channels can be purchased later, as required. The amplifier has a voltage gain of 20 and will handle input signals from 1mV to 250V d.c. or peak a.c. All the input connexions are floating, and the common-mode rejection at 50Hz is 80dB when driven from a 1000Ω source. When signals are fed directly into the amplifier,

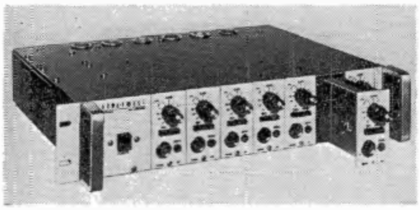

the input impedance is 100MΩ. The amplifier has a switched gain control, steps being bridged by a continuously variable Vernier. For signals greater than 5V, an attenuator is brought into circuit, reducing the input impedance to 1MΩ. Its frequncy range is 0-20kHz, flat to within ±5%, and it will deliver an output of ±3·0V at 40mA or ±10V at 1mA over the range. Noise referred to the input is less than 60μV peak-to-peak up to 10kHz, and drift (also referred to the input) is less than 50μV/degC under all conditions. The unit, suitable for 19in rack mounting, measures 19in × 3½in × 13in approximately; it can be used over the temperature range 0-50°C.

For more information circle **No. 303**

PRESET POTENTIOMETER

Rivlin Instruments Ltd, Doman Road, Camberley, Surrey

The type-500 preset potentiometer by Rivlin Instruments Ltd is now available with three different terminal arrangements: end solder tags (type-500) or side-exit wires for printed-circuit mounting, spaced at 0·2 and 0·7in (type-051·27) and 0·3in and 0·4in (type-501·34). The potentiometer is controlled by a multi-turn lead screw with a clutch mechanism to prevent overwinding. The lead screw is electrically isolated and the contact points are reduced to a minimum. Generated noise is low. The types 500 and 501 are 1·25in × 0·25in × 0·325in with 1in fixing centres, and they cover a resistance range of 10Ω to 20kΩ, with a ±10% tolerance.

For more information circle **No. 304**

MINIATURE NEON INDICATOR

Oxley Developments Co. Ltd, Priory Park, Ulverston, Lancashire

Oxley Developments have added to their range of miniature lampholders a neon version, which retains the 'Barb' press-fit principle, ensuring rapid assembly in

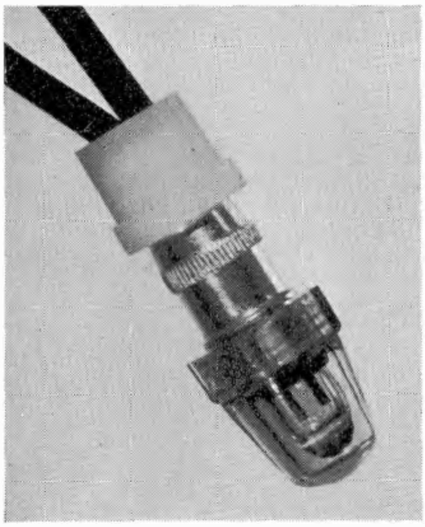

panels or chasses. The units are available for 250 or 110V and are supplied with 9in flying leads. The dimensions are as follows: overall (without leads) 1in maximum, overall diameter 0·35in, height above panel 0·5in, hole size required 0·281in, chassis thickness 10/16 s.w.g.

For more information circle **No. 305**

METER UNIT

Dymar Electronics Ltd, Whippendell Road, Watford, Hertfordshire

With the introduction of a new meter unit (type-70A), Dymar Electronics have modernized their complete range of plug-in instruments. The use of aluminium casting for the front panel makes the instrument more robust, smaller and lighter. The horizontal construction allows stacking of instruments one on top of the other, thus saving bench space; a simple conversion kit permits rack-mounting (19in standard rack, 7in panel height). The electrical specification

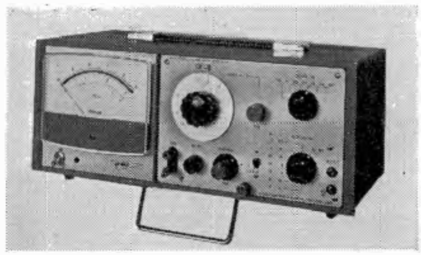

is identical to that of types-70 and 70/R meter units but design has been improved and all semiconductor components are now silicon. The type-70A will accept any of the entire range of existing plug-in instruments, which includes wave analyzers, distortion-factor meters, semiconductor test sets, r.f. power meters, as well as a range of a.c. and d.c. measuring plug-ins. The illustration shows the unit with a type-765 distortion-factor meter plug-in.

For more information circle **No. 306**

THERMOCOUPLE POTENTIOMETER

Croydon Precision Instrument Co., Hampton Road, Croydon, CR9, 2RU, Surrey

A thermocouple potentiometer is available from Croydon Precision Instrument. It weighs 3lb and its dimensions are 7in × 5½in × 3in. It is contained in a leather case with carrying strap, and its ranges will cover any thermocouple measurement that the service engineer could encounter. It reads directly in either millivolts or degrees Centigrade, with cold-junction compensation on all

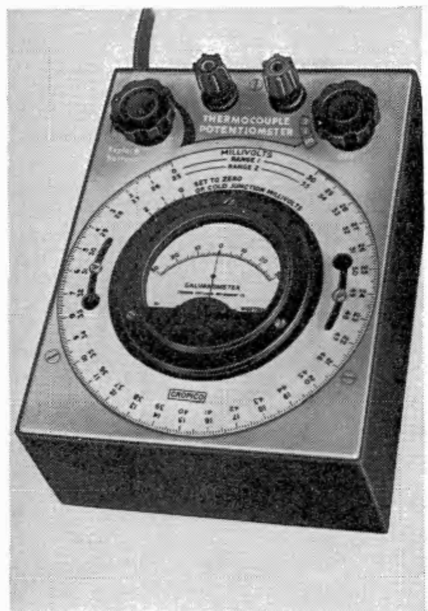

ranges. To cover all these ranges, eight quickly interchangeable scales are provided. Operation of this instrument is very rapid: to make a measurement, it is only necessary to rotate one scale to a position of galvanometer null-balance, and the sensitivity of the galvanometer is synchronized with that of the range scale to facilitate this adjustment. The operating current is 3mA, the power source being a 1½V dry cell LPU2, which will have a long life under these conditions. An unsaturated standard cell is incorporated as the reference voltage which has a low temperature coefficient (less than 5μV/degC); consequently, accuracy will be unaffected by adverse operating conditions.

For more information circle **No. 307**

SOLID-STATE MODULATOR

Microtest Ltd, 9 Old Bridge Street, Kingston-on-Thames, Surrey

The solid-state modulator type-703 available from Microtest is primarily intended as a compact bench supply, with comprehensive modulation facilities, capable of energizing 2-terminal solid-state devices such as Gunn diodes, l.s.a. diodes and other bulk-effect oscillators. The modulator provides a source of voltage suitable for medium-power diodes in c.w., pulse, squarewave and sawtooth form. The modulator may be used in experimental stages of design involving such devices, in production testing and in conjunction with fully engineered oscillators, as a source of microwave power. In the former case the modulator is particularly useful, as driving the device with short pulses will often prevent the destruction which would otherwise result due to accidental excessive power dissipation in the c.w. or squarewave mode. In the latter case, the modulator may be employed with an already engineered device for use as a test oscillator or source of microwave power, especially in the squarewave mode of operation, when the signal is normally amplified by means of selective amplifiers tuned to frequencies between 1 and 4kHz. In such circumstances, the modulator replaces the until now commonly used klystron power supply. The device current is continuously displayed on a built-in 3in meter. The output is *via* two B.N.C.

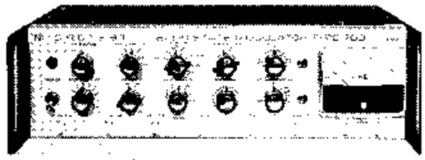

connectors in parallel, the second of which may be conveniently taken to an oscilloscope for the purpose of monitoring the waveform across the device.

For more information circle **No. 308**

THICK-FILM MICROCIRCUIT COMPOSITIONS

Du Pont Co. (UK) Ltd, 18 Bream's Building, Fetter Lane, London EC4

Compositions for screen printing of capacitors, fine-line printing of conductors, and crossover insulation, have been added to the range of Du Pont resistor and conductor compositions. The dielectric composition, designated 448-695OR, can produce capacitance densities of 4000 to 10000pF/cm², with a K of 500 to 700 and a dissipation factor lower than 2%. The high-conductivity compositions allow printing of fine lines with separations down to 50μm; the platinum-gold type is solderable, and the gold type can be used also for die bonding. The crossover composition 8190 provides an insulating layer between conductors, has a K of about 9 and a dissipation factor lower than 2%.

Another development is a glass encapsulant, which can be fired at low temperatures; colour versions are available for circuit identification.

For more information circle **No. 309**

SOUND-LEVEL CALIBRATOR

General Radio Co., West Concord, Massachusetts 01781, USA

The General Radio type-1562-A sound-level calibrator is a compact self-contained unit for making accurate field calibrations on microphones and other sound-measuring instruments. It generates five USASI-preferred frequencies (125, 250, 500, 1000 and 2000Hz, ±3%) at an accurately known sound-pressure level of 114dB (referred to 20μN/m²). Level accuracy with the Western Electric 640AA or equivalent microphone is

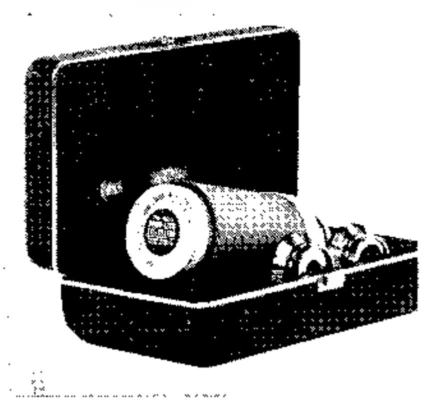

±0·3dB at 500Hz and ±0·5dB at other frequencies. Directly, or with the adaptors supplied, the 1562-A will calibrate many common types of microphones and associated sound equipment. An electrical output of 1V is provided for tests on instruments without microphones.

For more information circle **No. 310**

TEMPERATURE-TEST CHAMBER

Montford Instruments Ltd, 79 Lots Road, London SW10

The Montford universal laboratory environmental test chamber UCL/K25 combines the advantages of cryogenic refrigeration with the development of the solid-state temperature controller, using an electronic bridge in conjunction with a platinum-resistance probe, thus giving accuracy in temperature controlling together with a sensitivity of ±0·1degC in control switching. The temperature range extends from −70°C to +170°C, the lower temperature being achieved using liquid CO_2, as the refrigerant and the upper limit using fully enclosed stainless sheathed electric heaters to supply the heating agency. Facilities are provided for a higher temperature limit of +200°C should this be required. The inner chamber is constructed from stainless steel and forced-air circulation is employed to reduce the temperature gradient to a minimum, which, in the model is ±0·5degC after set temperature is reached. To cater for the testing of different-sized components or batches of components, four chamber sizes are available, with the following dimensions: 12in × 12in × 12in; 24in 12in × 12in × 12in; 24in × 18in × 18in; 24in × 24in × 24in. The outer cabinet is constructed from mild steel, with two-tone stove-enamel finish, all electrical controls being housed in a separate compartment and the unit being completely heat-insulated with mineral fibre lagging.

For more information circle **No. 311**

RESISTIVE PHOTOCELLS

Hewlett Packard Ltd, 224 Bath Road, Slough, Buckinghamshire

A series of resistive photocells is available from Hewlett Packard. The cells have relatively fast switching times without sacrifice of temperature stability and they are designed primarily for photochopper service in sensitive low-level d.c. amplifiers and instruments; they are also useful in a variety of other switching and control-circuit applications. Dark resistance of all the photocells in the series (4600-series) is typically 500MΩ and lighted resistances of 4, 10, and 100Ω are available (measured with an illumination level of 600μW/cm^2 obtained from high-brightness neon glow lamp (NE2U) operating with 1·5mA of current). Typical decay time is 1·2ms (time for resistance to change by a factor of 10 when illumination is removed). The cells are useful in choppers operating at rates up to 500Hz and achieve chopping efficiencies (output p-p voltage/d.c.) of 95%. Peak spectral response is 6550Å, making the cells sensitive to neon glow lamps as well as incandescent lamps.

The cells are hermetically sealed in a TO-5 package. Maximum permitted voltage (case to leads) is 200V. A transparent conducting layer on the window is available optionally for shielding a cell from electrical transients generated by switching the illumination.

For more information circle **No. 312**

SUBMINIATURE SEALED PRESS SWITCH

Thorn Special Products Ltd, Great Cambridge Road, Enfield, Middlesex

A subminiature switch with indicator lamp, announced by Thorn Special Products, is sealed internally to withstand a pressure differential of one atmosphere. The switch has a fully insulated body with an undercut integral flange and O-ring to form a panel seal. Including

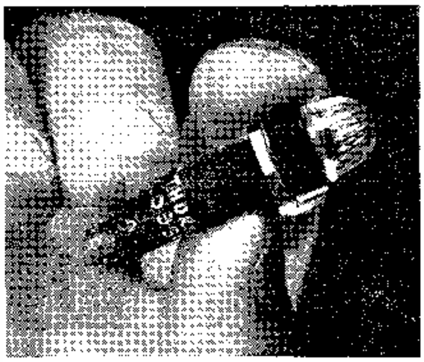

the conventional press-to-test arrangement, the switch is available with any one of the five standard circuits of press-to-make and press-to-break. An operating force of 1½-2½lbf is required for operation; a life of over 25000 switching operations in envisaged. The lamp required is the Thorn subminiature lamp L1123 with 60000h operation at 5V, 60mA. Lamp life at 6V, 70mA, is over 5000h; maximum rating of the switch is 30V. The fluted-glass cap is available colourless and in red, green, orange, blue and yellow.

For more information circle **No. 313**

DIGITAL MULTIMETER

Microwave and Electronic Systems Ltd, Lochend Industrial Estate, Newbridge, Midlothian, Scotland

The MESL digital multimeter provides complete multimeter capability with digital readout presentation. Employing solid-state circuitry with integrated circuits, the instrument offers reliability and high accuracy. Readout of any parameter within the instrument range is immediate, and the pushbutton mode selection ensures ease of operation. Autoranging is built in to the meter for all measurements, allowing readings to be made without recourse to a range switch, and with full overload protection. Similarly, automatic polarity indication for d.c., and sign indication for a.c., provides function recognition. The meter is capable of mains or battery operation, the latter giving good common-mode rejection. Nickel-cadmium batteries, complete with charger unit, are built in, allowing the batteries to be

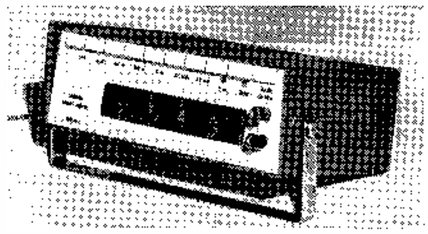

maintained automatically at full charge when the instrument is connected to the mains. A standby selector button is provided which maintains the input amplifier on while the remainder of the instrument is off. Servicing presents no problem, there being virtually no cables, and the use of printed circuits at certain points enables the entire instrument to be opened out flat for servicing accessibility. The charging system for the batteries is so designed that there is no possibility of overcharging, owing to the self-adjusting charging-rate circuitry.

For more information circle **No. 314**

Data Sheets and Catalogues

Silicon-diode data

Westinghouse Brake and Signal Co. Ltd, 82 York Way, London, N.1

Six new engineering publications give details of Westinghouse silicon diodes and stacks. 25-41 describes a 1·5A diode encapsulated in a moulded case which provides a high degree of protection from humidity and high insulation resistance; 25-21 and 25-36 describe medium-power silicon diodes of 18 and 37A rating, respectively, each with voltage ranges from 100 to 1500V; 25-17 describes 150A diodes of reverse polarity; and 25-22 and 25-37 medium-power silicon stacks for convection cooling.

For more information circle **No. 315**

Plastics materials data

Materials Data Ltd, 19-27 South Street, Farnham, Surrey

A new information system by Materials Data provides uniformly prepared data sheets on all thermoplastics materials commercially available in Britain. Application data on various aspects of forming, finishing and joining are recorded. Each data sheet records the name of the manufacturer of the material described. A feature card index is provided for random access to the information stored in the system. Selector cards, consisting of grids of numbered squares printed on translucent plastics film are punched appropriately to indicate materials having given properties—by superimposition, coincident dots indicate materials having the described combination of properties 'dialled' into the system.

For more information circle **No. 316**

Measuring instruments

Marconi Instruments Ltd, St. Albans, Hertfordshire

The Marconi Instruments 1967 Short-Form Catalogue is a reference guide giving brief specifications of the current range of measuring instruments arranged in logical order according to probable application. As it is intended as a means of rapid selection, the information given is much abridged, more details literature on any item being available separately.

For more information circle **No. 317**

Ignitrons

English Electric Valve Co. Ltd, Chelmsford, Essex

This pocket book, in addition to containing full data on all English Electric ignitrons, gives a type-number equivalents index, theoretical and practical information for designers and users, and a quick-reference selection chart of tabulated data.

For more information circle **No. 318**

Transistorized-static-control handbook

Simplex-GE Ltd, PO Box 2, Blythe Bridge, Stoke-on-Trent, Staffordshire

This new supplement to the Simplex-GE catalogue, covers the complete range of static-control units available. The handbook gives an introduction to, and the theory of, logic elements, and gives a wide variety of circuit configurations.

For more information circle **No. 319**

Custom-made cabinets

Bedco Ltd, Station Road, Harpenden, Hertfordshire

A 20-page illustrated booklet giving full details of a specialized cabinet and sheet-metal-components service is available from Bedco. Of particular interest to electronics, computer and allied industries, the booklet describes the design and planning service available.

For more information circle **No. 320**

Résumés des principaux articles

Les caractéristiques à signal fort et les critères de stabilité des circuits de conversion à impédance négative par A. C. Davies

Résumé de l'article aux pages 536 à 541

Les convertisseurs à impédance négative se divisent en deux catégories, à savoir les convertisseurs dits du type idéal et les convertisseurs de type pratique; ils se distinguent par le fait que le circuit du convertisseur idéal est symétrique tandis que les orifices du circuit pratique sont toujours dissemblables: l'un des orifices est instable par rapport au circuit ouvert et l'autre par rapport au court-circuit. L'auteur décrit en détail cet aspect du comportement des convertisseurs à impédance négative et analyse le rapport entre les conditions de stabilité à signal réduit et la nature des caractéristiques de courant-tension des orifices. Il démontre que le comportement observé peut être fonction des propriétés élémentaires des amplificateurs.

Système de télémesure des chocs à faible distance par J. Morrison

Résumé de l'article aux pages 542 à 545

Cet article décrit un système émetteur-récepteur à modulation de fréquence à faible portée, conçu pour la mesure d'accélérations d'impacts allant jusqu'à 1000g. Ce contrôle fut effectué pour la mise au point optima d'un prototype d'amortisseur et comportait la chute d'un cylindre d'acier de 272kg sur l'amortisseur d'une hauteur de 18m,

Les signaux obtenus à partir du bruit par l'emploi des méthodes numériques par A. B. E. Ellis

Résumé de l'article aux pages 546 à 552

L'auteur traite d'une instrument conçu pour améliorer les signaux sonores; la présence et la forme d'onde approximative d'un signal de 10mV peuvent être décelés d'un bruit de 100mV. La description de l'appareil porte tant sur son circuit que sur son fonctionnement. Certaines utilisations sont mentionnées, notamment dans les domaines de la recherche ionosphérique, des ultra-sons, de la recherche biomédicale et de la radioastronomie. Certains résultats sont indiqués dans le domaine de la recherche ionosphérique. Ils furent obtenus à l'aide d'un élément compact capable d'un bon rendement.

Déclencheur périodique linéaire à action rapide par E. A. Faulkner et J. B. Grimbleby

Résumé de l'article aux pages 565 à 567

Cet article décrit un déclencheur périodique à transistors planaires au silicium complémentaires. La circuit donne un temps de commutation de 5ns, avec des crêtes de courant négligeables, une linéarité inférieure à 0,1% et un coefficient de température de 0,04% par degK. Le déclencheur trouve des applications particulières dans les intégrateurs à longues impulsions séparées par de très courts intervalles et dans les détecteurs sensibles aux phases.

Convertisseur précis courant-fréquence par J. Korytkowski

Résumé de l'article aux pages 568 à 570

Cet article décrit un convertisseur analogique courant-fréquence dont la fréquence de sortie est proportionnelle au courant d'entrée. Cet instrument produit une sortie à impulsions répétées dont on peut faire varier la fréquence dans la gamme de 0 à 4 kHz par une gamme de courant d'entrée de 0 à 4 mA. Dans la gamme de 0 à 1 mA, le degré de précision est supérieur à 0,1%. Le fonctionnement du convertisseur est basé sur l'utilisation de diodes Zener à référence stable, d'un condensateur intégrateur et de transistors au silicium.

L'analyse de l'équilibrage des systèmes d'accord par les méthodes à matrices de dispersion par J. N. Saha

Résumé de l'article aux pages 571 à 575

L'emploi d'un diagramme Smith pour déterminer les caractéristiques de fréquence d'une ligne de transmission HF adaptée à un système d'accord nécessite un effort considérable, en particulier pour déterminer l'émission de courant par diffusion avant sur une ligne à très haute fréquence soutenue par le grand nombre de systèmes d'accord effectivement rencontrés. Une calculatrice numérique peut être employée utilement pour résoudre ces problèmes car elle permet d'obtenir des expressions convenant pour la programmation. Dans cet article, pour une ligne de transmission se composant de sections de réseau en deux parties reliées en cascade, les matrices de dispersion de chaque section ont été combinées pour produire une matrice de transfert général pour la ligne. Le coefficient de réflexion d'entrée du système a été déterminé à partir des éléments de cette matrice, tant pour les systèmes d'accord en dérivation que pour les systèmes série. On a obtenu ainsi des équations de réalisation d'un équilibrage parfait. La réponse de fréquence de la ligne adaptée à un système d'accord en dérivation ainsi que celle adaptée à un système d'accord série, ont été calculées par une calculatrice numérique et tracées en courbes sur un dispositif de report.

Antenne à lignes sinueuses et à arc en retour par S. C. Loh et J. Jacobsen

Résumé de l'article aux pages 575 à 577

Il s'agit ici d'une étude expérimentale des caractéristiques de radiation de l'antenne à lignes sinueuses utilisée dans des conditions d'arc en retour. Le comportement électrique en est généralement amélioré, particulièrement en ce qui concerne la largeur de bande de demi-puissance et la largeur de bande de la fréquence de fonctionnement.

La directivité d'un réseau de rainures à la surface d'un cylindre par L. J. Ricardi

Résumé de l'article aux pages 578 à 581

Des expressions générales ont été obtenues en ce qui concerne la directivité de réseaux de rainures axiales et circulaires sur un cylindre à conductibilité infinie. L'espacement optimum pour les réseaux à deux et à sept rainures sur un cylindre infini d'un diamètre de 1 à 4 longueurs d'ondes est présenté, ce qui permet de déterminer un dessin uniforme sur le plan équatorial.

La distorsion dans les oscillateurs de réaction à pont de résistance-capacité par V. B. Mehta

Résumé de l'article aux pages 582 à 585

Il est démontré que la méthode d'analyse de la distorsion dans les oscillateurs de réaction à pont de résistance-capacité, dont l'atténuateur résistif (parcours de réaction indépendant de la fréquence) est considéré comme faisant partie du réseau de réaction, comporte de nombreux avantages par rapport à l'autre méthode d'analyse. Les différents réseaux de résistance-capacité—le réseau de Wien, le réseau en T à pont de résistance-capacité et le réseau à T jumelé symétrique et équilibré—sont comparés dans l'analyse de la distorsion d'oscillateurs d'un système d'amplification particulier.

Zusammenfassung der wichtigsten Beiträge

Grossignaleigenschaften und Stabilitätskriterien von Wandlern mit negativer Impedanz von A. C. Davies

Zusammenfassung des Beitrages auf Seite 536-541

Ideale und praktische Wandler mit negativer Impedanz unterscheiden sich dadurch, dass die ideale Schaltung symmetrisch ist, die praktische Schaltung dagegen immer ungleichwertige Klemmenpaare hat: es stellt sich immer heraus, dass ein Paar im Leerlauf, das andere im Kurzschlussbetrieb unstabil ist. Das Verhalten von Wandlern mit negativer Impedanz wird nach diesem Gesichtspunkt eingehend behandelt und die Beziehung zwischen den Stabilitätsbedingungen für Kleinsignale und der Natur der Strom-Spannungscharakteristik an den Klemmen diskutiert. Es wird gezeigt, dass das beobachtete Verhalten mit Grundeigenschaften des Verstärkers in Beziehung gebracht werden kann.

Stossmessendes Telemetriesystem für kurze Entfernungen von J. Morrison

Zusammenfassung des Beitrages auf Seite 542-545

In dem Beitrag wird ein FM-Sende-Empfangssystem für kurze Entfernungen beschrieben, das zum Messen von Stossbremsungen von bis zu 1000g entwickelt wurde. Die Messungen waren für Optimisierung des Entwurfs eines Stossdampfers erforderlich. In Tests fiel ein etwa 272kg wiegender Stahlzylinder von Hohen bis zu 18,3m auf den Stossempfanger.

Ausblenden von Signalen aus Rauschen mittels Digitaltechnik von A. B. E. Ellis

Zusammenfassung des Beitrages auf Seite 546-552

Ein beschriebenes Gerät verbessert geräuschvolle Signale und gestattet Nachweis und Bestimmung der naherungweisen Wellenform eines 10-mV-Signals durch Ausblenden aus 100-mV-Rauschen. In der Beschreibung werden sowohl Schaltungs- wie auch Betriebsgesichtspunkte berücksichtigt. Einige Anwendungsmöglichkeiten werden erwähnt, besonders in der ionosphärischen Forschung, Ultraschalltechnik, biomedizinischen Forschung und Funkastronomie. Ergebnisse im Gebiet der ionosphärischen Forschung werden gebracht.

Lineare Schnelltorschaltung von E. A. Faulkner und J. B. Grimbleby

Zusammenfassung des Beitrages auf Seite 565-567

Der Beitrag beschreibt eine lineare Torschaltung mit komplementären Silizium-Planartransistoren. Die Schaltzeit des Tors ist bei vernachlässigbaren Überschwingspitzen 5ns, die Linearität innerhalb 0,1 Prozent und der Temperaturkoeffizient 0,04 Prozent/°K. Diese Torschaltung ist besonders für Anwendung in 'Boxcar'-Integratoren und phasenempfindlichen Gleichrichtern geeignet.

Präzisions-Strom-Frequenzwandler von J. Korytkowski

Zusammenfassung des Beitrages auf Seite 568-570

Ein Strom-Frequenzwandler wird beschrieben, dessen Ausgangsfrequenz dem Eingangsstrom proportional ist. Der Wandler gibt periodische Impulse ab, deren Frequenz fur einen Eingangsstrom von 0 . . . 4 mA uber den Bereich 0 . . . 4 kHz veränderlich ist. Für den Bereich 0 . . . 1mA ist die Genauigkeit besser als 0,1 Prozent. Die Arbeitsweise des Wandlers beruht auf der Verwendung konstanter Zener-Bezugsdioden, eines integrierenden Kondensators und von Siliziumtransistoren.

Analyse der Stichleitungsanpassung nach der Streumatrixmethode von J. N. Saha

Zusammenfassung des Beitrages auf Seite 571-575

Die Anwendung eines Smithschen Leitungsdiagramms bei der Bestimmung der Frequenzcharakteristik einer HF-Übertragungsleitung mit Stichleitungsanpassung ist sehr aufwendig, besonders wenn die Vorwärtsübertragung von Energie über eine VHF-Leitung mit der in der Praxis vorkommenden grossen Anzahl von Stichleitungen zu untersuchen ist. Bei Ableitung geeigneter Ausdrücke für die Programmierung kann ein Digitalrechner mit Erfolg für solche Probleme eingesetzt werden. Für eine aus Vierpolabschnitten in Kaskade bestehende Übertragungsleitung werden nach diesem Beitrag die Streumatrizes jedes Abschnittes kombiniert und ergeben eine Gesamtübertragungsmatrix für die Leitung. Der Eingangsreflexionsfaktor des Systems wird von den Elementen dieser Matrix sowohl für Parallel- wie auch Serienstichleitungen bestimmt und die Entwurfsgleichung für perfekte Anpassung abgeleitet. Der Frequenzgang der Leitung wird mittels Digitalrechner für Anpassung mit Parallel- sowie Serienstichleitung berechnet und aufgetragen.

Mäanderlinienantenne mit Reflektor von S. C. Loh und J. Jacobsen

Zusammenfassung des Beitrages auf Seite 575-577

Versuchsweise Untersuchungen der Strahlungscharakteristik einer Mäanderlinienantenne unter Rückstrahlungsbedingungen wird beschrieben. Eine allgemeine Verbesserung der elektrischen Eigenschaften wurde festgestellt, vor allem in bezug auf die Leistungshalbwertbreite und Bündelbreite bei der Betriebsfrequenz.

Richtwirkung eines Schlitzstrahlsystems auf der Oberfläche eines Zylinders von L. J. Ricardi

Zusammenfassung des Beitrages auf Seite 578-581

Es werden Allgemeinausdrücke für die Richtwirkung von Strahlersystemen aus Längs- und Umfangschlitzen auf einem unendlichen leitenden Zylinder abgeleitet. Der optimale Abstand für Systeme mit 2 bis 7 Schlitzen auf einem unendlichen Zylinder mit einem Durchmesser von ein bis vier Wellenlängen wird gegeben und die für die Erzeugung einer homogenen Charakteristik in der äquatorialen Ebene erforderliche Mindestanzahl von Schlitzen bestimmt.

Verzerrungen in RC-Brückenrückkopplungsgeneratoren von V. B. Mehta

Zusammenfassung des Beitrages auf Seite 582-585

Es wird gezeigt, dass von den beiden Verfahren zur Analyse von Verzerrungen in RC-Brückenrückkopplungsgeneratoren diejenige viele Vorteile hat, in der der ohmsche Abschwächer (frequenzunabhängiger Rückkopplungsweg) als Teil des Rückkopplungsnetzwerkes betrachtet wird. Bei gegebenem Verstarkersystem werden verschiedene RC-Netzwerke—Wien-Bruckenschaltung, RC-uberbrucktes T-Netzwerk und symmetrisches Doppel-T-Netzwerk—in bezug auf Verzerrungen im Generator verglichen.